DEPARTMENT OF INFORMATION ENGINEERING AND COMPUTER SCIENCE
DEPARTMENT OF INDUSTRIAL ENGINEERING
FONDAZIONE BRUNO KESSLER
Doctorate Program in Industrial Innovation

UV-CURABLE PROTECTIVE COATING FOR THE INNER SURFACE OF STEEL PIPES

Alessandro Condini

Advisor

Prof. Stefano Rossi

Università degli Studi di Trento

Co-Advisor

Prof. Flavio Deflorian

Università degli Studi di Trento

Industrial Tutor

PhD. Angela Giuliani

Elixe srl

October, 2024

Abstract

In recent years, the urgency of environmental and health protection regulations has significantly intensified the search for new, environmentally friendly anticorrosive coatings in heavy industry. While waterborne, high solids or powder coatings have emerged as alternatives, solvent-borne coatings still dominate the market, contributing to polluting and toxic volatile organic compound (VOC) emissions.

UV-curable coatings offer a compelling solution with low environmental impact and efficient production processes that avoid VOC emissions, reduce energy consumption significantly, and lower product costs. Applying UV-curable coatings, which cross-link with UV radiation in a few seconds and without temperature application, is an innovative strategy that could meet the current environmental protection needs. This technology's superiority over traditional ones is evident in its higher production efficiency, avoidance of VOC emissions, lower energy spending production processes, and low investment in the production plant, all of which contribute to reducing product costs and preserving the environment.

The technical-scientific aim of the proposed project is to develop a novel corrosion protective system cross-linked by UV radiation for the inner surface of piping. The system provides a new UV-curable coating formulation with outstanding performance and an effective technology for application and cross-linking inside a pipe's closed space.

The proposed project directly responds to the urgent need for innovation in the pipes industry. The current production processes, which rely on catalytic ovens operating between 80 ˚C and 130 ˚C and using solvent-borne epoxy-based coatings, are highly polluting and energetically expensive, significantly inflating the product's cost. By revolutionizing these processes with a more sustainable and cost-effective solution, we can potentially reduce the overall cost of production, a key benefit that will interest industry stakeholders.

Developing UV-curable coating technology for metal protection represents the new frontier of knowledge for the sustainability of corrosion protection treatments, respecting the environment, the workers' health involved in the process, and the economy of the production processes.

Keywords

#coating #anticorrosion #UVcuring #pipe

Contents

1 Introduction

Corrosion, the primary cause of steel infrastructure failures in harsh environments, is a pressing issue. The Nace International Report 2023 (1) estimates the global cost of corrosion at US$2.5 trillion, or 3.4 % of the global Gross Domestic Product (GDP) (2013). (2) Among the commonly used solutions to prevent corrosion, such as steel corrosion inhibitors (3) (4) , corrosion-resistant alloys (5), or fiber-reinforced plastics (6), protective organic coatings stand out for their cost-effectiveness and performance (7) (8) (9).

Organic coatings can be composed of organic polymers that can be thermoplastic or thermosetting, solvent-borne, or powder-based. Only organic coatings based on thermosetting resin have been investigated during this research. Until now, solvent-borne paints have been the most widely used protective coatings for steel-made products because of their high performance in terms of thermal and mechanical properties and ease of application. On the other hand, these paints can cause long-term adverse effects on workers' health and polluting effects because of VOC release and are characterized by a very high energy-consuming curing process due to the need for high-temperature application (10) (11) for long periods, using expensive and energy-consuming ovens (12) (13). In this context, UV-curable coatings represent a promising solution since they overcome the main drawbacks of thermally cured coatings, obtaining process efficiency through reduced curing time (from hours to seconds), lowering energy consumption, and improving environmental sustainability because of the absence of harmful VOCs in their formulation (14). Despite their evident advantages, UV-curable coatings have rarely been applied to the inner surfaces of pipelines and narrow geometries due to the dimensional difficulties of bringing a UV light source inside these spaces.

1.1 The Context

Even though the beneficial aspects of UV technology have been demonstrated, prejudices about its use must still be overcome. These limitations are due to a wrong analysis of the technology.

Despite the high productivity and efficiency resulting from applying UV technology, it is known that the cost of a thermal curing coating in raw materials is cheaper than that of a UV-curing coating. However, the price difference is negligible when it is considered that UV-curing coatings are 100 % solids compared to thermal-curing coatings. Thus, the latter are characterized by a lower efficiency per unit area and higher supply costs. To coat a particular area, more thermal curing paint drums are necessary than the drums of UV coating because UV coating is 100 % solids. In comparison, high solids solvent-borne coating could reach a maximum solid concentration of 65 %.

If we consider the object of the present research, a traditional production line for pipe treatment using thermal curing coating with ovens requires large spaces where the products can remain at high temperatures for 1-2 hours. The design of a curing oven requires huge investments before the installation and high-energy requirements to maintain it at the operating temperature during the process. For these reasons, even powder coatings are less sustainable than UV-curing coatings because they require thermal curing production lines.

The design and development of a new production line for pipe treatment using UV coatings would result in a smaller investment than a thermal curing line. The energy required to operate a UV light source, light-emitting diode (LED), or mercury lamp works for seconds or minutes is much lower than heating a natural gas oven to > 150 ˚C to cure thermal curing coatings.

1.2 The Problem

The heavy industry sector constantly challenges itself by protecting its extensive network of steel structures from corrosion, a natural process that degrades steel and reduces its structural integrity. Traditionally, solvent-based paints represent the primary method of corrosion protection, offering adequate barrier protection against external factors. However, these conventional methods exhibit several limitations in industrial use that hinder their widespread adoption, such as high energy consumption for thermal curing and significant investments in production plants and solvent filtration.

1.3 The Solution

UV curing emerges as a promising alternative to conventional corrosion protection methods, offering several advantages:

- Fast Curing: UV light instantly crosslinks the paint molecules, resulting in ultra-fast curing times of mere seconds. This accelerated curing process significantly reduces the time required for coating applications, improving production efficiency and minimizing downtime.
- Environmental Friendliness: UV curing eliminates the need for solvent evaporation, significantly reducing volatile organic compounds (VOC) emissions and environmental impact. This eco-friendly approach aligns with the growing emphasis on sustainability in industrial practices.
- Compatibility with Confined Spaces: UV curing does not require external heat sources, making it compatible with confined spaces that are challenging to access or where heat generation poses safety concerns. This adaptability is crucial for coating metal structures within pipelines, tanks, and other enclosed environments.

Developing a UV-based technology for heavy industry corrosion protection significantly advances industrial coatings. Combining a high-performance UV anti-corrosion coating and a simultaneous application and curing system offers a transformative solution for protecting steel structures from corrosion damage. This innovative approach is poised to revolutionize how corrosion is mitigated in heavy industry, contributing to improved operational efficiency, environmental sustainability, and extended structural lifespan.

In recent years, the progress of UV LED technology has brought devices with reduced size and limited heat emission (15) (16) onto the market that could be used for this purpose. In addition, compared to standard low-pressure mercury-arc lamps, UV LEDs represent a better choice due to their reduced size, improved energy efficiency, safety (17), and avoiding mercury waste management at its life-end. UV-LED can also be mounted in arrays, providing modularity to the UV source and better control over power and irradiance (18).

Based on my experience in work and the scientific knowledge acquired during the last years in the field of steel protection, I have set up a project aiming to develop a comprehensive UV-based technology for heavy industry to protect the inner walls of metal pipes, cylinders, and tanks. The key objectives include:

- Developing a High-Performance UV Anti-Corrosion Coating: The successfully developed UV-curable anti-corrosion coating exhibits exceptional properties, matching or surpassing the performance of the benchmark solvent-based coating, NG-coating. The new coating demonstrates superior corrosion resistance, adhesion, flexibility, and UV stability, ensuring long-lasting protection for metal structures.
- Creating a Simultaneous Application and Curing System: The project has also developed a sophisticated system that simultaneously applies and cures the UV coating on surfaces within confined spaces. This innovative approach overcomes the challenges of painting narrow-diameter pipes and other tight areas, ensuring efficient and uniform coating coverage.

1.4 Innovative Aspects

UV curing, a well-established technology in various sectors, has yet to thoroughly permeate the steel protection industry. This project aims to address this gap by developing a high-performance cationic photopolymerization paint and an innovative UV irradiation device tailored explicitly for coating the inner surface of downhole tubing.

Traditional two-component paints have long dominated the steel protection market, offering reliability and consistent results. However, UV-cured paints provide several advantages, including:

- Rapid Curing: UV light instantaneously crosslinks the paint molecules, enabling ultra-fast curing times of mere seconds. This accelerated curing process improves production efficiency and reduces waste.
- Environmental Benefits: UV curing eliminates the need for solvent evaporation, significantly reducing volatile organic compound (VOC) emissions and environmental impact.

- Thermal Efficiency: UV curing eliminates the energy-intensive drying process associated with traditional paints, making it a more environmentally friendly and cost-effective option.

Due to difficulties in the process, a steel protective coating using photopolymers and UV irradiation hasn't been developed in the past. A protective polymeric coating is based on fillers, which create a barrier to the ions and avoid their reaction on the steel surface. Still, while working as an impermeable membrane to ions, fillers are also a barrier to irradiation, interfering with the UV reaction and the paint curing. During this study, I have demonstrated that the right choice and combination of fillers creates a barrier to ions but lets UV rays penetrate the paint. Moreover, excellent adhesion to the surface has been guaranteed to avoid the formation of reaction zones on the steel surface.

The proposed project addresses the specific challenges of coating the inner surface of downhole tubing, where chemical, thermal, and mechanical stresses are highly demanding. The developed high-performance photopolymerization paint exhibits exceptional properties, including:

- Corrosion Resistance: The paint effectively withstands the harsh corrosive environment within oil-well pipes, protecting the underlying steel structure.
- Adhesion: The paint adheres tenaciously to the pipe's surface, ensuring a durable, long-lasting protective barrier.
- Flexibility: The paint maintains its flexibility even under extreme temperature fluctuations and mechanical vibrations, ensuring the integrity of the coating.

Coating the inner surface of oil-well pipes presents a unique challenge: accessing and curing the coating at narrow diameters. To address this challenge, I have developed a compact and efficient UV irradiation device designed explicitly to cure inside small-diameter tubes.

The device utilizes the latest UV-LED technology, offering several advantages:

- Compact Size: An LED array's compact design allows easy access to the pipes' narrow interiors.
- Low energy consumption: UV-LEDs emit high-intensity UV radiation with minimal energy consumption and low heat emission compared to mercury gas UV lamps, making them ideal for this application.
- Controlled Curing: The device controls UV irradiation intensity, ensuring consistent and uniform curing across the pipe's inner surface.
- Energy efficiency: UV curing energy is wholly focused on the surface to be cured, avoiding energy dispersion like in a thermal process.

Combining a high-performance UV-cured paint and a sophisticated UV irradiation device represents a significant advancement in steel protection technology. This innovative approach offers several benefits for the oil-well industry, including:

- Extended Pipe Lifespan: The durable protective coating enhances the lifespan of oil-well pipes, reducing the need for premature replacements.
- Reduced Maintenance Costs: Coated pipes' longer lifespan leads to lower maintenance costs and improved operational efficiency.
- Enhanced Environmental Protection: Reducing solvent-based paints and eliminating drying emissions contribute to a more sustainable oil-well operation.

This project paves the way for the broader adoption of UV-cured coatings in the metal protection industry, offering a transformative solution for various applications. The combination of advanced material science, innovative technology, and rigorous testing demonstrates the potential of UV curing to revolutionize steel corrosion mitigation and enhance industrial processes.

1.5 Structure of the Thesis

Developing a steel protective coating using UV technology significantly advances corrosion mitigation strategies, introducing innovative protection with high performance in terms not only of corrosion resistance but also high adhesion and resistance to external agents such as acids and temperature. The collaboration with the Polytechnic University of Turin significantly contributed to the project, bringing specialized expertise in photopolymers. At the same time, the work carried out at the host company, MPR srl (Trento), specializing in pipe coating equipment, enabled the manufacturing of the necessary equipment. This multifunctional and

well-structured approach ensured the project's overall success, combining scientific expertise with production capabilities synergistically and achieving the set objectives.

The project commenced with thoroughly investigating UV-curing coating materials tailored explicitly for steel protection. A novel combination of resin and fillers studied in collaboration with the Turin Polytechnic gave a formulation with exceptional corrosion resistance, adhesion, flexibility, and stability properties.

The work has parallel created the inner pipe's painting and UV curing equipment developed in the MPR facility. In the corrosion laboratories of the University of Trento, extensive experimental work has been spearheaded to evaluate the coating application process and the performance of the new UV-cured coating under various environmental conditions. This meticulous testing involved applying the coating to diverse steel substrates, subjecting them to simulated exposure to harsh environments, and measuring their resistance to corrosion, mechanical wear, and degradation. The insights gained from these experiments guided further optimization of the coating application process and paint formulation.

Advanced characterization techniques, such as surface analysis, adhesion testing, and corrosion resistance assessments, have been employed to culminate the project and verify the coating's properties under controlled laboratory conditions. This comprehensive evaluation at the University of Trento's laboratories proved that the coating met or exceeded the project's stringent specifications.

The seamless integration of theoretical expertise, experimental rigor, and sophisticated characterization techniques underscores the project's adherence to a high standard of scientific rigor. The collaboration between leading institutions, extensive experimental testing, and thorough characterization have established a solid foundation for developing a revolutionary UV-based coating protection solution for steel.

The successful completion of this research holds the potential to revolutionize the field of corrosion mitigation, offering enhanced protection for steel structures and components across various applications. The project's meticulous methodology and unwavering commitment to scientific excellence exemplify the efforts involved, setting a benchmark for future innovations in coating technology.

2 State of the Art

2.1 Protecting Steel Pipes

Most metals exist in nature as stable oxides, carbonates, or sulfide compounds. They are refined to obtain them pure or in alloys to make them useful for human purposes. Refining processes require energy. Corrosion is nature's way of reversing an unnatural process back to a lower energy state. (19)

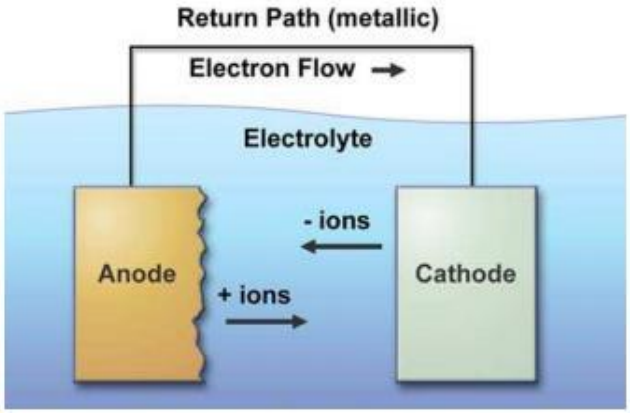

Figure 1 - Basic corrosion cell (Source: NACE Corrosion Training Material)

The primary corrosion mechanism follows the principle of a battery. Figure 1 below reports a scheme of a primary corrosion cell.

A battery requires two dissimilar metals connected and immersed into an electrolyte. The metal characterized by a higher tendency to rust (oxidize) forms the negative pole of the battery, named anode. The other metal, which creates the battery's positive pole, is called the cathode. The formation of metal-positive ions onto the anodic surface and its resulting release into the electrolyte solution triggers the release of electrons. This reaction is named the oxidation reaction. The build-up of the electrons generates an electrical potential, causing them to flow through the conductor to the cathode. Excess electrons are neutralized or taken up at the cathode by ions in the electrolyte. This reaction is called the reduction reaction. The anode will continue to rust if the electric circuit is maintained and the metal cations are removed from the electrolyte solution and combined with other elements to make up corrosion products. (19) (20)

There are many sources of corrosion and many more methods to slow the process down. A common strategy to avoid corrosion depends on a) corrosion source/mechanism identification and b) the working condition of the part of an industrial plant that can suffer the corrosion process. (19) (20)

The reported research project focuses on preventing corrosion of pipes used for oil and gas, water transport, chemical transport, or production.

Corrosion can involve the external or internal wall of the pipe. The present study investigated only the prevention of corrosion of the inner wall of pipes. However, a summary of external corrosion prevention has been reported as the best topic of knowledge.

2.2 External Corrosion

The corrosion of the external wall of pipes is different depending on whether they are buried in the soil or not. Usually, pipes can be suppressed when they are part of water, sewerage, and oil & gas distribution plants. They can be exposed to atmospheric phenomena when part of chemical transport/ production plants or offshore structures. (21)

When pipes are buried, the characteristics of the soil and its corrosivity play a critical role in corrosion phenomena. As it is known, corrosion requires the movement of ions through an electrolyte, the soil, and factors that can increase the electrical conductivity of the soil, such as a) moisture contents, b) poor drainage, and c) high salt contents, can favor the increase of its corrosivity. Thus, differences in the soil characteristics from place to place along a pipeline, such

as a) differences in aeration, b) moisture content, and c) the soil composition, can produce strong driving forces for corrosion.

Soils characterized by low conductivity, as expected, tend to exhibit lower corrosivity, although, through practical experience has been found that the low conductivity of the soil can retard the flow of cathodic–protection currents resulting in the occurrence of corrosion phenomena greater than what can be expected.

To prevent or mitigate external corrosion of buried pipelines, three approaches can be applied:

a) cathodic protection application.

b) protective coatings application.

c) "pipe–in–pipe" method.

Cathodic protection cannot be used as a unique approach. A very high current would be required to be very effective because the necessary current is proportional to the pipeline exposed area to protect. Thus, cathodic protection and protective coatings application strategies are usually applied together. Protective coatings application reduces the pipeline exposed area to protect.

In the end, the "pipe–in–pipe" method involves placing a metal pipe within another pipe containing a nonconductive filler in its annular space.

2.3 Internal Corrosion

The focus of this research project is the prevention or mitigation of internal pipeline corrosion. Generally, internal pipeline corrosion can occur only in the presence of corrosive agents like water or other aqueous compounds like glycols; carbon dioxide (CO_2) for the formation of dilute organic or inorganic acids; or sulfur for the formation of acids or growth of bacteria. The corrosive agents continue the corrosion until they have been removed or consumed in the corrosion reactions.

Typically, the internal wall of gas pipes is corroded because gas comes from a well and may contain fewer substances, such as water, CO_2, and hydrogen sulfide (H_2S). If the water condenses, it can react with CO_2 or H_2S to form acid adducts that can cause internal corrosion. (92)

Another example of internal corrosion is represented by the hazardous liquid transporting pipes. Hazardous liquids can consist of corrosive liquids or liquids containing corrosive contaminants. Corrosive contaminants react where electrolytes or solids drop out and wet the surface or provide a place for electrolytes to collect. Figure 2 shows a picture of a pipe damaged by internal corrosion.

Figure 2 - Pipes damaged by internal corrosion (Source: Mihir S. archive).

Common approaches applied to prevent internal corrosion of pipes are (93)(94)(96):

a) ***Dehydration***: is the most used strategy to prevent internal corrosion of gas pipes. The method consists of removing free water from the gas stream using a device to chemically scrub the gas stream by eliminating moisture and decreasing the gas dew point. Even physical approaches can be used, such as applying cyclone separators. However, applying these approaches to reduce the gas stream dew point is impossible. Thus, the chemical scrub is periodically applied too. The method is very effective. However, there is always the potential to introduce water into a gas pipeline. Thus, the issue is partially erased. Dehydration is also applied to liquid pipes

transporting crude oil. Water is removed from crude oil by gravity separation or by using the salt dryer. However, because the systems are not reliable or practical, there is always the possibility of introducing water or other corrosive contaminants into the pipeline.
b) ***Inhibitors***: This approach uses chemical substances that can be absorbed onto or react with the metal surface, forming a protective layer or with the corrosive agent, creating a less corrosive species. Several substances are available for this purpose. However, selecting the right one depends on the nature of the liquid transported into the pipeline, corrosive agents, cost, availability, toxicity, and environmental risks. (97)
c) ***Protective coatings***: This approach involves applying a protective coating layer onto the pipe's internal layer. The coating layer can provide a smooth surface, reducing drag and improving the flow of the transported fluid. However, the uniform application of the coating onto the internal wall of the pipe is complex. It requires knowledge of the physical features of the coating, such as viscosity and drying time. For a successful coating application, a device able to uniformly spray the coating onto the internal cylindrical surface and dry the coating, avoiding the formation of defective spots on the coating layer, is pivotal. (98)(99)
d) ***Buffering:*** This method adds buffering agents to the fluids remaining in the pipes, raising their pH above seven. However, this approach is often ineffective because covering the entire pipe surface is difficult.
e) ***Cleaning pigs***: This method consists of using pigs to scour the internal surface of the pipelines. The choice of which type of pigs to use depends on the product carried by the pipe and the contaminant to be removed. Cleaning pigs can effectively direct both liquids and corrosive solids to pig traps for removal from the pipeline. It has been shown that even the build-up of solids can start internal corrosion since solids can entrap corrosive or low pH liquids into the solids agglomerate. The effectiveness of this approach depends on pigging velocity to scour the entire pipeline, pigging distance, and characteristics of the material targeted by the pig run.
f) ***Biocides***: This method can prevent corrosion due to bacteria's corrosive actions. Biocides are injected into the pipeline in the stream of a non-electrolyte carrier. An active agent can also form a passive barrier at the pipe surface. Many of these agents are very expensive, and depending on the gas flow, they may miss the location where the microbes are trapped.

All these strategies can help protect pipelines' internal walls from corrosion. However, due to the geometrical features of the pipes targeted in this research project and the complexity of the plants of which they can be a part, the approach to avoiding internal corrosion investigated during this study has been the application of protective coatings. Efforts have been spent developing a UV-curable protective coating to make this corrosion protection strategy more effective and greener.

Corrosion protection of the internal surfaces of steel pipes is critical, especially in industries such as oil and gas, water distribution, chemical processing, and energy. The internal environment of pipes often involves contact with aggressive substances, such as seawater, chemicals, hydrocarbons, or gases, which accelerate corrosion. The state-of-the-art methods to protect the inner surfaces of steel pipes include coatings, linings, corrosion inhibitors, cathodic protection, and advancements in smart materials. Here is a breakdown of the leading literature concerning corrosion protection of inner steel pipes:

2.4 Protective System for Inner Pipe

Many steel protection systems have been analyzed and implemented to safeguard pipelines' internal surfaces from corrosive agents. The literature presents various challenges and solutions that depend on the type of fluid being transported and the preferred technologies within the specific application area.

Three approaches to this issue are mainly used: applying a barrier between steel and fluid using a coating, inhibiting corrosion with an additive to the fluid, or creating a nonaggressive environment by cathodic protection. Hereafter, we will discuss these main approaches and their variants.

Protective coatings:

- Epoxy-based Coatings are widely used for internal pipe surfaces due to their excellent chemical resistance, adhesion, and durability. Modified epoxy coatings with additives (such as glass or ceramic particles) improve performance under severe conditions, such as high temperatures or aggressive chemical environments. (108) (109)

- Fusion-bonded epoxy (FBE) is often applied to the internal surfaces of pipelines, especially in the oil and gas industry. It provides strong corrosion resistance, especially in pipes transporting hydrocarbons, water, or aggressive chemicals. (110) (111)
- Polyurethane coatings are used for internal protection in water and wastewater pipelines. They offer flexibility, abrasion resistance, and protection against corrosive fluids, and they are instrumental in municipal water supply systems. (112)
- Cement Mortar Linings are widely used in water supply pipes to protect steel from corrosion caused by water. They act as a physical barrier and help neutralize acidic water conditions. (113) (114)

Corrosion Inhibitors:

- Corrosion inhibitors are chemicals added to the fluid inside the pipe to prevent or slow down corrosion. Organic inhibitors (amines, fatty acids) and inorganic inhibitors (chromates, phosphates) are commonly used for internal corrosion protection. Recent research focuses on developing green inhibitors, which are eco-friendly and derived from plant extracts or natural sources (115). Corrosion inhibitors are essential in oil and gas pipelines, where they prevent internal corrosion caused by CO_2, H_2S, and other aggressive components. Studies focus on optimizing inhibitor formulations and improving their efficiency in multiphase flow conditions (116) (117).

Cathodic Protection:

- Although Impressed Current Cathodic Protection (ICCP) is more commonly applied to external surfaces, it can also be adapted for internal corrosion protection, especially in large-diameter pipelines. This is especially relevant in systems that cannot effectively use coatings or inhibitors. (118)
- Sacrificial Anodes of zinc, magnesium, or aluminum can be installed inside pipelines to provide localized cathodic protection. This method is commonly used in pipelines carrying water or brine.

Emerging technologies and research directions are shaping the future of corrosion protection for internal steel pipe surfaces across various industries. Among these technologies, the following advanced coatings are particularly promising:

- Nanocomposite Coatings using nanoparticles (e.g., graphene, silica, or carbon nanotubes) in internal coatings enhance corrosion resistance, mechanical strength, and durability. These nanocomposite coatings are particularly promising in pipelines exposed to aggressive chemicals or high pressures. (119) (120)
- Self-healing coatings are an emerging technology that can automatically repair minor cracks or damages in the coating, thus preventing corrosion initiation on the exposed steel. These coatings have been studied for internal and external pipeline protection applications. (121) (122)

Smart coatings and real-time monitoring technologies are becoming increasingly integrated into pipeline maintenance, offering proactive rather than reactive solutions. Hybrid systems combining coatings, inhibitors, and cathodic protection are often used in extreme environments to maximize corrosion resistance.

International standards for internal corrosion protection provide guidelines for selecting and applying coatings, inhibitors, and other protection methods. These standards also include best practices for monitoring and maintaining the internal surfaces of steel pipelines, such as NACE SP0208-2008, “Standard practice for the application of coatings for corrosion control on internal surfaces of water pipelines,” and ISO 15741, “Paints and varnishes – Wetting balances and their use for assessing internal corrosion protection of pipelines.”

2.5 Corrosion-protective Organic Coatings

Organic coatings are the most widely applied method for corrosion protection of metallic materials and infrastructures. (22) A protective organic coating consists of various discontinuous solid functional additives, commonly called pigments, contained within a continuous polymeric phase known as the binder. The pigments and the binder contribute to defining the functionality of the protective organic coating. The pigments create a barrier that hinders the percolation of water and other environmentally corrosive substances through the coating film, preventing corrosion. At the same time, the binder contributes to the adhesion of the coating to the substrate. The heterogeneity of the binder structure has an essential role in creating a tortuous

percolating pathway for water and ionic species ingress due to variations in the network crosslink density across the 3D polymer volume.

Protective coatings generally provide a barrier between the substrate and the environment, ideally providing high resistance to ionic movement. (22)

Due to the high intrinsic complexity of the coatings, it is presumed that their excellent performances are due to better adhesion to the metallic substrate, directly or via an undercoat or primer. At the same time, the failure of the coating and the corrosion occurring could be ascribed to a) coating intrinsic defects, b) damage accumulated in service, or c) surface contamination under the coating.

However, the role of coating and substrate heterogeneity in the coating performances must be clearly defined. Thus, several studies have been carried out.

A preliminary study by Mayne et al. demonstrated that an unfilled lacquer such as polystyrene 25 µm thick onto a rust–free steel plate allowed the migration of ions. A red-brown deposit was observed on the surface of the lacquer. The red-brown residue on the surface suggested that Fe^{2+} ions had migrated from the substrate into the polymer. The growth of the deposit indicated that oxygen and water migrated from the electrolyte into the polymer. Mayne et al. reported that the typical corrosion rate of steel of 70 mg cm^{-2} y^{-1} required 11 mg cm^{-2} y^{-1} of water and 30 mg cm^{-2} y^{-1} of oxygen. These permeation rates were easily achieved in many unfilled polymeric coatings. (22) (23) Appropriately filled coatings with lamellar fillers can retard the movement of water and other species. Deflorian et al. reported a reduction of 80% of the oxygen diffusion rate and 88% of the water diffusion rate for nano–clay composite coatings compared with unfilled epoxy coatings. (22) (24)

Self–evidence and studies have reported that the protective organic coatings' resistance to corrosion decreased over time due to environmental factors. According to Nguyen's hypothesis, water uptake by the coatings was non–uniform and concentrated in low molecular weight regions characterized by low cross-linking density. During the service, the low molecular weight regions of the coatings grew until they became wide enough to give rise to a percolating network. (25)

Indeed, Mayne and coworker, in a preliminary study, highlighted the existence of regions characterized by different conductivities by immersing the films of linseed oil pentaerythritol alkyd, tung oil phenol-formaldehyde, and epoxy-polyamide into an electrolyte solution for a short time of around ten minutes. (22) In particular, they found centimeter scale regions characterized by conductivities proportional to the solution conductivity, called the D–areas (ex., low molecular weight regions), having low resistance within the range 10^{6} – 10^{8} Ωcm^{-2}, and centimeter scale regions characterized by low conductivity, inversely proportional to the solution conductivity named I–areas, characterized by resistance higher in the range of 10^{9} – 10^{11} Ωcm^{-2}. Thus, the film can be defined as a percentage of D–areas and I–areas. Water uptake into the film was believed to control the "I" type conduction, whereas ion uptake controlled "D" type conduction. (22) (26) (27)

Later, Jamali and Mills confirmed Maine's findings by studying the electrical properties of the coatings using a wire beam electrode with a millimeter spatial resolution. They concluded that most of the film's area was made of I – areas. (22) (28)

These findings were consistent with the delay period observed before the total failure of a protective organic coating. Electrochemical Impedance spectroscopy (EIS) analysis performed on coatings immersed for a long time in the electrolyte solution demonstrated that the resistance of the coating can decrease from values of 10^{9} – 10^{11} Ωcm^{-2} to 10^{6} – 10^{8} Ωcm^{-2} over time, supporting the growth of the size of D – areas, with depletion of the wideness of the I – type areas. (29)

Recently, surface analysis such as sub-diffraction limit infra-red analysis using atomic force microscopy has permitted imaging at the nanometer scale, allowing the successful study of the coatings' nanostructures. Such works have demonstrated that the water uptake process inside epoxy–phenolic coatings was characterized by a very heterogeneous mechanism, strictly correlated to the coating areas where the polymer showed low cross-linking density. Thus confirming a chemically and physically heterogeneous nanostructure. (30) (31) (32)

Despite Funke and coworkers' great emphasis on the importance of high wet adhesion of the coatings on the metal substrate to achieve good performance (33) (34), experimental evidence achieved by cathodic disbonding has supported Mayne and Nguyen's hypothesis. They claimed that ionic migration and development of the percolating pathways appeared independently of good adhesion. Thus, good adhesion is necessary, but more is needed for good coating performance.

Lyon et al. reported that applying an epoxy coating to a substrate pretreated with 3–3-glycidol propyl silane, an adhesion promoter, has increased wet adhesion and improved resistance to cathodic disbonding. Similarly, pretreating with 3–3-aminopropyl silane, a metal plate coated with an alkyd coating, caused an increase in wet adhesion, but no such improvement to the cathodic disbonding resistance was observed. (35) Cathodic disbonding is a chemical effect controlled by interface and binder chemistry.

More than coating adhesion, the quality of the surface to treat appears more essential to increase the service life of the organic coatings. To improve surface quality, a treatment may be applied to the substrate to provide a consistent surface free of contamination and deleterious phases. Surface preparation influences the coatings' heterogeneity nanostructure. (36) (37) Using mechanical removal of oxide, salt contaminants, and other debris, the metal surface may be chemically reacted to produce a more protective or more consistent salt layer as a "conversion coating." (38)

3 The Problem

Corrosion: A Pervasive Threat and the Quest for Sustainable Solutions

Corrosion, the gradual deterioration of materials due to chemical or electrochemical reactions with their surroundings, poses a significant threat to infrastructure, machinery, and industrial equipment. The oil and gas industry faces the constant challenge of protecting its vast network of pipelines, tanks, and storage facilities from corrosion's destructive effects. (39) (40)

Traditionally, applying paints and coatings has been the primary method of corrosion mitigation. These coatings act as a protective barrier, shielding the underlying metal from the environment's corrosive elements. However, using conventional solvent-based coatings has raised concerns about their environmental impact.

The Environmental Footprint of Solvent-Based Coatings

The production and application of solvent-based coatings lead to the release of volatile organic compounds (VOCs) and hazardous air pollutants (HAPs). These compounds contribute to air pollution, posing health risks to workers and the surrounding communities. Additionally, the energy consumption associated with solvent evaporation and drying processes further exacerbates environmental impact. (41) (42)

There is a growing interest in developing sustainable and eco-friendly solutions to address corrosion challenges and the environmental concerns associated with traditional corrosion protection methods. Several approaches are being explored to achieve adequate corrosion protection while minimizing the negative impact on the environment. Some of these include:

- **Green Coatings and Inhibitors:** Researchers focus on developing environmentally friendly coatings and corrosion inhibitors. Water-based coatings, powder coatings, and other eco-friendly alternatives to solvent-based coatings are being investigated. Naturally derived corrosion inhibitors, such as plant extracts and bio-based compounds, are also gaining attention.
- **Nanostructured Materials:** Nanostructured materials, such as nanoparticles and nanocomposites, show promise in providing enhanced corrosion protection. These materials can be incorporated into coatings to improve their barrier properties and resistance to corrosion. Nano-scale additives can offer better coverage and adhesion, providing more durable and adequate corrosion protection.
- **Electrochemical Protection:** Cathodic protection and impressed current systems are electrochemical methods employed to mitigate corrosion. These techniques involve applying an electric current to the metal structure, which helps to counteract the electrochemical processes responsible for corrosion. These methods can be more sustainable than traditional approaches.
- **Self-healing Materials:** Self-healing materials are designed to repair damage autonomously, reducing the need for frequent maintenance and reapplication of coatings. Incorporating microcapsules containing corrosion inhibitors or other healing agents into coatings allows for releasing these agents when damage occurs, promoting self-repair.
- **Biodegradable Materials:** Developing biodegradable materials for corrosion protection is gaining traction. These materials break down naturally over time, reducing the environmental impact of coating degradation and disposal.
- **Advanced Surface Treatments:** Innovative surface treatments, such as plasma coatings and ion implantation, are being explored to enhance materials' corrosion resistance. These techniques modify the surface properties at the atomic or molecular level, providing improved protection against corrosive environments.
- **Corrosion Monitoring and Predictive Maintenance:** Implementing advanced corrosion monitoring systems and predictive maintenance strategies can help identify and address corrosion issues before significant damage occurs. This approach enhances safety and reduces the need for frequent and extensive maintenance, contributing to sustainability.

The quest for sustainable corrosion solutions involves a multidisciplinary approach, combining materials science, chemistry, engineering, and environmental science. As industries prioritize sustainability, ongoing research and development efforts aim to create corrosion protection methods that balance effectiveness, longevity, and minimal environmental impact.

4 The Proposed Approach

4.1 UV-curable Steel Protective Coatings

4.1.1 Thermal Curing vs. Radiation Curing

During the last few years, the numerous provisions for protecting the environment and health have intensified the research of new anticorrosive coatings for heavy industries with lower environmental impact, such as water-based, high solids, or powder coatings. However, solvent-based coatings remain dominant, even if they cause emissions of hazardous air pollutants (HAPs) and toxic volatile organic compounds (VOCs) into the environment. (43) (44)

Thermal curing coatings are currently used to protect metal materials and infrastructures. They usually need a long-term or high-temperature application for the cross-linking reaction to be successful. Most thermal curing coatings used for corrosion protection for metal materials are epoxy resin-based. Epoxy resin-based coatings can ensure high solvents and strong acid resistance and improve mechanical properties. They can be classified as liquid and powder coatings. Liquid coatings, in turn, may differ by the nature of the diluent: a) solvent-borne, with organic solvents; b) waterborne when diluted in water; c) or solvent-free, without diluent in the formulation, and for this reason, with zero VOC emissions. The cross-linking reaction of solvent-based coatings requires a long reaction time, even seven days, if carried out at room temperature, affecting production time and sometimes quality. If the crosslinking reaction occurs in the oven at high temperatures (even 150 ˚C), the production time is reduced to a few hours. Still, it involves a significant expenditure of energy. (43) (45)

Despite promulgating new restrictive laws for emissions into the atmosphere, solvent-borne coatings are still the most widely used. A greener choice to avoid VOC and HAP emissions can be represented by applying powder coatings, which are also widely used. However, even these coatings require high temperatures for polymerization, ranging between 160 ˚C and 200 ˚C, and reaction time is in the order of hours. Therefore, these coatings require long reaction times and high temperatures for polymerization and cannot be easily used in the field. (44)

The introduction of UV-curable coatings represents a solution to the drawbacks of thermal curing coatings. UV curable coatings crosslink by irradiation with ultraviolet (UV) radiation in minutes, without applying temperatures. This technology also stood out because it is efficient, enabling technology, economical, energy-saving, and environmentally friendly. (44) (46)

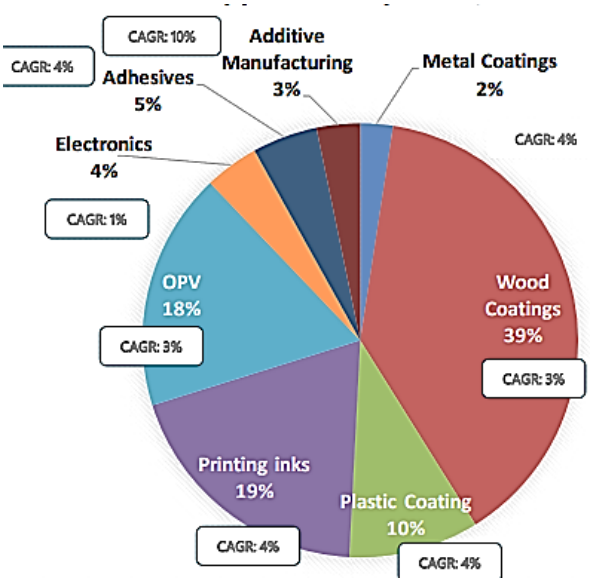

Figure 3 - UV technology market during 2019 (Source: Radtech)

UV-curable coating technology has been applied in graphic art, food, automotive, and medical fields, as well as the coating of wooden floors and furnishings. (44)

Anticorrosive coatings for heavy industry represent a new frontier to be explored. In 2019, only 2 % of the UV technology market was addressed to the metal protection field application. (47) Above is a representative plot of the UV technology market during 2019 (Figure 3).

In the end, UV technology can be easily used in production sites as in the field, and this is due to a) reaction times of the order of minutes, b) no VOC and HAP emissions, c) UV-curing production lines that do not require lots of space and are very simple to resize. (44)

4.1.2 The UV Curing Mechanism

As reported above, UV coatings technology presents several advantages (100), the most important are the following: a) low capital cost (UV lamps instead of oven or furnace); b) shallow energy requirement for cross linking at room temperature (Figure 4); c) reduced solvent emission and d) protection against corrosion. (104)

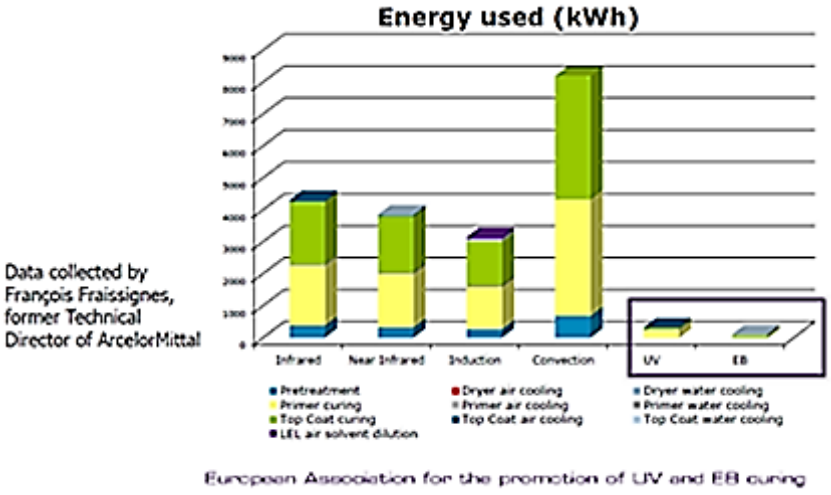

Figure 4 - Shallow energy requirement for cross linking at room temperature

A UV-curable coating consists of a) multifunctional oligomers, b) reactive diluent (reactive monomers), and c) photoinitiators (PI) (101).

Due to their high functionality, multifunctional oligomers provide a high degree of crosslinking to the coatings (102). The most used oligomers are acrylates and methacrylate, in particular:

a) epoxy, urethane, polyether, and polyester – full acrylate.

b) epoxy, urethane – methacrylate.

c) oligo amines and co–resins, which are specialties.

The molecular weight of these groups of oligomers is within 450 – 5000. Reactivity and flexibility depend on these weights and the inherent concentration of double bonds. The higher the molecular weight, the lower the reactivity, coupled with increasing viscosity and flexibility. The more double bonds, the higher the reactivity.

The reactive diluent has a double role: a) it acts as a thinner, controlling the rheology of the coating and reacting with the photoinitiators, forming the polymeric matrix and promoting the successful occurrence of cross-linking. Most have a low molecular weight and one or more functional acrylate groups—the more doubled linkage by the same molecular weight, the better the film's reactivity and hardness. (105)

The photoinitiator molecules can undergo electronic excitation after radiation absorption, which generates initiating species (106). Depending on their chemical nature, the photoinitiators can trigger free radicals or cations, initiating chain growth polymerization (103). Thus, two curing mechanisms can be distinguished: a) the radical mechanisms and b) the cationic mechanism (107).

During this research project, both mechanisms were investigated; the cationic mechanism was investigated in preliminary studies before finding the optimal UV-curable coating formulation, which was reported later based on radical mechanism polymerization.

The radical mechanism starts from the photogeneration, by UV irradiation, of a radical that initiates the crosslinking by adding to vinyl double bonds. Figure 5 below reports a general scheme of the radical polymerization mechanism.

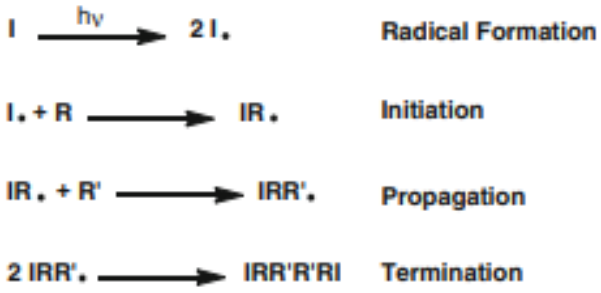

Figure 5 - Scheme of the radical polymerization mechanism

Depending on the photo cleavage mechanism the photoinitiator undergoes, two radical mechanisms can be distinguished:
a) If the photoinitiator is type I (or first class) PI, it undergoes a homolytic cleavage, generating two radical fragments of the original photoinitiator. These radicals then initiate polymerization. The Type I PI is irreversibly incorporated into the polymer matrix. Below, in Figure 6, a type I PI example cleavage reaction is reported.

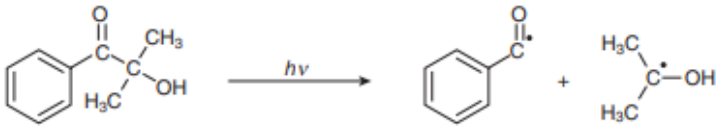

Figure 6 - type I PI example cleavage reaction

b) If the photoinitiator behaves as a type II (or second class) PI, upon UV irradiation, it generates a biradical species that reacts, abstracting a hydrogen atom from a hydrogen donor (usually amines) and forming two radicals. These radicals, like the Type I photoinitiators, can initiate the polymerization reaction. Type II PI is typically not incorporated during the reaction, while the hydrogen donor deriving radical is. Below, in Figure 7, an example of the cleavage reaction of a

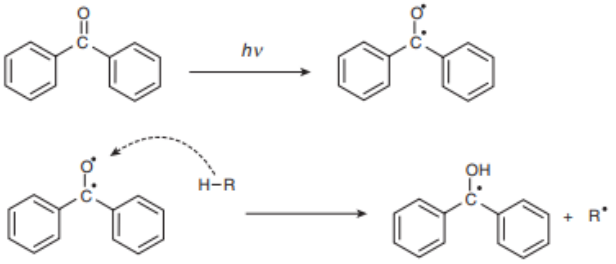

Figure 7 - type II PI example cleavage reaction

type II PI is reported.

The UV curing cationic mechanism is based on the growth of the cationic chain process. Figure 8 below reports the general mechanism of cationic polymerization of an epoxide monomer.

A strong acid is formed when the photoinitiator is irradiated by UV light. The strong acid generated, a Lewis acid or a Brönsted acid, initiates polymerization. Generally, the cationic

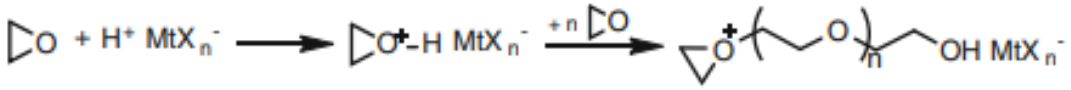

Figure 8 - mechanism of cationic polymerization mechanism of an epoxide monomer

photoinitiator comprises onium salts of strong acids. Mainly, iodonium and sulfonium salts are employed as cationic photoinitiators. When irradiating these salts with UV light, they undergo homolytic bondage cleavage, like Type I photoinitiators. The formed radicals react with a proton donor to a Brønsted or Lewis acid. The generated acid then initiates polymerization. Below, Figure 9 depicts the mechanism reaction.

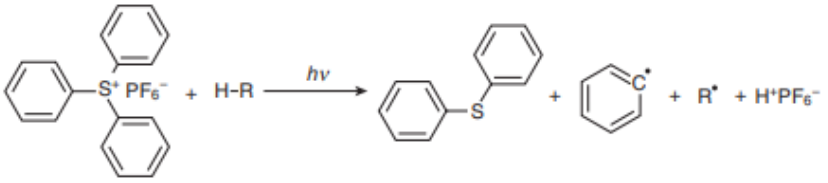

Figure 9 - mechanism of reaction of the polymerization by the generated acid

The chemical nature of the photoinitiator and the oligomer is pivotal in designing a UV-curable coating because the crosslinking rate depends on the oligomer's character and the photoinitiator's effectiveness.

4.1.3 Steel Protection Using UV Coating.

UV technology coatings are widely used for decoration and protection in many industries. (44)

UV technology is not only environmentally friendly, as previously reported, but it is also a faster cure, increases production speed, and improves process efficiency, source reductions, and sustainability. Faster drying under UV lamps avoids using the oven and hinders curing plants, corresponding to energy cost savings and little production infrastructure. UV technology can provide a healthier work environment because UV-curable coatings formulation does not contain flammable solvents.

Due to the large dimensions of a gas-mercury lamp, UV technology has never been introduced to coat inner pipes. In recent years, compact UV-LED sources have overcome the problem of presenting a compact UV source inside narrow spaces. However, many issues remain unsolved, such as optimizing the irradiation inside a space, the barrier of fillers in the paint, and the limited wavelength range of UV LEDs.

Despite the limited diffusion of this technology in the anti-corrosion field, UV technology can provide high-performance protection to metal surfaces such as steel and high-strength aluminum alloys in industrial and aerospace applications. UV-curable coatings can provide toughness, solvent resistance, and abrasion resistance.

Moreover, UV technology can be easily used in production sites as in the field, and this is due to a) reaction times of the order of minutes, b) no VOC emissions, c) UV-curing production lines that do not require extensive manufacturing space and are very simple to resize.

UV technology application in the corrosion protection field still needs to be widely applied due to prejudices about the technical value of the UV curable coatings, even if, by formulation with urethane acrylates and chromium-free corrosion inhibitors, high-performance corrosion protection has been demonstrated with solvent-free UV Below is a summarizing table of a comparison study between UV curing coating corrosion performance and thermal curing coating corrosion performance.

As reported in Table 1 above, accelerated corrosion testing on steel has shown, after 672 hours of ASTM D117 salt fog testing, that superior corrosion resistance can be obtained with high-performance UV coatings compared to conventional epoxy and urethane corrosion resistance coating with much higher thicknesses. UV cure was complete within seconds, and improved performances were obtained using 100 % solids UV technology with significantly lower material usage and coating weight than conventional coatings. Applying a UV coating topcoat can also improve the corrosion resistance performance of thermal curing coatings. (44)

Table 1 - Corrosion resistance ranking based on ASTM D 1654 ratings of scribed steel panels after 672 hours of ASTM D117 salt fog testing (from RADTECH REPORT FALL 2011)

Corrosion resistance rankings for high-performance coating systems				
Coating layer description	Layer wet mils	Total wet mils	Total dry mils	Corrosion resistance ranking
UV topcoat UV Primer	2 2	4	4	1 = Best
Epoxy	22	22	16	2
UV coating	2	2	2	3
Urethane Epoxy	5 10	15	10	4
Epoxy	14	14	10	5
Urethane	10	10	6	6
Urethane	3	3	2	7 = Worst

O'Keefe et al. have also demonstrated the suitability of UV coating technology for high-performance corrosion protection of high-strength aluminum alloys for aerospace applications. Multifunctional UV (MUV) curable pigmented coatings have been developed to replace the strontium chromate epoxy primer and isocyanate-containing polyurethane topcoat for aerospace applications. (48)

MUV coatings have demonstrated excellent corrosion protection for aluminum alloys, even when applied to different treated surfaces. Their performances have also satisfied the requirements of aerospace primer specification MIL—PRF—23377 and aerospace topcoat specification MIL—PRF—85285, including low-gloss camouflage appearance, good adhesion, hardness, solvent resistance, and ASTM B—117 salt fog testing. 2024 – T3 aluminum alloy panels underwent 3000 hours of salt fog testing and remain shiny.

As scientific literature has reported, UV technology's versatility extends to its ease of involvement in designing intelligent anti-corrosion coatings.

Zhang et al. have demonstrated that UV curing technology can be easily applied to self-healing coatings for anticorrosion. They provided a simple way to achieve self-healing UV curable waterborne polyurethane (WPU) coatings that conform to the development trend of high-performance and environmentally friendly anticorrosive coatings. Disulfide groups were introduced into the polyurethane chain as critical components for the self-healing properties using polysulfide as chain extenders. Then, vinyl and thiol groups were introduced into the end of the polyurethane chain and UV-cured. As revealed by corrosion and electrochemical tests, disulfide bonds showed repeated crack remendability. The study of thermal stability, hardness, and adhesion force of the disulfide-modified WPU coatings indicated that introducing a suitable proportion of polysulfide can improve the comprehensive performance. Since the raw materials used are all commercially available, the UV-curable WPU coatings are hoped to be applied to metal anti-corrosion. (49)

Jafarzadeh et al. reported successfully introducing a conducting polymer into polyester acrylate resin to apply to galvanized steel and UV cured. They used a polyaniline (PANI) synthesized by chemical oxidative polymerization using sulphonic methane acid (Mesa) as a dopant and ammonium peroxydisulfate as the oxidizer. The PANI-Mesa conducting polymer was used as an active corrosion inhibitor as an alternative to hazardous phosphate–chromium surface treatments, minimizing health risks and environmental damage. This study has highlighted the advantages of conducting polymers containing coatings concerning conventional barrier coatings, where minor defects may lead to quick system failure. The achievement of the successful introduction of conducting polymers in the UV curable coatings technology is one step forward in long-term corrosion protection of metallic structures by providing active protection with a thin one-layer system, non-toxic surface treatment, and environmentally friendly solvent-free coating thanks to UV technology. (50)

Rahman et al. reported a nano ferrite dispersed waterborne epoxy-acrylate resin as a nanocomposite anticorrosive coating. They proved that the successful dispersion of nano ferrite particles into the resin provided an intimate interaction between them, improving the mechanical properties of the coating, which was evident from the higher values of scratch hardness, bend

test, and impact test. Polarization and EIS measurements have shown that the coating, as obtained, can successfully inhibit the deterioration of the metal substrate in different corrosive media through barrier action. This is further confirmed by the decrease in their corrosion current density and corrosion rate, besides shifting corrosion potentials to the more noble direction. (51)

4.1.4 UV Curing Protective Coating: Cationic and Radical Reaction.

However, the UV light source selection depends on the PI selected because the effective activation of the PI occurs if there is a considerable overlap of its UV absorption spectrum with the emission spectrum of the light source. (52)

UV curing can occur through two different mechanisms: a) cationic mechanism and b) radical mechanism. The UV curing cationic mechanism is based on the growth of the cationic chain process. A strong acid is formed when the PI is irradiated by UV light. The strong acid generated, a Lewis acid or a Brönsted acid, initiates the polymerization. The radical mechanism starts from the photogeneration, by UV irradiation, of a radical that begins the crosslinking by adding to vinyl double bonds. The general scheme of both mechanisms is reported above in Figures 5 and 8.

The cationic reaction can ensure better performance and cure widely used epoxy-based resins such as diglycidyl ether of bisphenol A and branched resins, as commonly reported in the literature. (53) (54) The possibility of curing a highly functionalized epoxy novolac resin was exciting.

The cationic reaction is better and naturally activated at UVC wavelengths such as 330-350 nm.

The UV-curable coating reported here has been developed in cooperation with the Polytechnic of Turin chemical team. They have defined the formulation of the paint and the parameters of the curing process, such as a) the kind of reaction, radical, or cationic; b) the UV wavelength, irradiance, and dose; c) environment conditions like temperature, air, humidity, and similar, and d) the surface to be coated conditions like roughness, temperature, and cleanliness.

Scientific literature reports several studies about novel protective coating for metal structures based on UV-curable coatings. However, only a few studies about filled coatings have been reported in the literature, such as the study by Deflorian et al. about the improvement of UV coatings' corrosion protection using montmorillonite nanoparticles. Using EIS, they analyzed the corrosion behavior of three different UV coatings: a) UV-curable waterborne urethane acrylic coatings, b) modified montmorillonite nanoparticles in UV-cured epoxy coatings, and a c) a combination of the sol-gel route with UV curable moieties in urethane acrylic coatings. Through their analysis, they found that nanoparticles dramatically affected the corrosion protection properties of the UV-cured coatings. The best corrosion results were obtained using functionalized montmorillonite nanoparticles. (46)

Thus, to evaluate the protective performance of the UV-coating designed and developed during this study, two different benchmarks have been taken as reference: a) NG paint to evaluate the corrosion performance of the UV-coating for oil & gas application and b) the latest study of Sangermano et al. to evaluate the electrochemical performance of the multifunctional oligomers and PI blend selected for the corrosion application. (55) They have applied UV-curable epoxidized vegetable oils (EVOs) as an anti-corrosion coating, and the protective properties have been investigated. They characterized the corrosion protection effectiveness of the coatings by potentiodynamic polarization and electrochemical impedance spectroscopy measurements. They found that the coating may delay the diffusion of water molecules and other species through the coating, resulting in an improved barrier effect against the corrosive medium.

4.1.5 The Use of Inorganic Fillers.

It is found that the introduction of inorganic fillers can improve the corrosion properties of UV-curable coatings. (46)

An example is the montmorillonite nanoparticles that can provide remarkable barrier properties to gases and moisture and excellent resistance to staining to the containing UV-cured coatings. (56)

They even thought it was possible to get good results by designing properly functionalized pigments using the sol-gel route. The sol-gel method to form inorganic domains directly into the polymeric matrix in situ was investigated. They found it very promising because it allowed them to design the pigments' dimensions, reactivity, and functionalization by choosing the metal

alkoxide precursors. They even found auspicious results by preparing functionalized nanoparticles separately from the UV-curable matrix using the sol-gel method and subsequent dispersion of the preformed particles in the polymeric paste. Using this last approach, they could functionalize pigment nanoparticles formed before the distribution in the polymeric matrix, having better control of the sol-gel process and, thus, of the final properties of the performed particles. (46)

4.1.6 Hydrophobic Properties of UV Coating

UV technology has even been applied to develop biomimetic superhydrophobic non-polymeric surfaces for advanced anticorrosive coatings. Peng et al. reported the preparation of a polymer surface structure directly replicated from a lotus leaf that exhibited the same hydrophobic properties as the original leaf. The surface they created showed both micro- and nanostructures consistent with the lotus leaf and expressed the same superhydrophobic behavior. The surface morphology of as-synthesized epoxy-acrylate coatings was found in many microscaled mastoids, each decorated with many nano-scaled wrinkles. They noted that the water contact angle of coating with biomimetic natural leaf surface was 153°, which was found to be significantly higher than that of the corresponding polymer with a smooth surface, 81°. Electrochemical corrosion protection measurements in saline conditions demonstrated that the superhydrophobic polymeric surface coating provided excellent corrosion protection, good adhesion of the cold rolled steel substrate, and an effective barrier to aggressive species. (57)

4.1.7 Paint Formulation

The primary objective of the Polytechnic of Turin chemical team was to ensure that the UV-curable coating developed would maintain or even improve the performance of the thermal version currently used on the field. Thus, they created a library of resins and PIs blends based on the resin DEN 425, an epoxy novolac manufactured by Dow Chemicals, that gives high chemical and mechanical performance and is already used in other thermal-cured coatings. DEN 425 is the resin used in the NG coating formulation, and it was possible to make it UV-curable by using the cationic curing reaction.

The chemical and physical studies performed using the UV-curable blends based on the resin DEN 425 have demonstrated that a commercially available epoxy novolac resin can be successfully cured with UV radiation through cationic photopolymerization using a mercury vapor lamp.

Despite the exciting results achieved, the mercury vapor lamps cannot be applied to the treatment of small-diameter tubes because they need optical auxiliary systems to bring the light into the pipe to treat, which cannot ensure the required curing irradiance onto the inner surface of the tube. Therefore, the cationic curing mechanism cannot be applied. Thus, the UV-curable coating must be designed considering the weaknesses and the strengths of using the radical mechanism for the curing.

Thus, a new library of blends made with acylated oligomers and PIs has been developed, investigated, and improved to be efficiently cured using 395 nm UV-LED light through the radical curing mechanism. The features of the optimal formulation are reported, and it is named RAD03.

The formulation of RAD03 is confidential and the property of Elixe Srl; therefore, it cannot be disclosed in this thesis. However, the method to achieve it has been described here.

The formulation RAD03 has been obtained by investigating how changing the photoinitiator concentration and the concentration ratio between the functionalized oligomer and reactive diluent affects the coating's mechanical properties.

All coating samples were crosslinked using a flood-type DYMAX mercury lamp with an intensity of about 130 mW/cm^2 and a wavelength between 200 and 400 nm.

4.2 UV-curing Light Source

Generally, the UV curing process of a coating occurs as depicted below in Figure 10.

As expected, the UV light source plays a crucial role in successfully occurring a UV curing

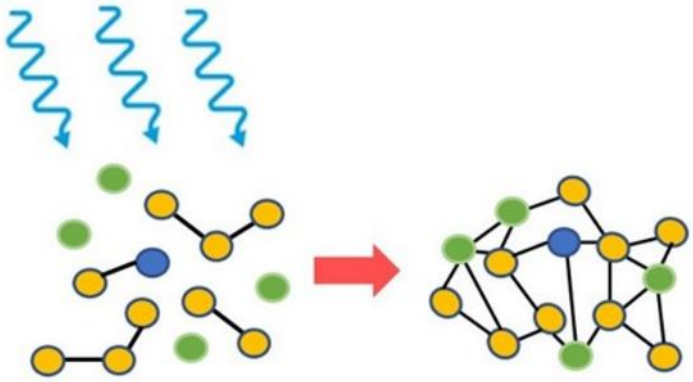

Figure 10 - UV curing process (Source: Excelitas Technolgies)

process because, for the effective activation of the PI, a considerable overlap of its UV absorption spectrum with the emission spectrum of the light source is pivotal. (52) The penetration of the UV light into the coating layer depends on a) the optical thickness of the coating, which determines to what extent irradiance will affect the depth of the cure and adhesion; b) the spectral absorbance of coatings affects which wavelengths can more effectively penetrate and how the irradiance level can achieve the depth of the cure and c) Absorption spectrum of the PI determines the wavelength responsivity. (58) Thus, the proper selection of the UV light system to apply to the studied UV curing process is very important for the correct occurrence of the process.

Two types of UV lamp systems can be used to perform a UV curing technology: a) UV pressure lamp (usually medium pressure) and b) UV light emitting diode (LED) lamps.

Moreover, it is essential to consider the following during the selection of the correct lamp for the designed UV curing process:

a) the thickness of the applied coating because the curing process initiates at the surface, and when polymerization starts, the viscosity of the mixture changes due to the increase of the molecular weight distribution of the oligomers, forming an insoluble network when the gelation point has been reached. This inhibits the curing process, and longer wavelength radiation is necessary for complete curing because it is more penetrating. Indeed, literature has reported that for better UV curing using UV LEDs, applying two wavelengths has been suitable, one in the far UV for the surface initiating curing process and one in the near UV for the deep curing process. (59)

b) optical properties of the resin.

c) the type and the constitution of the PI.

d) filler particles and pigment size.

e) geometry of the surface to be cured.

4.2.1 UV Lamps

UV pressure lamps are polychromatic light sources containing mercury or noble gases. These lamps emit a broad multiple-line spectrum from 200 to 400 nm. These lamps operate at very high temperatures; thus, a significant part of the energy is wasted as heat, which can be ascribed to the reduction of the lamps' lifespan by the bulb's degradation. Moreover, since they emit a broad multiple-line spectrum, the large amount of radiation is only helpful if the PI absorbs these distinct wavelengths. (52) (60) Heat production requires an efficient air-cooled system to avoid undesirable effects during the polymerization reaction, such as even the thermal degradation of the polymer to be cured.

On the other hand, the UV LEDs are monochromatic light sources and can emit at 365 nm, 385 nm, 395 nm, and 405 nm. Thus, the light emitted has a relatively narrow wavelength range, which can be tailored for a particular PI. Since they emit a minimal wavelength range, no infrared radiation is emitted; thus, overheating does not occur, resulting in the long lifetime of the diode

(10,000 – 20,000 hours). Moreover, since the energy consumption is lower than UV pressure lamps, they can be used with a battery power supply. Thus, small mobile devices have been developed and are available on the market. For these reasons, they are also used when UV-curing coatings are applied directly on the field.

The key characteristics of a lamp to consider before being selected for a UV curing process are:

a) The operating power for the tubular lamp is expressed as W/cm. It is the ratio between the electrical power input and the effective length of the bulb, as reported below in Equation 1.

$$Power\ (W/cm) = \frac{electrical\ power\ input}{effctive\ lenght\ of\ the\ bulb} \qquad (1)$$

This parameter cannot provide any information about a) the output efficiency of the lamp, b) the spectral conversion efficiency, and c) the UV irradiance delivered by the work surface.

b) The energy density is expressed as J/cm^2. It is related to the total energy arriving at the coating surface and inversely proportional to the line's speed. In particular, the energy density is proportional to the lamp's power and rows. Below, in Figure 11, a plot relative to the comparison between a lamp 240 W/cm and a lamp 120 W/cm has been reported. The 240 W/cm has a total energy higher than the 120 W/cm lamp. The total energy of both lights decreases by increasing the line speed. This means that given the correct energy density, curing with more power increases the speed of the process.

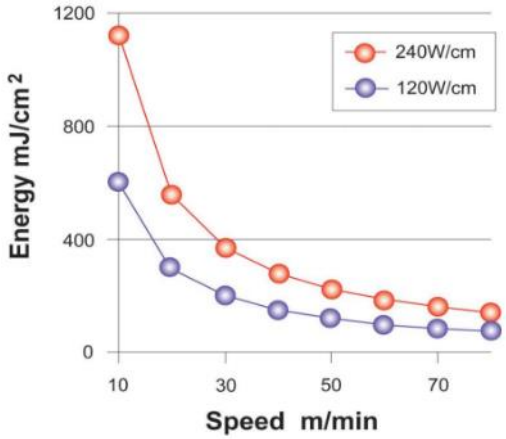

Figure 11 - comparison between a lamp 240 W/cm and a lamp 120 W/cm (Source: Luminus Devices Inc.)

c) The peak irradiance is expressed as W/cm2. It is the radiant power arriving at a surface per unit area. It is related to a) the power of the light at the coating surface, b) it is characteristic of the lamp and the geometry of the reflector, and c) it is independent of the speed. The irradiance at the cure surface decreases quickly as the distance between the source and the cure surface increases. However, research reveals that, in many cases, excessive irradiance can negatively affect or hamper proper curing. Sometimes, reducing the irradiance and providing more energy density can improve the cure for faster line speeds. Since the light source's proximity to the substrate is essential because irradiance decreases with distance, lamp manufacturers usually use optics to manipulate a higher irradiance over a greater distance.

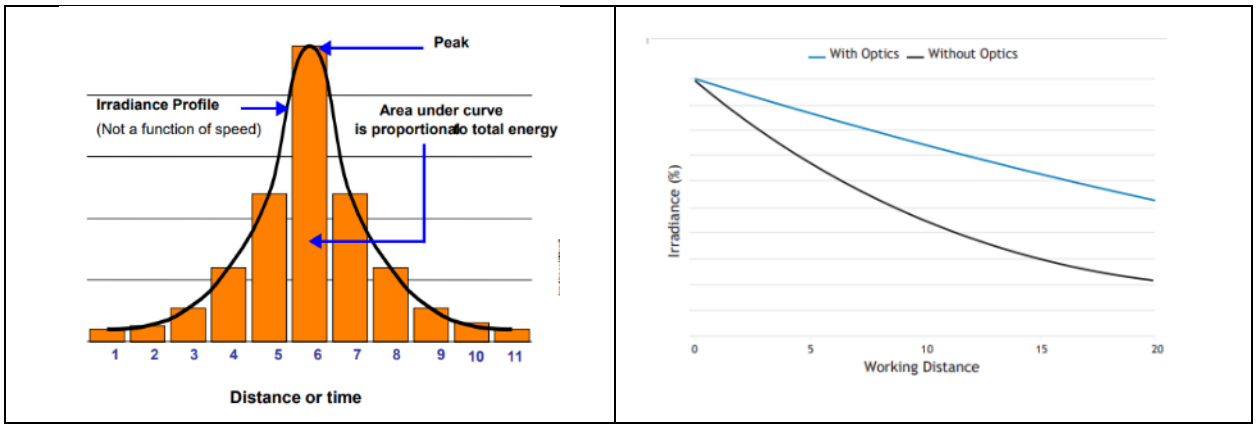

Figure 12 - Peak irradiance and working distance (Source: Luminus Devices Inc.)

d) The bulb's spectral output is consistent with the wavelength distribution. Below, in Figure 13, the emission spectra of a medium-pressure mercury UV lamp and the near-infrared UV – LEDs are reported.

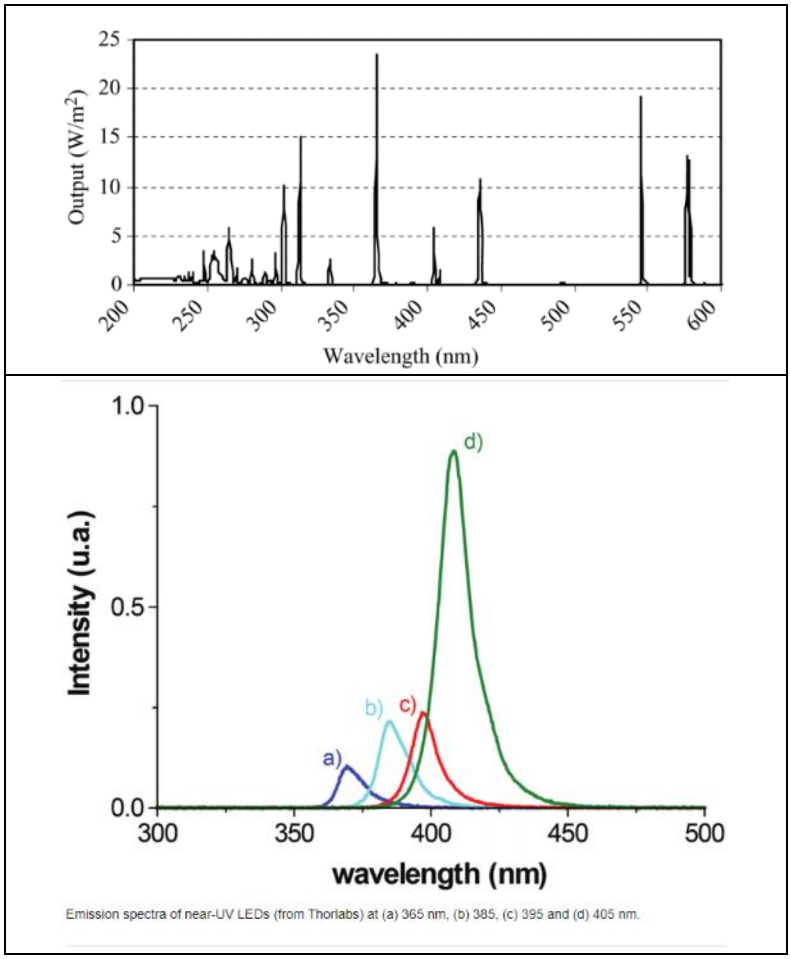

Figure 13 - emission spectra of a medium-pressure mercury UV lamp and the near-infrared UV – LEDs (Source: Luminus Devices Inc.)

4.2.2 UV LED Lamps

Both UV system lamps were used during this research project. However, the medium-pressure mercury lamp was used only during the preliminary study due to its impossibility of UV curing the coatings applied to the inner wall of the pipes, which is the target of the following survey. The research attention moved very fast on using UV LED lamps.

More literature on applying UV LED lamps to cure different systems has reported promising results. Vandervalle et al. compared five LEDs with a halogen lamp applied to cure a micro-filled composite resin. They evaluated the effectiveness of the curing even using different UV light sources–surface to fix distance, ranging from 1 mm to 5 mm. They found that UV LEDs provided similar or even better curing results than the halogen lamp at 5 mm. This study used camphor quinone as PI, having a maximum absorption band at 470 nm. (61)

Neckers et al. compared the effectiveness of a 395 nm UV LED module and a single 5 mm 395 nm UV LED (having the lower output) to an H – bulb and an Xe – lamp for the curing of a polycarbonate coating for wood protection (thickness 100 µm) and a corrosion resistant metal paint (thickness 150 µm). They found that the fastest curing was achieved using the H–bulb. However, the exact double bond conversion was performed from the other light sources within the 20 s, even though 90% of conversion was performed using the Xe – lamp and the UV LED module after 2 s. As expected, the single UV LED converted nearly the same amount of double bonds achieved using the H–bulb lamp after 30 seconds due to the lower irradiance. These results suggested the comparability of the UV LED to the other UV lamps used. The properties of the coatings obtained, like crosshatch adhesion, solvent resistance, gloss, and abrasion resistance, were the same. (62)

This study suggests that UV LEDs are a valid alternative to medium-pressure UV lamps.

4.3 UV Curing Process Inside a Pipe

Curing the inner surface of a pipe is a dynamic process that requires a UV light source moving inside a cylinder, running the entire length while curing the coating. The movement of the UV source can be defined by a linear translation along the cylinder's longitudinal axis and by a rotation around the same axis. To limit possible oscillation during the linear translation and avoid inaccuracies during the curing process, using a source with a 360° circular light can replace an erratic rotational movement and is a preferred solution. The total amount of energy reaching the paint surface must be accurately tailored based on the paint chemistry to fully cure the paint into a coating with the desired mechanical properties. This energy value is generally called energy dose (J/cm^2), the power per surface unit to be applied for a specific time to provide enough energy to cure a liquid film into a hard coating (63). If this value is not reached, the final performance of the polymer will be affected, and it is thus of the utmost importance to accurately measure this value spatially during the curing process.

This study developed a lamp composed of several UV LEDs with a 360° radiation emission pattern to cure a photosensitive coating in difficult-to-reach surfaces such as the inner surface of pipelines. In particular, the light source was designed to fit inside pipes with diameters ranging from 40 to 200 mm, the most common dimensions of pipelines used in the oil and gas industry. The radiation wavelength of 395 nm was selected to crosslink the photocurable coating. To allow optimal photopolymerization in all points of the coating, the irradiance pattern of the lamp was evaluated using software in both the radial and linear coordinates as a function of the LED arrangement and the pipe diameter. Once the optimal LED configuration was selected, it was constructed, and the spatial irradiance was measured to validate the simulated irradiance profile, as described in the experimental phase.

Legros et al. 2015 published a patent reporting their invention of a UV-curable internal resistance reduction coating for steel pipes and application/curing equipment. (29) The equipment, suitable for pipes with ID > 50 cm, consists of two UV lamps mounted onto a rail. The rail was concentrically arranged concerning the pipe, which had already been treated with a UV-curable coating on its inner surface. A bulb and a reflector made the UV lamps. The latter was used to focus the UV rays emitted from the bulb. Since the bulb also generated infrared radiation, air or water was used to cool the lamp to maintain the internal temperature below reasonable values, T< 80 °C. The cooling system avoided excessive heat generation because it may lead to a temperature that had a detrimental effect on the bulb's efficiency and lifetime. In Figure 14, a scheme of the patented equipment is reported below.

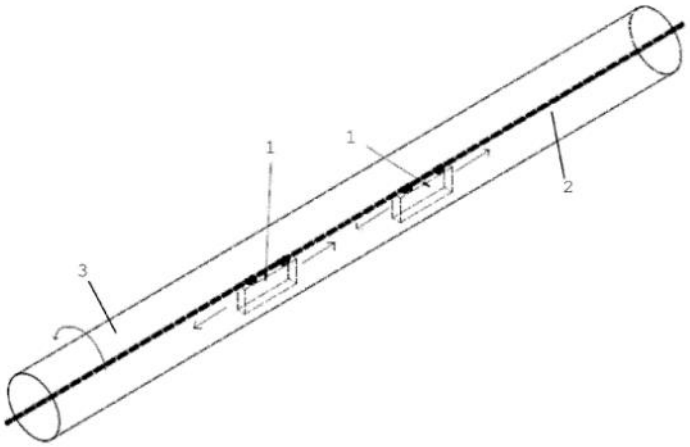

Figure 14 - scheme of the patented equipment (Source: patent)

During the curing, the pipe was rotated around the rail on which the UV lamps were mounted. The lamps were maintained at a given position while the pipe turned. Thus, a portion of the pipe surface corresponding to the length of the lights was cured. After that, the lamps were moved to the next part, and the process was repeated. Once the inner pipe surface was cured, the UV lamps were turned off before being removed from the treated pipe and starting with another. However, this operation was suitable for the operator but detrimental to the lamp's lifetime and curing efficiency due to the time needed to reach total UV irradiance after the light was shut off.

The patent described an alternative if pipes with ID < 50 cm needed to be processed. Since no space was available for a UV lamp made from a bulb and reflector, the rail was fitted with liquid-cooled UV bulbs. These bulbs were made with a double-walled quartz envelope in which water was circulated to avoid excessive heat generation. Since the quartz envelope absorbed some UV radiation, higher-powered UV lamps were needed to achieve efficient curing.

The equipment described in the patent was claimed to be optimal for pipes with an ID of about 100 cm and 12 m long. The inner diameter dimension allowed us to use UV bulbs because a UV–LED application was not claimed.

The equipment described by Legros et al. is the most critical example of a UV-coating curing system used to treat the inner surface of pipes, and it has been used as a benchmark for the design and development of the equipment designed during this research project. As it is known, the target pipes of the study were characterized by an ID < 62 mm. Thus, as anticipated, bulbs were not used to reach the study purposes.

4.3.1 UV LED Radiation Pattern

The irradiance produced by a single LED is defined as the power per unit area incident on the surface to be illuminated by the source, and it is usually expressed as $E = d\Phi/dA$ and measured in W/m^2 (64). The relative intensity of the radiation field around the emission source depends on the viewing angle and, in standard LEDs, is expressed by Lambert's equation:

$$I_\theta = I_0 \cos\theta \qquad (2)$$

I_0 is is the maximum intensity at the surface perpendicular to the LED, and theta is the viewing angle. The spatial distribution of irradiance obtainable with equation (2) represents the radiation pattern, which is specific for every LED. This case study is given in Figure 15.

The irradiance distribution (E_θ) can also be expressed as a cosine function according to:

$$E_\theta = \frac{d\Phi}{dA} = \frac{I_0 \cos\theta}{r^2} \qquad (3)$$

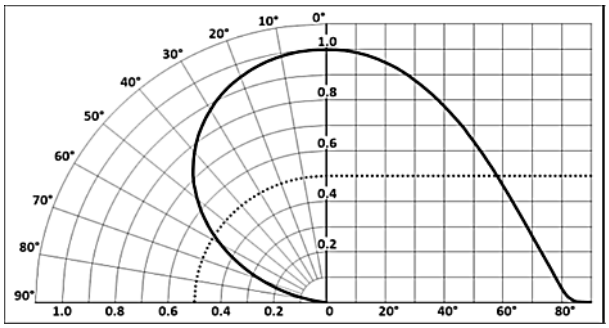

Figure 15 - radiation pattern of a LED
(Source: Luminus Devices Inc.)

Where Φ is the radiometric flux, A is the incident area, and r is the distance between the viewing point and the source (65)

Several mathematical models have been reported describing the resulting radiation pattern in a system with more than one LED (64) (66) (67), but none explain the radiation pattern inside a cylindrical shape. For polymerizing a coating inside a pipe, the radiating source resulting from the LED arrays disposed around the cylindrical support is required to emit light at 360°. The total radiation pattern resulting from combining the single LED radiation patterns in polar and cartesian coordinates referring to the lamp axis must be as homogeneous as possible.

The radiation pattern simulation was performed using the analytical software GNU Octave®. The model developed used the UV LED relative position, viewing angle, radiation pattern, and radiation angle (Figure 15). Two model versions were generated. The first one produced a linear profile on a section parallel to the axis of the cylinder, taking as input the number of lined LEDs (n), their relative distance (step), the inner radius of the cylinder to be irradiated (p_r) and the radius of the lamp body (l_r). The second radial, on a section perpendicular to the cylinder's axis, takes as inputs the number of LEDs distributed radially (n) or the number of sides of the polygon, the radius of the cylinder to be irradiated (p_r), and the radius of the lamp body. The models do not consider the contribution of the light reflected by the painted surface of the pipe, as this is considered neglectable.

The total irradiation generated by the lamp was analyzed using a simplified model considering the internal pipe surface to be flat. The irradiance distribution, in this case, was evaluated as the total radiometric flux divided by the inner surface of the pipe:

$$E = \frac{\Phi}{A} = \frac{\Phi}{2\pi p_r L} \qquad (4)$$

Where E is the irradiance [mW/cm^2], Φ is the total radiant flux of the lamp [W], p_r is the radius of the pipe to be irradiated by the source [mm], and L is the length of the pipe [cm].

4.3.2 Radial Radiation Patterns

Using the simplified flat surface model, the radial irradiation profiles generated by several lamp geometries were evaluated on a cylindrical surface with an inner radius (pr) ranging from 10 mm to 100 mm. The results, plotted on polar diagrams, show the radial level of irradiation ranging from 0 to 100 %. The distance of the light source from the center of the cylinder (lr) was assumed constant and equal to 7 mm for all polygonal profiles.

Starting with small pr values, the radial emission diagrams obtained were non-uniform as the radiation intensity oscillated considerably, reaching 100 % values only in correspondence with the LED position. This can be seen in Figure 16, where the radiation pattern generated by a hexagonal lamp on a cylinder with pr = 10 mm.

When the distance from the source to the surface, given by pr-lr, is too small, each LED can

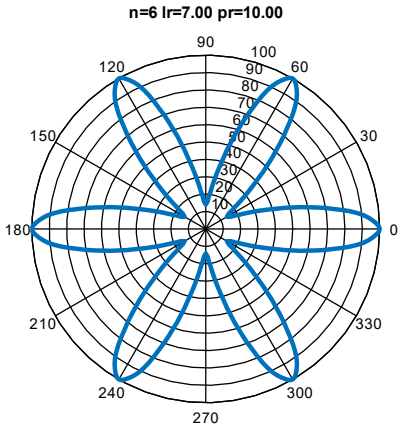

Figure 16 - Radial radiation pattern generated by a hexagonal UV LED source on a cylindrical surface of inner radius pr =10mm.

irradiate only a tiny portion of the surface immediately in front of it, and no side contribution is given to adjacent LEDs.

Considering the same hexagonal source, when the cylinder radius is increased from 10 to 30 mm (Figure 17), the radiation pattern becomes more evenly distributed on the cylindrical surface, reaching an average level of irradiation of around 95%. Increasing the p_r value, the irradiance becomes constant at about 100 %, with a profile closer to a circumference.

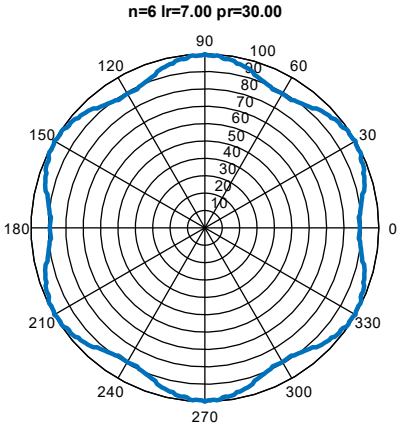

Figure 18 - Radial radiation pattern generated by an hexagonal UV LED source on a cylindrical surface of inner radius pr = 30mm.

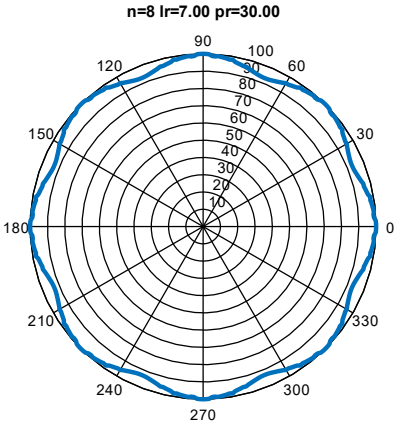

Figure 17 - Radial radiation pattern generated by an octagonal UV LED source on a cylindrical surface of inner radius pr = 30mm.

This tendency is particularly true for lamp geometries with more sides n. As the distance from the source increases, the contribution of each LED to the adjacent LED emission pattern becomes more critical, and the areas where there is no radiation become smaller because of irradiance overlapping.

Increasing the number of sides (n) of the light source does not affect the radiant flow, which is

uniform inside cylinders of small diameters. This situation is visible in Figures 18 and 19, where 8- and 10-sided sources (n=8, n=10) uniformly irradiate a cylindrical surface diameter of 60 mm (pr 30 mm).

Despite the excellent result in uniformity of the radiant flow, a light source with more than six sides is too large compared to the diameters of the cylinders we want to access, thus limiting the range of cylinders that can be cured.

Therefore, considering the size of the UV LEDs and the dimensional results of the radial radiation analysis, the hexagonal geometry is the suggested source for our purposes.

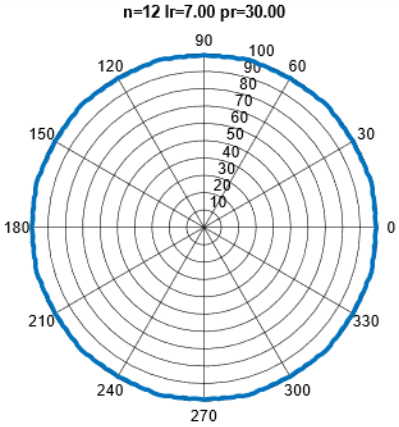

Figure 19 - Radial radiation pattern generated by a dodecagonal UV LED source on a cylindrical surface of inner radius pr =30mm

4.3.3 Linear Radiation Patterns

Once the optimal lamp radial configuration was defined, the linear irradiation was analyzed as a function of the step between LEDs and cylinder size. Figure 20 shows the linear radiation pattern obtained for a hexagonal lamp at a close distance to the cylindrical surface; as expected, at low p_r values, the radiation pattern has no room for overlapping, and a discontinuous profile is generated.

The minimum pr value at which the linear radiation pattern becomes uniform is 20 mm,

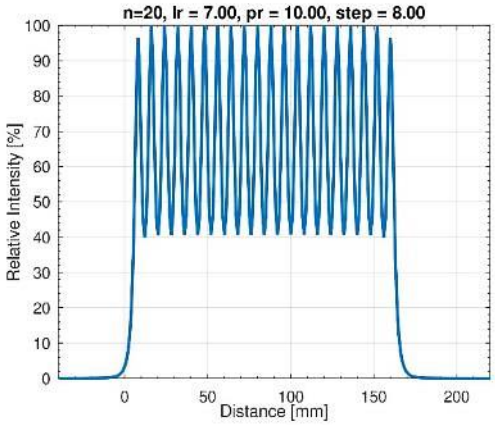

Figure 20 - Linear radiation pattern generated by a hexagonal UV LED source on a cylindrical surface of inner radius pr = 10mm.

corresponding to a cylindrical surface diameter of 40 mm (Figure 21).

Thus, the higher the p_r values, the lower the oscillations in the linear profile. While increasing the p_r value generates less irradiance at the surface, raising it too much causes a parabolic shape.

This effect causes the maximum intensity value to be maintained for a shorter length compared to cases where the surface to be irradiated is closer to the source. This effect must be considered when evaluating the lamp speed along the pipe.

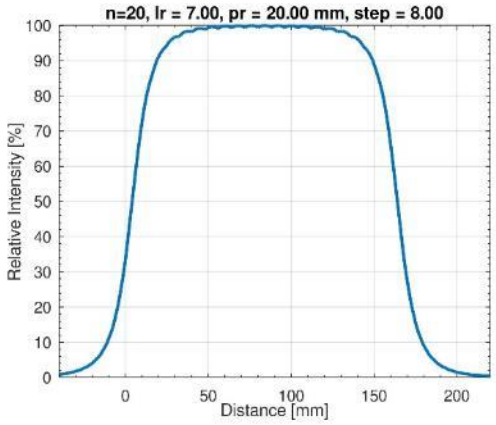

Figure 21 - Linear radiation pattern generated by a hexagonal UV LED source on a cylindrical surface of inner radius pr = 20 mm.

Finally, the effect of changing the distance between LEDs was evaluated. Decreasing the step resulted in a smoother profile with a lobe shape. However, reducing step size means having a shorter lamp and, thus, lower movement along the pipe. In addition, increasing the density of LEDs in each array would result in heat dissipation issues. For these reasons, a step size smaller than 8 mm was not considered. On the other hand, the effect of increasing the step on the linear radiation pattern is depicted in Figure 22.

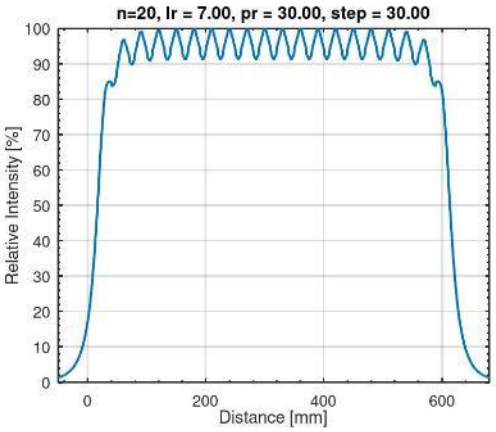

Figure 22 - Linear radiation pattern generated by a hexagonal UV LED source on a cylindrical surface of inner radius pr = 30 and step = 30 mm.

With a step size of 30 mm, the profile appears less uniform, with an irradiance oscillating between 90 and 100% of the maximum (Figure 23). In this case, the lamp's length will be increased from 160 mm to 570 mm, with a higher lamp speed.

Following the information collected in this paragraph, a UV LED light was manufactured for the experimental part of the project.

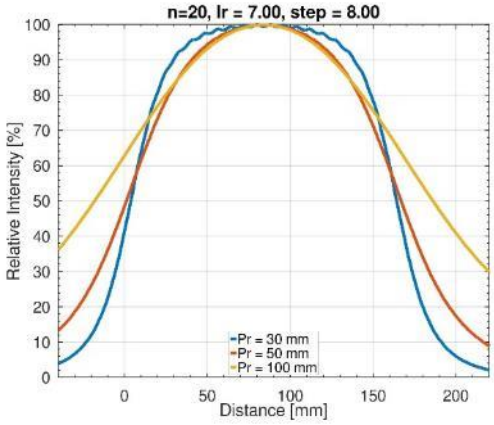

Figure 23 - Linear radiation pattern generated by a hexagonal UV LED source on a cylindrical surface of inner radius pr = 30, 50, and 100 mm.

5 Experimental Work

5.1 Materials

The experimental work has been developed using the new UV-curable coating called VRAD03 and RAD03 (property of ELIXE, Trento, Italy), where RAD means that polymerization is activated with radiation, V is the variant without fillers, based only on the resin with additives, and 03 is the code of the final formulation. The reference thermal curing coatings are VNG and NG (property of ELIXE, Trento, Italy), where NG is the name of the epoxy paint owned by MPR and used on down-hole tubing; V is, in the same way, the formulation based only on the resin with additives, without fillers. All the coatings specimens have been prepared in the ELIXE chemical laboratory. The general coating formulations are reported in Table 1 because the detailed coating formulations are companies' properties and are confidential information.

Steel substrates used for coating application consisted of API 5 CT steel with an inner diameter of 62 mm and wall thickness of 5.5 mm, employed as a standard in the oil and gas industry for oil wells. The chemical composition of API 5 CT steel consists of 0.34-0.39 carbon, 0.20-0.35 silicon, 1.25-1.50 manganese, 0.020 phosphorous, 0.015 sulfur, 0.15 copper, 0.20 chromium, 0.20 nickel, and 0.020 aluminum. Before application, each pipe's internal surface was sandblasted according to ISO 8501-1 to achieve a 2 ½ - 3 cleanliness standard, having a roughness average of 65 µm.

Thermally cured and UV-cured coatings were formulated and tested with an inorganic fillers' mixture of quartz, talc, and TiO_2 in fixed concentration, whose specific concentration is withheld due to a confidentiality agreement with the paint supplier. The weight percentage of fillers used in the thermal formulation was given as critical pigment volume concentration (CPVC). CPVC represents the transition point above or below which substantial differences in the appearance and behavior of paint films will be encountered. It is that point in a pigment-vehicle system at which just sufficient binder is present to fill the voids left between the pigment particles incorporated in the film after volatilization of thinner. It represents the densest degree of packing of the pigment particles commensurate with the degree of dispersion of the system. (68) CPVC of the thermal formulation was defined during the research and development activities of ELIXE laboratories using several corrosion protection tests on a bibliography of formulations with different filler content. The selected thermal formulation was also tested on the field six months before the market placement.

In contrast, concentration in UV formulation was determined after a series of tests as maximum concentration allowed to obtain a fully cured film of 100 µm thickness after exposure to 380 mW/cm2 for 60 seconds. A bibliography of UV-coating formulations with different fillers' concentrations has been prepared to evaluate which one might be optimal for successful curing and corrosive protection effectiveness through performance tests in the laboratory. RAD03 fillers' concentration higher than 40% w/w hinders the complete curing of a 100 µm coating layer with detrimental effects on mechanical and protective coating performance.

A table of the definition and general composition is given below.

Table 2 - General composition of the four formulations used

Coating		Composition (g)				
Name	**Curing type**	**Epoxy**	**Amine**	**Solvents**	**Additives**	**Fillers**
VNG	T	25	55%[1]	13.0	2.5	0
NG	T	25	55%[1]	13.0	2.5	58.5
Name	**Curing type**	**Epoxy acrylate**	**Diluent**	**Photo initiator**	**Additives**	**Fillers**
VRAD03	UV	34	20.5	2	3.5	0
RAD03	UV	34	20.5	2	3.5	40

[1] Amine curing agent used in wt.% to the concentration of epoxides.

5.2 Coating Machine

The standard procedure for painting steel is spraying, which can be performed manually or using an automated device. Spray application allows for adjusting the amount of material applied

and obtaining a uniform distribution. Indeed, applying protective coatings inside small-diameter pipes of significant length (the final pipes can be 12 m long) presents significant technological challenges, as tight spaces make it difficult to operate with existing equipment.

The best solution, already applied to industrial equipment, is to enter the tube with a device mounted on top of a rod. The main difficulty with this solution is optimizing the dimensions of the devices applying and curing the paint to allow them to enter and operate in a small-diameter pipe.

Another issue in applying protective coatings is the curing time, which is typically quite long, ranging from 8 to 12 hours. However, this duration can be reduced to 1 to 3 hours by utilizing ovens that heat the polymer, accelerating the reaction. The UV curing on a photopolymer paint dramatically reduces the curing time to minutes.

Referring to Figure 24 below, the layout of the machine works with two rods entering alternately a central chamber [1] where the tube sample is positioned [2]. The tube height is adjusted to allow both rods to enter the center of the cylinder. On the left [8], the rod inserts a sprayer [7] that applies the paint, while on the right [4], the rod inserts a UV lamp [3] that performs the curing. A cooling system [5] is connected to the UV lamp, while a heating system is connected to the insulated paint feeding tube [6]. Thanks to the limited length of the specimen, both lances cantilevered into the tube without the need for support. A motorized system controls the linear movement of the rods, connecting it through software to the respective painting and curing

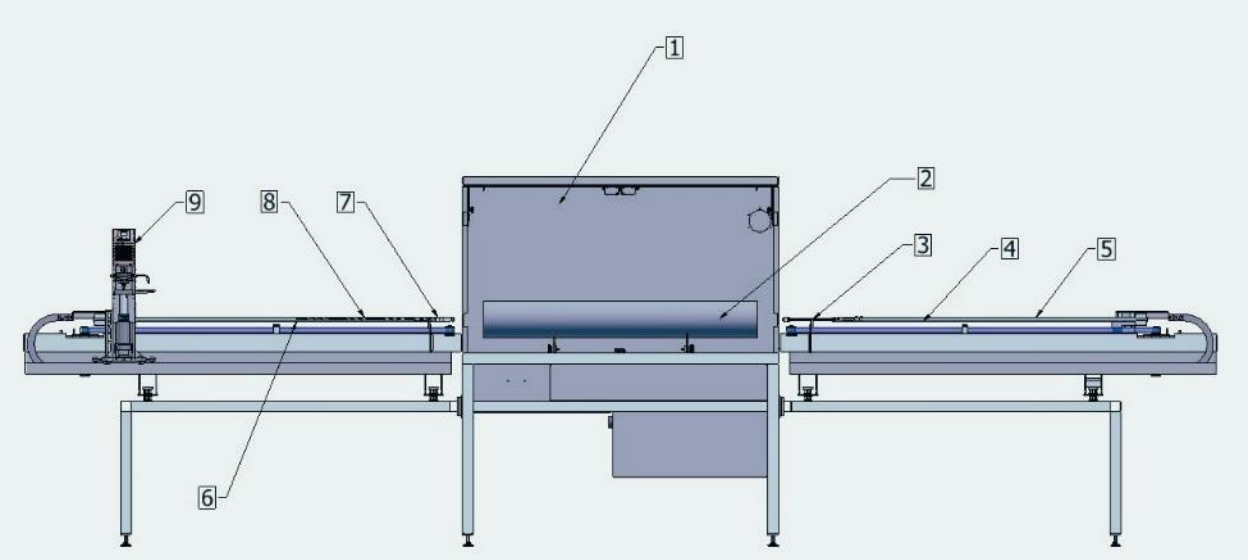

Figure 24 - Scheme of the coating and curing machine

processes. The spray rod links the speed to the amount of paint fed into the sprayer by the pump [9] to achieve the required layer thickness. The UV curing lance links the speed with the amount of irradiation needed and, thus, the irradiation time to achieve cross-linking.

5.2.1 Coating Inside a Pipe

Coating a steel surface means spraying by pulverizing the paint into tiny particles. This process can be achieved using one of the three different technologies (126):

- Airless spray: pushing the paint at very high pressures (about 250 bar) through a nozzle with a controlled and geometry-defined jet opening, which breaks the flow into tiny particles and sprays them with a directional jet. (123)
- Air spray: pushing the paint onto a nozzle, where pressurized air (6-7 bar) breaks the flow and creates a jet. (124)
- Rotary atomizer: The paint is pushed towards a high-speed (30-40,000 r.p.m.) rotating bell, which, with centrifugal force, separates the jet into tiny particles and sprays them in a cone pattern. Due to the particles' lateral direction, this process is often combined with an electrostatic charge to avoid material loss. (125) (127)

To define the preferred technology for the inner coating of a pipe, we must focus on the needed

features, notably protecting the steel surface from corrosion and improving the flow by decreasing the friction of the liquid. While a coating well adhering and without defects is needed for the best corrosion protection, a smooth and uniform surface enhances the flow inside the pipe. Moreover, UV curing is particularly sensitive to the polymeric layer and requires precise coating thickness control.

Given these requirements and from experience in the field of pipe coating, a rotary atomizer [2] with a bell [1] mounted on a rod [4] and connected to the paint feeding tube [3] is particularly suitable for painting the inner surface of small-diameter pipes up to 200-250 mm in diameter (Figure 25). Such pipes are closed inside, and their tight surface prevents the dispersion of paint particles, a typical problem of centrifugal spraying with a rotary atomizer, avoiding the use of

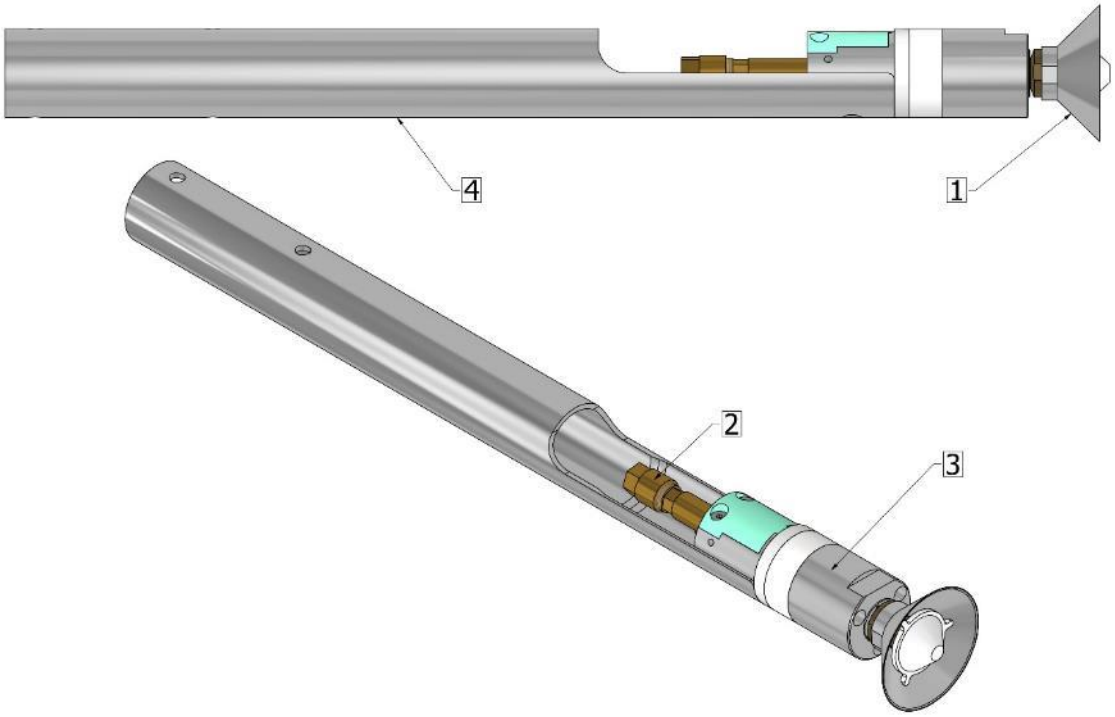

Figure 25 - Rotary Atomizer mounted on the top of a rod

Finish quality is improved using a rotary atomizer as it provides the best particle finesse, circular spray uniformity, and reasonable control of the paint flow. The rotary atomizer also produces a uniform spray pattern, which reduces mottling or striping caused by inconsistent film buildup caused by spray pattern uniformity issues.

Due to the difficulties in controlling the application in confined spaces such as inside pipes and vessels and the need to ensure a uniform and smooth coating, a stroboscopic device with an electronic control has been integrated into the axe of the rotary atomizer to regulate the speed of the bell, particularly when variations in paint viscosity or other factors could affect the force needed to rotate and to keep a constant volume of paint dispensed. This control operates through a valve on the compressed air flow that gives the axe the rotational force, keeping a constant rotation speed.

A precise cylinder pump guarantees a consistent and steady paint flow from the tank to the machine.

This process operates as airless, meaning that the paint is applied without being mixed with air. This airless approach has several advantages, including preventing external contaminants from entering the paint during application. It also contributes to a cleaner application process, minimizing the risk of defects or impurities in the coating.

The finishing industry has been trending toward the transition from air-atomized applicators to rotary atomizers. This trend started about 20 years ago in automotive assembly plants. Although the initial interest was related to improved transfer efficiency or reduced paint usage,

additional benefits, such as improved finish quality and simplified application programming, were also realized. (128)

5.2.2 The Rotary Atomizer

Rotary atomizers utilize centrifugal force to shear the coating material into droplets. An air-bearing turbine with a "bell" cup mounted on it is typically rotated between 25,000 and 40,000 rpm. In a rotary atomizer, the bell is the main element that affects the characteristics of the flow of particles that reach the surface. This flow should be uniform and constant to obtain a good surface and thickness and can be modelized through different simulation processes (69) (70). Electrostatic forces between the paint and the surface to be covered are commonly applied to control the flow (71) (72), but working inside a closed space, we can assume that all paint will be deposited on the steel surface.

The rotational movement is obtained with pressurized air at 6-7 bars propelled into a turbine that generates the necessary centrifugal force to push the bell cup and the paint particles. This allows efficient force without air admixing and ensures the paint is broken into fine particles. The flow field depends on the rotational speed, the flow rate, and the liquid viscosity and is independent of the surface tension coefficient. (73)

The coating material is introduced through a fluid tube into the backside of the rotating bell cup. The liquid column initially impacts a splash plate and then transfers to the face of the bell cup, where the rotation draws it to the edge (Figure 26). The edge of the bell cup often has serrations that the material is forced through, causing it to form into ligaments, which then shear off the edge of the rotating cup. Shaping air can be introduced outside and behind the edge of the bell cup, which is used to shape the spray pattern and provide additional forward momentum. Although it will vary based on coating material, flow rate, and rotational speed, rotary atomizers generally produce droplets in the 20 – 45 micron range.

The bell-cup painting process can be roughly divided into three regions, as shown in Figure 27:

Figure 26 - Cross section of a Rotary Atomizer

near field, transport field, and target field. In the near field, the paint supplied through the liquid supply nozzle [1] flows over the bell-cup surface by centrifugal force, forming a liquid film [2]. The fluid film flows off the bell-cup edge as ligaments [3] and disintegrates into droplets [4]. The atomized droplets transit through the transport field, which is the space between the bell cup and the target, and adhere to the target (the inner cylinder surface).

The stream of paint particles emitted by the rotary atomizer has a circular conical shape, which, when placed in the center of a tube, allows uniform application on the internal cylindrical surface.

The uniformity of the paint layer is critical when applying UV-cured paint, as it enables uniform irradiation penetration within the polymer layer.

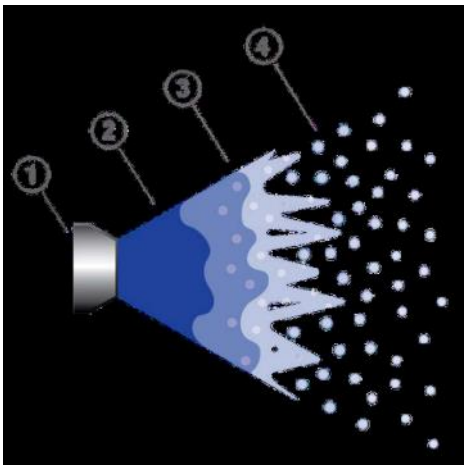

Figure 27 - bell-cup paint spray

The paint flow is controlled with a pump feeding at 2-3 bars by an electric motor driving a screw pushing the piston of a paint chamber filled every cycle. With this system, the flow is well controlled, and we can even define the thickness of the layer by combining the flow of paint with the linear movement of the atomizer in the pipe.

5.2.3 Definition of the Processing Parameters

5.2.3.1 The rotational speed

Assuming a linear conical bell, the geometric parameter that affects the paint jet is the diameter in the zone where the paint leaves the bell with the maximum centrifugal force. The exit diameter defines the centrifugal force F_c released to the paint particles:

$$Fc = m\ \omega 2r \qquad (4)$$

Where m is the mass of the particles, ω is the angular velocity, and r is the radius. At an angular velocity between 400 and 600 revolutions per second over the 20 mm diameter of a standard bell used for a 60 mm diameter pipe, we have an acceleration of around 5000 m/s², hugely higher than the gravity acceleration. According to the literature and our experiments, an acceleration of more than 3000 m/s², corresponding to 20-25,000 r.p.m., does not further affect the separation of the paint into small and uniform particles. The chemical composition and viscosity of the liquid determine the minimum drop size, but it is relatively insensitive to significant changes at bell speeds higher than 20,000 rpm. Therefore, our machine will work with a range of 20-25.000 r.p.m. rotational speed.

5.2.3.2 The paint feeding

As shown in Figure 28, a piston pump [2] regulates the paint flow drawing from a tank [1] that stores sufficient paint for one pipe coating process. This reservoir ensures a continuous and consistent paint supply to the atomizer, avoiding interruptions during the application. A valve [4] sends the flow of paint to the atomizer [3] or cleaning exit [5]

The pump and the atomizer are connected using feeding copper tubes with an internal diameter of 6 mm. The small diameter of the feeding tubes decreases the unused paint but increases the pressure and, consequently, deforms the tube, raising the possibility of irregular waves of paint feeding. This issue can cause waves of different thicknesses during the paint application.

Due to the high viscosity of a 100 % solid content, photopolymer paint also experiences a similar high-pressure and wave-feeding problem. To avoid this problem, a heating system has been added to the machine to decrease viscosity and facilitate the paint's flow through the feeding tube. Following the technical specification of the paint, a temperature of 40 ˚C has a viscosity of 3000 cp, which is smooth enough for this application.

The paint is fed from the end of a rod that penetrates the pipeline. This rod supports the spraying device, allowing the paint to reach and cover all internal surfaces of the pipeline evenly.

The paint is pressurized around 2-4 bars before being propelled to guarantee the correct flow quantity. Pressurization is critical as it enables the paint to be forcefully and uniformly applied to the pipeline's interior surfaces.

5.2.3.3 The paint flow

The paint flow must be defined according to the bell's exit border. This limits the quantity of paint and establishes the quality of the droplets. The best way to study the quality of the paint droplets is to use a stroboscopic light and a camera that collects pictures of the paint spray.

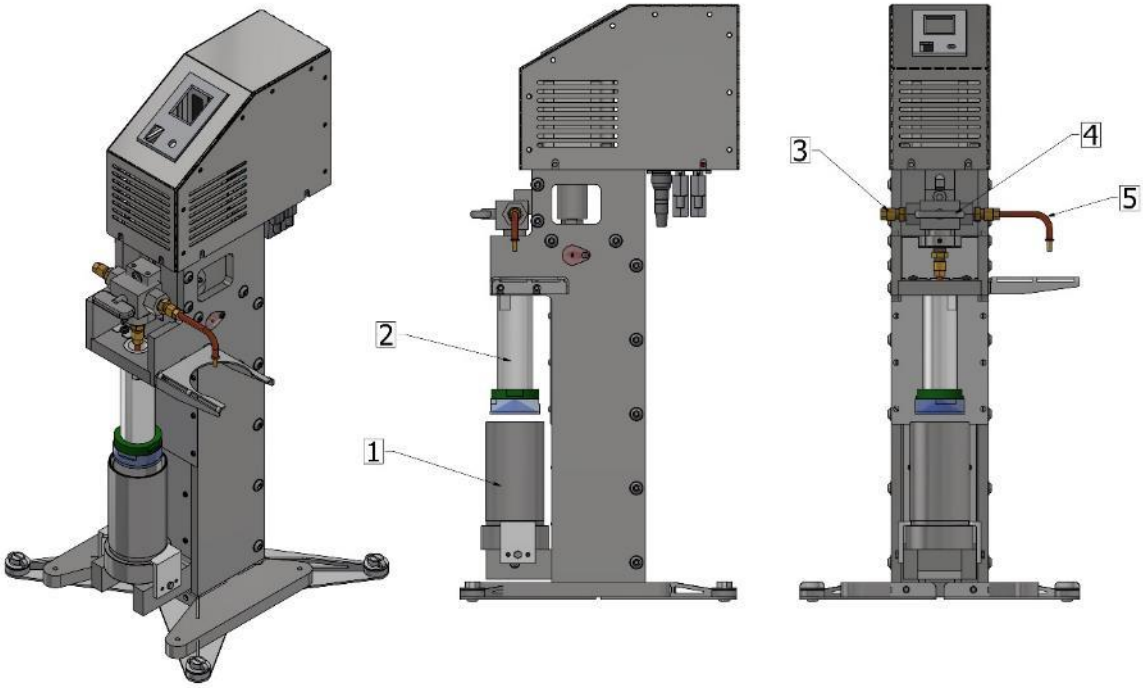

Figure 28 - Paint piston pump

The experiment has been developed using two bells of different diameters, the first 36 mm and the second 46 mm. The paint flow has been tested at three levels: 1 l/min, 2 l/min, and 3 l/min. The result is shown in the photo in Figures 29 to 34.

When the paint flow exits the bell, but the rotation does not break the flow into droplets, the spraying will not result in a uniform application.

With this consideration, we have evaluated the pictures in the paint. We can consider that, using a smaller bell, the defect appears at a smaller quantity, notably at 2 l/min, while increasing the diameter of the bell, the defect appears at 3 l/min (Figures 30, 31, and 34). This is due not only to the higher centrifugal force but also to the broader surface of detachment that gives a larger surface to extend the paint flow.

This is coherent because working on larger pipes needs more giant bells. Our machine uses a bell with a 36 mm diameter for pipes with an internal diameter of 60mm, and the paint flow is limited to 1 l/min.

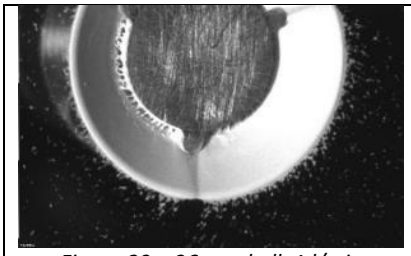

Figure 29 – 36 mm bell, 1 l/min

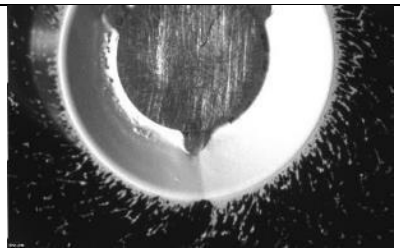

Figure 30 - 36 mm bell, 2 l/min

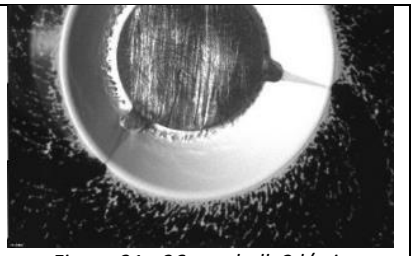

Figure 31 - 36 mm bell, 3 l/min

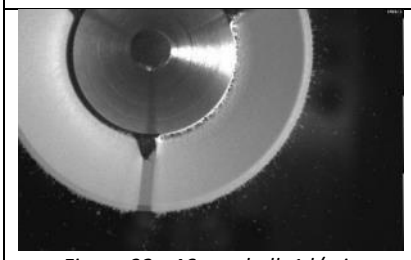

Figure 32 - 46 mm bell, 1 l/min

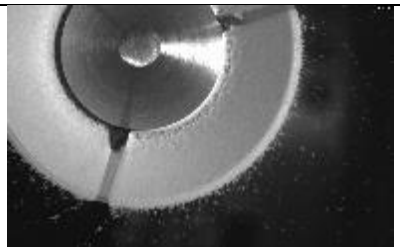

Figure 33 - 46 mm bell, 2 l/min

Figure 34 - 46 mm bell, 3 l/min

5.2.3.4 The linear speed.

The spraying process is also defined by the linear speed v of the spraying device in the pipe. This parameter, together with the paint's feeding flow p_f, defines the quantity of sprayed paint per linear unit and, consequently, the thickness of the layer t, obtained as follows:

$$t = p_f / v \qquad (5)$$

In our application, the constraint is the thickness of the coating, assumed to be 0,150 mm; using a paint flow of 1 l/min on a standard 60 cm internal diameter pipe results in an atomizer's linear speed of 60 mm/s. The two parameters can be regulated according to the process's efficiency.

In summary, integrating controlled-flow atomizers, pressurization, and an airless system in the paint application process ensures the effective and controlled coating of pipeline interiors, addressing the critical parameters necessary for successive efficient and reliable UV curing.

5.3 UV Curing Machine.

The UV curing process is obtained on the same machine, working with the opposite rod, where the UV-LED lamp is mounted on its top. While the coating process inside a pipe is already in use even at the industrial level, UV curing in tight spaces is an entirely new issue, and it is possible only with the new UV-LED technology, using a small source at low energy. A prototype lamp will verify the parameters studied and analyzed in the previous paragraphs.

5.3.1 UV curing process.

The issues in developing this part of the machine are essential for defining the paint layer's polymerization and, consequently, the quality of the protective coating. Even minor defects can allow corrosion agents to attack the metal, expanding the reaction under the coating.

The cross-linking of a photopolymer coating is obtained by the dose of UV light, which is the light flow for the irradiation time. Since the source moves inside the tube along a constant motion, the irradiation time depends on the speed and length of the lamp. Increasing the movement speed or the lamp's length can improve efficiency but reduce the irradiation time.

5.3.2 Irradiance Patterns Validation

This application's standard UV LED source was a 1 W power UV LED, SST-10-UV [20], with a 395 nm peak wavelength (Luminus Devices Inc, Brussels, Belgium).

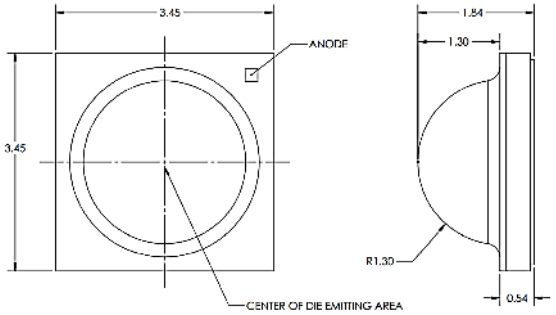

Figure 35 - PDS Product Data Sheet (Source: Luminus Devices Inc.)

Figure 35 gives the dimensional features reported by the manufacturer. In particular, the LED is a square of 3.5 x 3.5 mm^2, has a height at the center of 1.3 mm, and a viewing angle of 130°.

Table 3 - Technical characteristics of the SST-10-UV LED [20].

UV LED					
Parameter	Symbol	Value			
Wavelength Range [nm]	λ	365-375	380-390	390-400	400-410
Peak Wavelength [nm]	λ_p	370	385	395	405
Forward Voltage [V]	V_f	3.7	3.4	3.3	3.3
Radiometric Flux [mW]	Φ_{typ}	875	1015	1015	930
Viewing Angle [deg]	$2\Phi_{1/2}$	130	130	130	130

The printed Circuit Board (PCB) where the UV LEDs were placed was designed using KiCAD®.

To generate a 360° radiation profile, the LED arrays were distributed around cylindrical support in a configuration where each PCB occupies a side of a polygon. Considering the PCB width to be 4.2 mm, the side of each polygon was set to be constant and equal to 6 mm, and the dimension of the final lamp was calculated accordingly for each configuration analyzed.

Table 4 - Polygonal geometries and number of LEDs on 16 cm length

Polygon	**R_{ext} [mm]**	**l_r [mm]**	**n LEDs**
Square	4.24	3.00	80
Hexagon	6.00	5.20	120
Octagon	7.84	7.24	160
Decagon	9.71	9.23	200

Table 3 reports the support characteristics for the analyzed polygons, each defined by the radius of the circumscribed circle (R_{ext}), the radius of the inscribed circle (l_r), and the total number of LEDs per lamp, considering each array composed of 20 LEDs.

The irradiance profiles were evaluated as a function of the number of LEDs, the arrangement along the lamp structure, the LED spacing (step), and the distance from the source to the pipe's internal surface. The dependence of linear and radial profiles from the parameters above was evaluated, and it was found that a lamp with hexagonal geometry consisting of 6 arrays of 20 LEDs with an 8 mm step between one another was the best configuration to achieve the optimal radiation pattern with the minimum encumbrance. The chosen lamp was then constructed, and the absolute irradiance was measured at various distances using a radiometer.

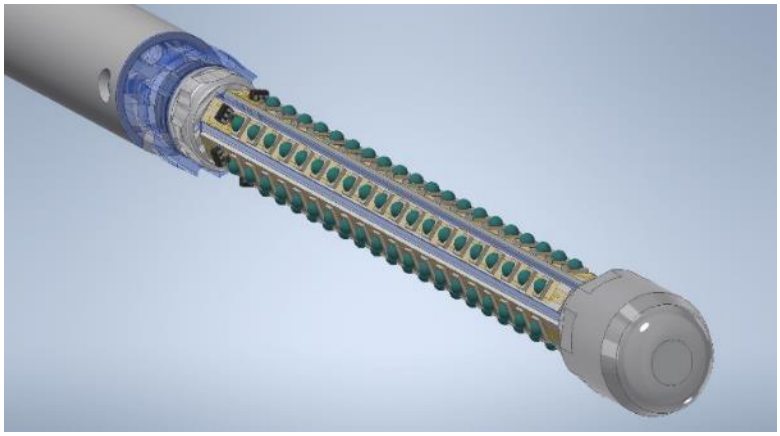

Figure 36 - 3D model of the hexagonal UV LED source.

Following the analysis's results, the UV LED source chosen to continue the experimentation is based on an array of 120 UV LEDs Luminus SST-10-UV distributed in 6 strips of 20 LEDs spaced 8 mm apart and fixed on hexagonal aluminum support. Figure 36 shows the 3D model of the described hexagonal UV LED source.

The overall resulting radiant flux is Φ = 120 W, and the achievable irradiation on a cylindrical surface having the same length as the UV LED source results from the following formula:

$$E = \frac{120W}{2\pi P_r \; x \; 16cm} = \frac{1{,}19}{P_r} \; W/cm^2 \qquad (6)$$

When the inner surface of a cylinder is characterized by a radius (P_r) between 10 mm and 100 mm (meaning a source-surface distance between 3 mm and 93 mm), we obtain irradiation between 1200 mW/cm2 and 120 mW/cm2; consequently, the irradiation needed for the correct UV curing can be tuned using the power of the UV LED.

Larger diameters of the cylinder to be irradiated need more extensive supports, which can be obtained by increasing the number or the dimension of the sides.

A UV radiometer X1-5 equipped with an RCH-119 detector (Gigahertz Optik GmbH, Türkenfeld, Germany) was used to measure the absolute irradiance after the constructed lamp. The radiometer measuring device was fixed on a support while the light was mounted on a moving rod operated by an inverter motor. A value of irradiance was registered every 4 mm distance for the linear profile or every 10 degrees for the radial profile. The irradiance value for each measurement point was obtained as an average of 3 different results.

The radial and linear irradiance profiles were evaluated on the prototype lamp by measuring the intensity values while rotating and translating the lamp along its axis. Except for the pattern corresponding to a p_r value of 10 mm, where the collected points were too few to have a reliable curve, all the radiation patterns were consistent with the ones obtained by computer simulation (Fig. 11). The experimental irradiance values were calculated by increasing the distance from the LED source ($d = p_r - l_r$). It was found that the values of intensity registered by the instrument corresponded to the theoretical values obtained with equation (6) with a maximum error of less than 6%, which can be ascribed to the operator error in measuring the distance d.

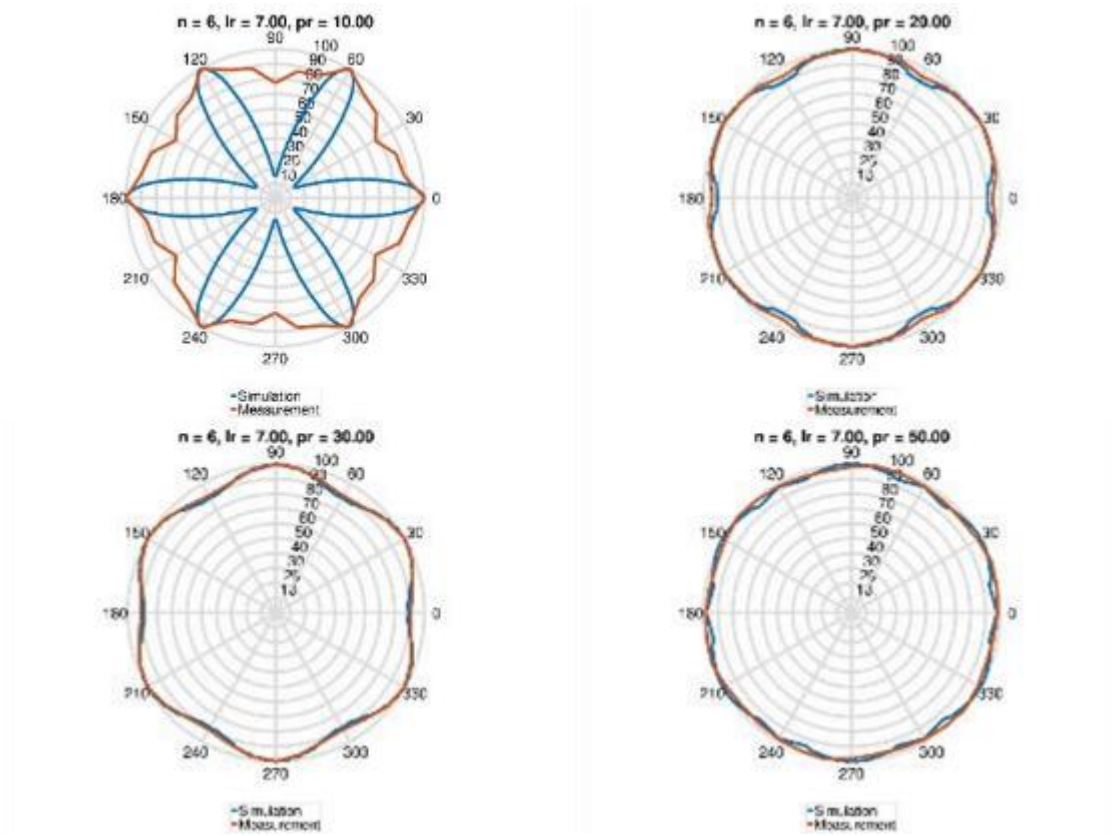

Figure 37- Comparison between simulated radiation patterns an experimental data for radial (a-d) radiation patterns for different pr values.

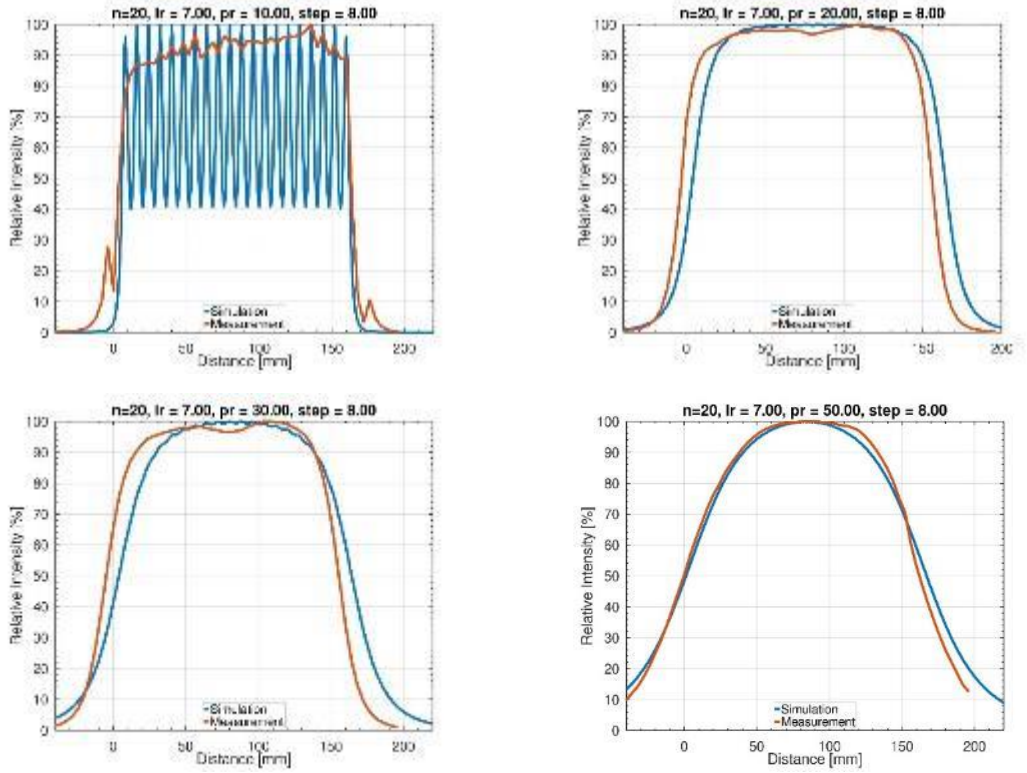

Figure 38 - Comparison between simulated radiation patterns and experimental data for linear (e-h) radiation patterns for different pr values.

Table 5 - Irradiance values are measured with a radiometer at increasing distances from the source.

Distance from LED (d) [mm]	Theoretical I [mW/cm²]	Measured Irradiance [mW/cm²]	Abs Error [%]
1	702,5	710.1	1.08
2	442,3	450.5	1.85
3	322,8	328.2	1.68
4	254,1	250.7	1.34
5	209,5	210.0	0.23
6	178,3	175.8	1.37
7	155,1	150.3	3.09
8	137,3	129.8	5.44
9	123,1	120.2	2.37
10	111,6	105.0	5.93

Despite good validation obtained from intensity measures, the simulation remains an approximation of the intensity of the UV light on a flattened surface. For more complex systems in which different geometries are present (e.g., closed vessels and curved pipes), a more detailed simulation should be preferred to have more accurate patterns. In addition, the values of pipe diameters used in this study cover only a small range of the ones commonly used. With more considerable distances from the source to the surface, a different lamp design should be introduced to avoid the intensity of light reaching the coated surface being too low to allow the crosslinking reaction.

5.3.3 UV Light Definition.

After the developed model was validated by the data collected through the radiometer, the simulation was used to determine the optimal radiation pattern to cure UV paint formulations applied on the inner surface of different pipe sizes. For each pipe of various diameters, lamp designs with optimized radiation patterns with the lowest oscillation intensity along the whole length of the lamp should be chosen.

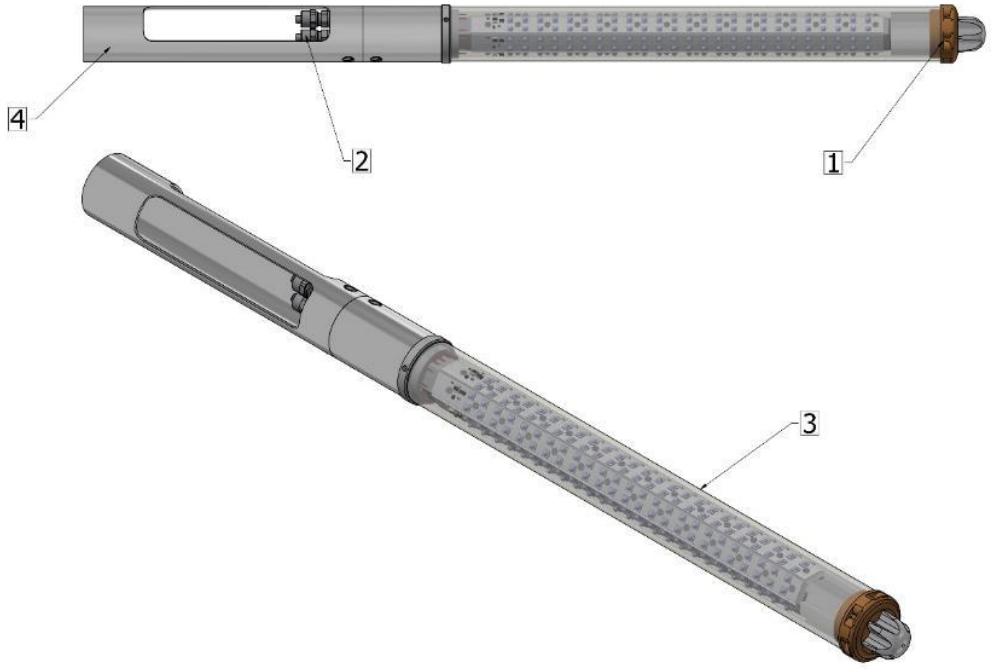

Figure 39 - UV lamp mounted on a rod

Figure 39 displays the lamp where the UV LED array defined above (3) has been applied to the top of the right rod (4), connected to the water cooling system (2), and protected with quartz glass (1). The resulting device has been used to verify the curing parameters of the UV paint inside a pipe with a 60 mm inner diameter.

5.3.3.1 UV light dose.

Depending on the UV paint formulation, the correct UV intensity (W/cm^2) required for the right cure can be tailored by acting on the number of LEDs and the power regulation. If a different peak intensity is needed, the LED current can be increased or reduced to 50 to 200 % of the nominal power or radiometric flux [20]. Consequently, the dose regulation (J/cm^2) can be obtained using a certain number of LEDs by increasing or decreasing the lamp speed across the pipe.

During the chemical development of the formulation based on photopolymers (Paragraph 4.1.7), the suggested parameters for UV curing have been defined as follows:

Radiation source LED (UVA):	395 nm
UV Radiation intensity:	600 - 1000 mW/cm^2
Dry Film thickness:	40 - 120 µm
Exposure time:	15 - 60 s

Based on Formula 6, the 120W, 160 mm long lamp irradiates a 60 mm diameter pipe at 400 mW/cm^2 on the pipe's inner surface. To increase the intensity, a new lamp has been manufactured with the same parameters but using a double strip of UV LED on the sides of the support, giving an intensity of 800 mW/cm^2, which was considered optimal for our experiments.

Considering the intensity and time given for our paint, the resulting dose for correct curing is 20-50 J/cm^2. Using the new lamp at 800 mW/cm^2, the curing time is 25-60 s. Considering that this time is needed to move for the 160mm of lamp length, the resulting speed is about 5 mm/s.

5.3.3.2 Cooling and protecting the UV light

Heat deteriorates the LEDs, shortening their life or burning the circuit. LED breakage is a significant problem in the curing process because it occurs with incorrect irradiation parameters and leads to considerable damage to the coating. Despite the high energy efficiency of LED systems, the heat generated by the lamp while in use is an issue that can lead to a critical temperature increase on the PCB chip. This temperature should never surpass the threshold value of 80 °C to avoid consequent power reduction, LED damage, or desoldering [20]. For this reason, a possible solution would be to introduce an internal water cooling system to avoid overheating. The cooling system has been integrated into the LED support, optimizing the flow of the liquid and the cooling transfer.

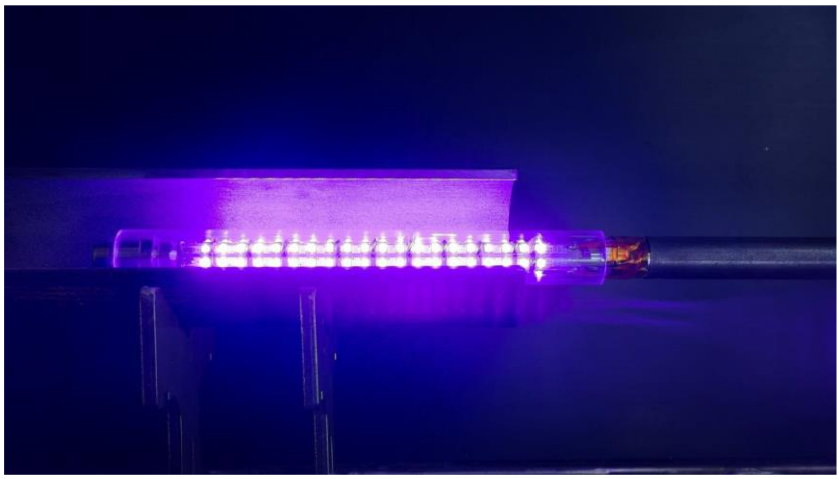

Figure 40 - UV light moving inside a pipe

Another common issue with using LED units in a chemicals-rich environment is VOC contamination of LED silicon lenses. The outgassing of adhesives, gaskets, or coatings in close contact with the LED generally causes this contamination. The VOCs produced this way will penetrate the lens and occupy the free space within the silicone polymer; with subsequent exposure to high photon energy and heat produced by the LED, the volatile compounds trapped will undergo discoloration, which will cause the LED to lose intensity [25-26]. To avoid this effect, LEDs must be screened from the VOCs produced from the curing coating with a transparent cover with optimal light transmittance properties (e.g., quartz).

Figure 41 - Final render of the coating and curing machine

6 Characterization

6.1 Chemical–Physical Characterization

Chemical-physical characterization has been developed to provide information about the curing process, the viscoelastic properties, and the adhesion to the substrate; all this information is essential for defining the steel's coating protection characteristics. The tests used in this study are the FTIR, the DMTA, and the pull-off, and the procedures for analyzing the results are detailed hereafter.

6.1.1 Conversion

6.1.1.1 Fourier-Transform Infrared Spectroscopy (FTIR)

FTIR measures the absorption of infrared light by molecular vibrations corresponding to different functional groups. Each functional group absorbs at a specific wavelength, allowing for identification and quantification.

Procedure.

Prepare the samples (the thin coating film has been directly applied on the flat silicon support of the instrument) and place them in the FTIR spectrometer. Record a background spectrum without the sample to remove any ambient interference. Run the FTIR analysis before and after the reaction. The key absorption peaks corresponding to the functional groups of interest are identified. Compare the intensity or area under the peaks before and after the reaction. A decrease in peak intensity indicates the consumption of a functional group, while an increase indicates the formation of a new group.

Standards.

ASTM E1252-98: Standard Practice for General Techniques for Obtaining Infrared Spectra for Qualitative Analysis

ASTM E168-16: Standard Practices for General Techniques of Infrared Quantitative Analysis

6.1.1.2 Analysis of Results

The curing process of the two formulations was evaluated by measuring the relative concentration of their respective functional groups before and after the reaction using the Fourier-Transform Infrared Spectroscopy (FTIR). Figure 42 reports the FT-IR spectra of the two formulations before and after irradiation. For the thermally cured epoxy reference coating, the distinctive peaks are the stretching of the C-O bond of the oxirane functionality at 915 cm^{-1} and the stretching of the C-O-C ring at 831 cm^{-1}. Here, the signal at 915 cm^{-1} was used because it was more easily readable. Another signal that can be used to confirm the ongoing reaction is the strengthening of the signal at 3500 cm^{-1} relative to the stretching of the -OH group. The formation of more hydroxyl groups directly affects the oxirane group ring opening reaction. Differently, the response in the radical formulation can be followed by looking at the disappearance of the peak at 1635 cm^{-1}, which can be ascribed to the C=C double bond of the acrylate function, which reacts after UV exposure. The aromatic ring C=C double bond stretch peaks at 1610 cm^{-1} and the C-O bond stretch at 1510 cm^{-1} were used as reference peaks for the epoxy-based and acrylate base coating, respectively. The conversion degrees ($\propto$) after 120 seconds of curing of RAD03 and NG coatings were found by applying equation (1) to the absorbance data of the FTIR spectra obtained before and after curing. RAD03 showed a $\propto$ value of 0.7 while NG revealed a $\propto$ value of 0.6. These values are lower than the conversion values calculated for VNG and VRAD03, respectively 0.7 and 0.8. The decrease in the conversion degree can be ascribed to the different concentrations of fillers inside the coatings. The higher concentration of fillers in NG coating hinders the curing reaction, bringing it to a lower $\propto$. (74)

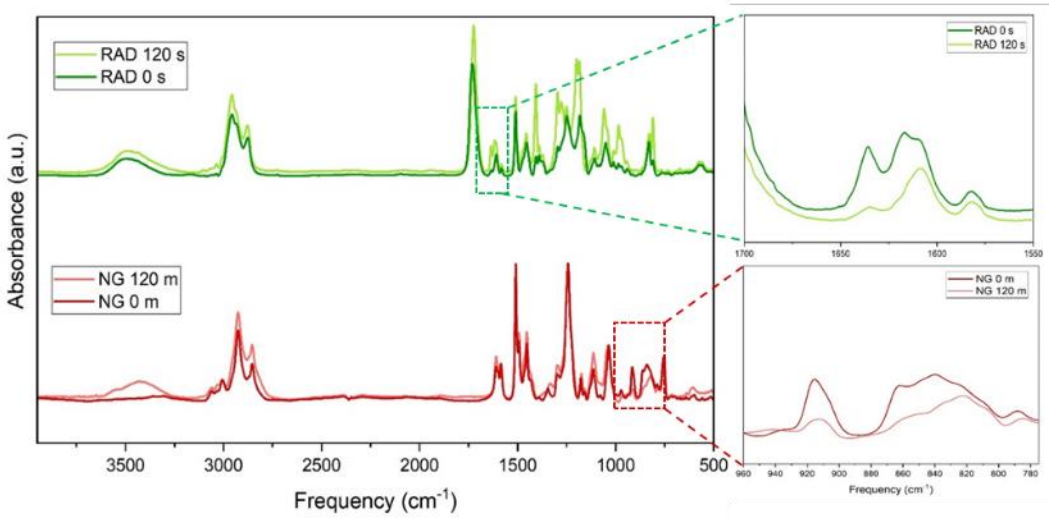

Figure 42 - FTIR spectra of VRAD03 and VNG formulations before and after curing

6.1.2 Viscoelastic Properties

6.1.2.1 Dynamic Mechanical Thermal Analysis (DMTA)

This test is used to study the viscoelastic properties of materials, such as polymers, under varying temperatures and dynamic stress. The procedure involves applying sinusoidal stress to the material and measuring its response to evaluate properties like storage modulus, loss modulus, and damping factor (tan δ) over various temperatures.

Procedure.

Prepare a rectangular flat sample and set the instrument:

- Deformation Mode: tension
- Temperature Control: from 20 °C to 180 °C (T_g).
- Frequency: 0.1 Hz
- Heating rate of 10 °C/min

The Storage Modulus (E') represents the elastic or "storage" component of the material's response and indicates the material's stiffness. The DMTA measures the deformation in phase with the applied stress. Modulus vs. Temperature Curve: The instrument plots the storage and loss modulus as a function of temperature. These curves provide information on the material's stiffness and ability to store energy across the temperature range. A higher storage modulus indicates a stiffer, more elastic material, while a lower modulus suggests greater flexibility or softness.

The Glass Transition Temperature (Tg) is observed as a peak in the tan δ curve as the temperature increases. A high tan δ value indicates that the material has good damping properties, which can effectively dissipate mechanical energy. In a DMTA test, the dry polymer will show a higher glass transition temperature. When the same polymer absorbs moisture, a DMTA test will be rerun to show a lower Tg (wet Tg), reflecting the water's plasticizing effect. A decrease in the storage modulus and an increase in the loss modulus are usually observed as the material becomes more flexible.

Standards.

ASTM D4065 - 12: Standard Practice for Plastics: Dynamic Mechanical Properties: Determination and Report of Procedures

ASTM E1640 - 18: Standard Test Method for Assignment of the Glass Transition Temperature by Dynamic Mechanical Analysis

ISO 6721-1: Plastics — Determination of dynamic mechanical properties — Part 1: General principles

ISO 6721-11: Plastics — Determination of dynamic mechanical properties — Part 11: Glass transition temperature

6.1.2.2 Analysis of Results

Dynamic mechanical thermal analysis was used to determine the viscoelastic properties of the four coatings samples as a function of increasing temperature. The storage modulus (E') has been used to determine stiffness, filler/matrix interfacial bonding, and degree of cross-linking, as reported in Figure 43. The material's glass transition temperature (T_g) is the maximum value of the tan delta curve, as reported in Figure 44.

Figures 43 and 44 display can be used to evaluate the effect of the two curing approaches investigated, thermal and UV irradiation, and the impact of adding the fillers to the pure resins.

In the E'(Pa) vs T(°C) graph, three different regions can be identified: glassy region, transition region, and rubbery plateau. (75) In the glassy region, the components of the composite result in a very compact state, like they were frozen, and E' shows higher values. (76) Increasing temperature E' decreases for all the coating samples because the resins become increasingly fluid and finally soft upon the glass transition occurring and reaching the rubbery plateau. Generally, the thermal curing samples VNG and NG reveal the highest value of E' in the glassy region, suggesting higher stiffness than the coating samples obtained by UV irradiation curing, VRAD03, and RAD03. The difference in stiffness between thermal-cured and UV-cured samples could be ascribed to the unreacted resin inside VRAD03 and RAD03 layers due to the scattering effect of the fillers' particles, which limits UV light penetration, hindering the resin curing.

Finally, as shown in Figure 44, VNG and NG coating samples show tan delta peak values higher than VRAD03 and RAD03, indicating a higher degree of molecular mobility than VRAD03 and RAD03 samples. These latter appear broader due to the non-homogeneity of cross-linking density inside the coatings' layers, likely due to different polymer chain lengths in the case of broad polydispersity. The wide shape of the storage modulus curves in Figure 43 supports this behavior. (75) (76) (77)

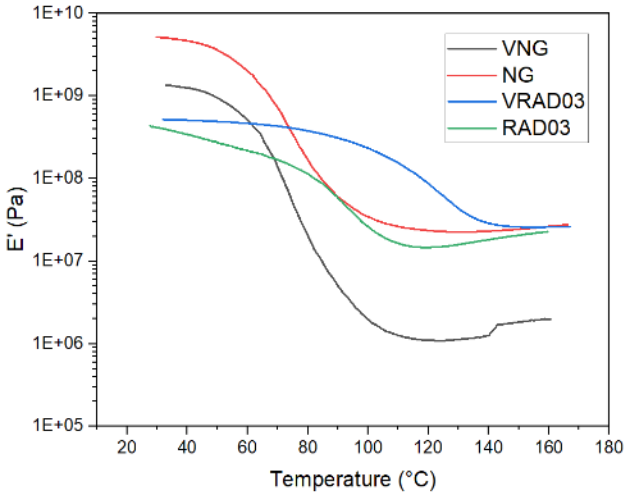

Figure 43 - Storage modulus in the function of temperature obtained from DMTA measures of VNG (black), NG (red), RAD03 (green), and VRAD03 (blue).

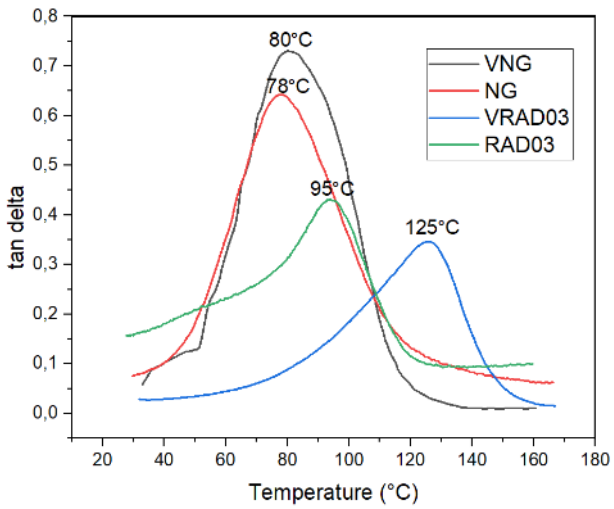

Figure 44 - Tan delta curves in the function of temperature obtained from DMTA measures of VNG (black), NG (red), RAD03 (green), and VRAD03 (blue).

Concerning the effect of fillers addition to the resin, as reported in Table 6, the reduction of the E_r can be observed for the UV-cured formulations, from 2.9 x 10^7 Pa of VRAD03 to 1.7 x 10^7 Pa of RAD03. The reduction of the modulus can be ascribed to the hindering of the curing process of the polymer matrix due to the presence of fillers, as supported by the noticeable decrease of T_g, going from 125 °C for the VRAD03 formula to 95 °C for RAD03. This effect arises from the scattering effect of the fillers' particles, which limits UV light penetration inside the polymeric matrix during the curing process and reduces the T_g of the UV-cured coating. Moreover, as suggested by the shape of the storage modulus curves (Figure 42) in the glass transition region, adding fillers into VRAD03 negatively affects the crystallinity of the UV-cured resin. (76) This behavior is also supported by the reduction of T_g. Inside VRAD03, more polymer chains are constrained to a greater degree at the crystal/ amorphous interface and require higher temperatures to mobilize, resulting in the increased transition temperature. (77)

As reported in Table 6, T_g of VNG coating measured with DMTA is not significantly affected by adding fillers to obtain the NG sample. Indeed, it varies from 80 °C for VNG to 78 °C in NG. The effect of the fillers can be observed in the increase of E_r from 1.1 x 10^6 Pa of VNG to 2.7 x 10^7 Pa of NG. This finding can be ascribed to strong interactions between fillers and epoxy matrix that make NG stiffer than VNG. (75)

Table 6 - DMTA measures reporting glass transition temperature (Tg) and modulus at rubbery plateau (Er). Wet Tg has also been reported.

Coating	Dry T_g [°C]	Dry E_r [Pa]	Wet T_g [°C]
NG	78	2.7 e07	41
VNG	80	1.1 e06	40
RAD03	95	1.7 e07	38
VRAD03	125	2.9 e07	48

6.1.3 Adhesion

6.1.3.1 Pull-Off Test

This test uses a portable adhesion tester to measure the tensile force required to detach the coating from the substrate. High cohesive adhesion guarantees uniform surface coating coverage, avoiding the inclusion of air on the substrate.

Procedure.

Prepare a rectangular 20x50mm flat-coated sample. Ensure the coating is clean, dry, and contaminant-free. Abrade the coating's surface to ensure proper adhesion of the dolly (pull-off fixture). Apply an epoxy adhesive to the dolly (a cylindrical metal fixture) and press it firmly onto the coating. After the adhesive has cured, the portable adhesion tester is attached to the dolly. A gradual and uniform tensile force is applied perpendicular to the coating surface. The force is increased until the dolly detaches from the coating, and the pull-off strength is recorded. The test provides a quantitative value of adhesion expressed in megapascals (MPa). Examine the failure mode to determine whether the coating failed cohesively (within the coating) or adhesively (at the interface between the coating and the substrate).

Standards.

ASTM D4541: Standard Test Method for Pull-Off Strength of Coatings Using Portable Adhesion Testers.

ISO 4624: Paints and Varnishes — Pull-Off Test for Adhesion.

6.1.3.2 Analysis of Results

Adhesion tests were performed on four specimens right after curing and after immersion in HCl, 20 % solution for three days at ambient temperature and pressure (25 °C and 1 atm) to simulate the aggressive environment of oil and gas wells. (78) (79) The standard used to evaluate this test is a common practice of coating suppliers in the oil and gas sector in Europe and Asia: the minimum initial pull-off adhesion of 10 MPa is required for a coating to be considered suitable for metal protection. The adhesion cannot decrease over 50% of the adhesion value of the right prepared specimen (adhesion pristine), which is considered ideal for the test after acid immersion (indicated in brackets in Table 7).

As shown in Table 7, the adhesion of both thermal and UV-cured coatings improves significantly after filler addition. Although the retention of an adhesion higher than 10 MPa required by the quality standard applied by ELIXE srl is apparent, all the samples, UV and thermal cured, showed a reduction of adhesion upon immersion in a 20 % HCl solution.

Table 7 - Pull-off adhesion data were obtained for RAD03 with fillers, RAD03 without fillers, and NG coatings pristine after immersion in a 20% HCl solution.

Coating	Adhesion Pristine [MPa]	HCl a 20% three days [MPa]	Adhesion Loss (%)
NG	20.21 ± 0.66 (SE)	10.35 ± 4.00 (51%)	49 (cohesive failure)
VNG	16.80 ± 2.26 (SE)	8.15 ± 0.54 (49%)	51 (adhesive failure)
RAD03	25.00 ± 0.00 (SE)	14.91 ± 0.64 (60%)	40 (cohesive failure)
VRAD03	16.60 ± 0.50 (SE)	10.30 ± 1.50 (62%)	38 (adhesive failure)

RAD03 and NG coatings revealed a cohesive failure, while VRAD03 and VNG coatings had an adhesive failure. The adhesive failure of VRAD03 and VNG has been addressed to interaction forces between the polymer chains greater than those generated between polymer molecules and the metal substrate. Cohesive failure of the coatings can be addressed by the swelling of the coating by absorption of the 20 % HCl solution or degradation reactions of the resins, such as the epoxy ring opening reaction (80).

Further, NG adhesion is higher than VNG adhesion, 20.21 MPa and 16.80 MPa, respectively. RAD03 has an adhesion of 25.00 MPa, which is the upper limit of the instrument used, meaning that the coating does not break from the substrate. As expected, VRAD03 has an adhesion of 16.60 MPa, lower than RAD03, because of the filler's absence. The increasing adhesion conferred by the filler can be explained by the effect the inorganic particles have on the crack propagation inside the polymeric matrix: fillers create bridges across the initial forming cracks, hindering delamination. (81) After HCl immersion, RAD03, both filled and unfilled, also shows a more excellent adhesion compared to the tests performed in standard conditions, with 62% of initial adhesion for the unfilled version and 60% for the filled one respectively, and overall higher than 10.00 MPa.

Figure 45 shows pictures of the pull-off test adhesion samples.

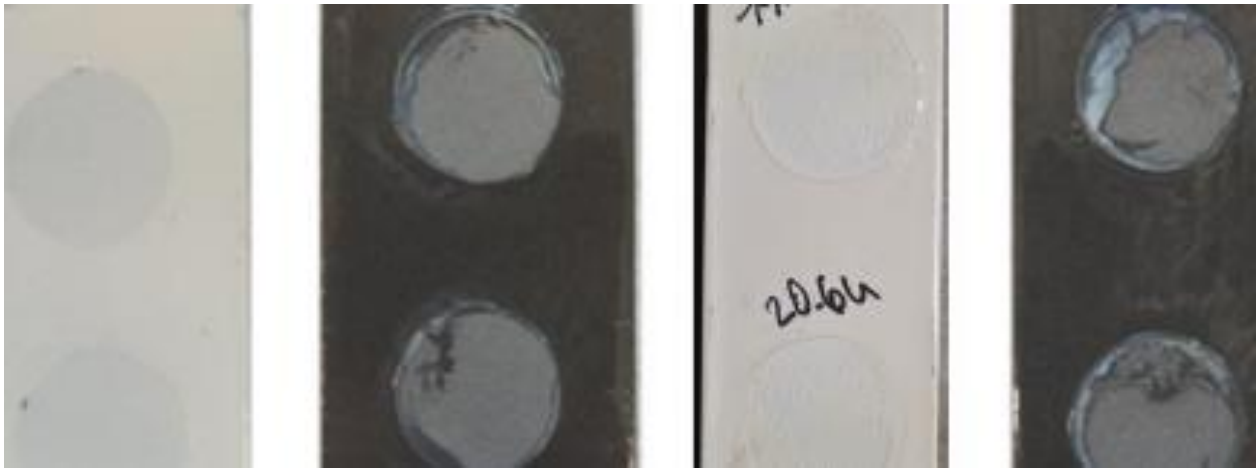

Figure 45 - Picture of the pull of test adhesion of NG, VNG, RAD03, and VRAD03.

6.2 Electrochemical Characterization

Impedance analysis allows us to analyze the electrochemical process of metal under corrosion. To simulate a longer process, the EIS test was conducted with varying immersion times in 3.5 % NaCl water, spanning 1, 7, 14, and 28 days, with results showing minimal variation between different periods, demonstrating the coating's integrity over the given timeframes. To accelerate the time-based verification, the ACET test was introduced, which applies a stress cycle to accelerate coating aging. Since the primary objective is to conduct a comparative test between the UV-cured and reference coating, the long-term durability verification was replaced with the ACET test.

6.2.1 Electrochemical Impedance Test

6.2.1.1 Electrochemical Impedance Spectroscopy (EIS)

The EIS is a powerful, non-destructive technique widely used to evaluate the corrosion protection performance of coatings, inhibitors, and materials in a corrosive environment. It provides detailed information on materials' resistance and capacitive behavior by measuring their response to an applied alternating current (AC) signal across various frequencies.

Procedure.

To better reproduce the objective conditions, the cylinder containing the solution is obtained using a 120-mm-long, 63-mm-diameter pipe coated with the paint sample to be tested and sealed on the bottom with a 3-mm-thick methyl-methacrylate plate (Figure 46). The electrolyte solution is water with 3.5 % NaCl to simulate a highly corrosive environment.

Figure 46 and 47 - Electrochemical cell using a coated pipe cylinder

The coating was applied using the machine presented in Section 5, obtaining a 100 µm thick layer on the inner surface of the pipe

The electrochemical cell positioned in the pipe cylinder consists of three electrodes:

- Working Electrode (WE): connected to the pipe-pot
- Counter Electrode (CE): platinum.
- Reference Electrode (RE): silver/silver chloride (Ag/AgCl).

The Frequency Response Analyzer (model Autolab with Nova software) is connected to the electrochemical cell. The potentiostat applies a small AC potential and measures the current response. The frequency range is between 10^{6} and 10^{-2} Hz, and the AC signal amplitude of 10 mV is set to ensure a linear system response.

Measurement Procedure: Stabilize Circuit Potential for 10 minutes before starting the impedance measurement. Apply the AC voltage perturbation over the selected frequency range. The system's impedance is recorded at each frequency, recording both the magnitude and phase angle of the impedance. The data are then represented in two plots:

- Impedance |Z| and phase angle vs. frequency (Bode Plot) measured at different temperatures
- Real impedance |Z'| vs. imaginary impedance |Z''| (Nyquist Plot) not considered for our study

The extracted parameters are used to evaluate the system's electrochemical properties, such as corrosion resistance and the effectiveness of protective coatings.

Comparing the impedance spectra at different conditions, such as time, temperature, or exposure to corrosive environments, assesses the system's stability and performance.

As a result, a third plot has been evaluated in this study:

- impedance |Z| vs. Temperature at 0.1 Hz frequency

Standard.

ISO 16773: Electrochemical Impedance Spectroscopy (EIS) on Organic Coatings on Metallic Substrates

6.2.1.2 Analysis of Results

Impedance |Z| and phase angle vs. frequency (Bode Plot) at different temperatures.

Generally, the higher the coating's impedance at low frequencies at a defined temperature, the higher its barrier properties and corrosion protection; a coating is considered to have good corrosion protection if its impedance measured at low frequencies is higher than 10^6 Ω cm^2 (82) (83) (84) (85). On this basis, all the tested coatings demonstrated excellent corrosion protection behavior at room temperature as their impedance at low frequency is between 9.5 $x10^8$ Ω cm^2 and $2x10^{10}$ Ω cm^2

When the coating behaves primarily as a capacitor, only charge and discharge processes occur at the interface of the WE and the electrolyte; no electrochemical reactions occur because the diffusion of the electrolyte through the coating network is hindered by its barrier properties microstructure. In this case, the Bode plot of the coating is a straight line with a slope of -1 (82), as can be seen on the low-temperature EIS curves of the NG coating in Figure 48 and RAD03 in Figure 50.

On the other hand, when the electrolyte starts to penetrate inside the polymer microstructure, the coating begins to swell due to electrolyte absorption. It has less capacitive behavior, facilitating the possibility of electrochemical reactions on the metal surface. In this case, the |Z| curves show a plateau at low frequencies, and the coating behaves less as a capacitor. This behavior can be observed in the coatings specimens formulated without fillers VNG and VRAD03 in the temperature range studied, from 20 °C to 90 °C, respectively, Figure 49 a and Figure 51. As expected, VNG and VRAD03 do not contain fillers; thus, they cannot hinder electrolyte permeation even at low temperatures.

While in RAD03, the behavior change occurs at 30 °C, NG coating shows the change at 50 °C. For RAD03 and NG coating, the permeation of electrolytes inside the coating layer starts when heating stress affects the viscoelastic properties of the coating, bringing to a change of the microstructure and, of course, a change of the barrier properties. Even if the filler species and their relative concentration are the same, for both RAD03 and NG, the total amount in RAD03 is lower than in NG coating; for this reason, the change of behavior in RAD03 occurs first, then in NG coating.

Moreover, as demonstrated from the Tg data achieved by DMTA, the faster electrochemical behavior change of RAD03 can be ascribed to a less uniform cross-linking of the resin matrix due to the scattering of the UV curing light of the filler particles, resulting in a RAD03 Tg lower of 30 °C than the one obtained for VRAD03. The poor cross-linking uniformity of RAD03 explains even the electrochemical behavior difference to NG coating, for which, as supported by their Tg values, the cross-linking occurs with negligible difference by its relative without fillers, VNG.

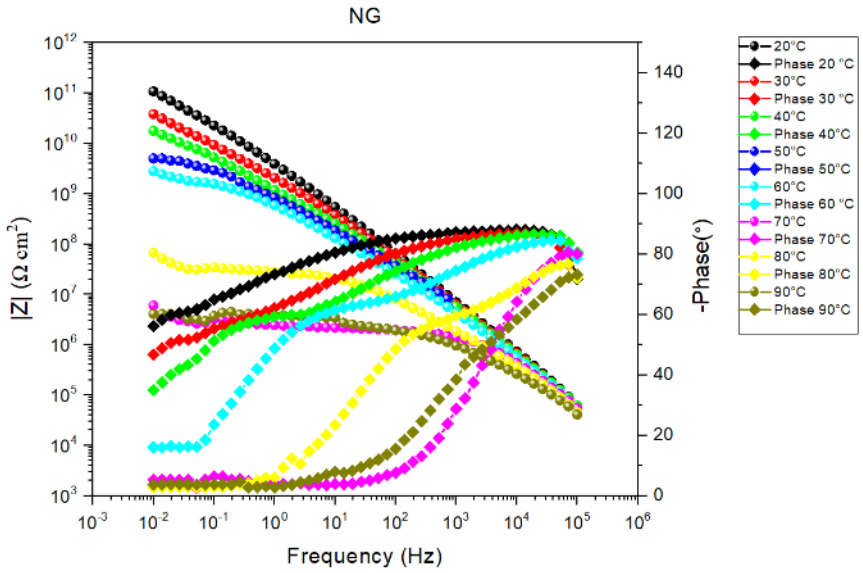

Figure 47 - EIS Bode plots of NG at different temperatures

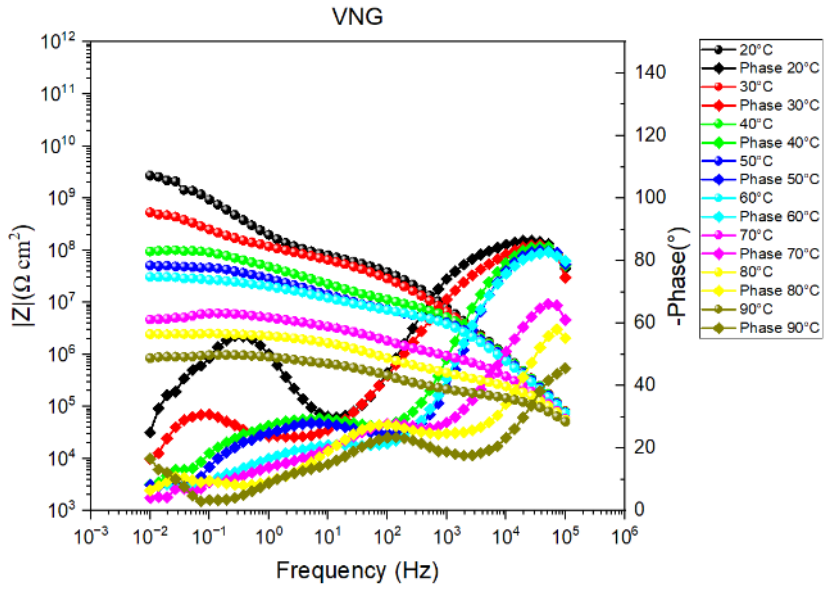

Figure 48 - EIS Bode plots of VNG at different temperatures

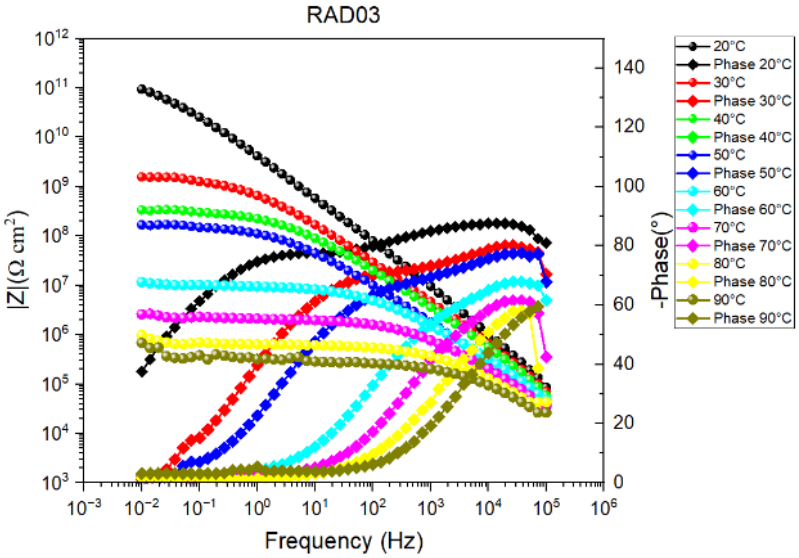

Figure 50 - EIS Bode plots of RAD03 at different temperatures

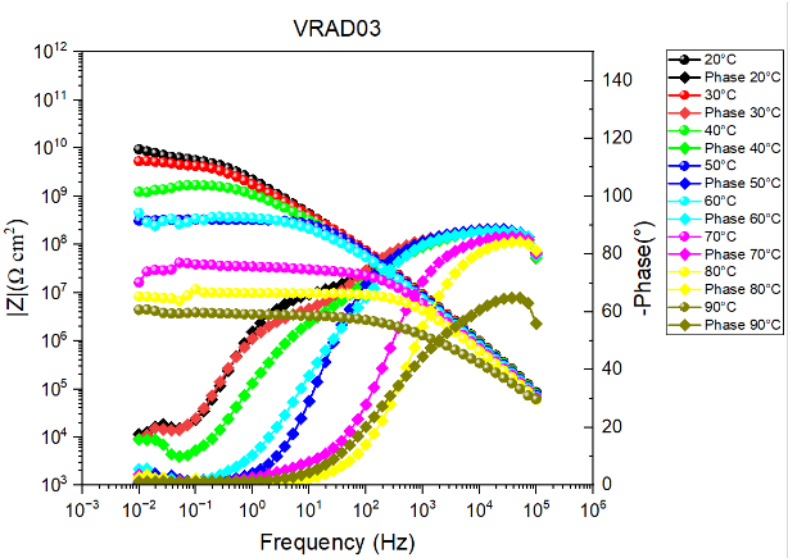

Figure 49 - EIS Bode plots of VRAD03 at different temperatures

Impedance |Z| vs. Temperature at fixed frequency

The impedance modulus |Z| generally decreases with increasing temperature for all the coatings, as the combined effect of heat and electrolyte penetration influences their mechanical properties. This impacts the coating's corrosion protection and causes its behavior to change from mainly capacitive to mainly resistive. As a result of increasing temperature, the impedance varies differently for the different coatings (Figure 52).

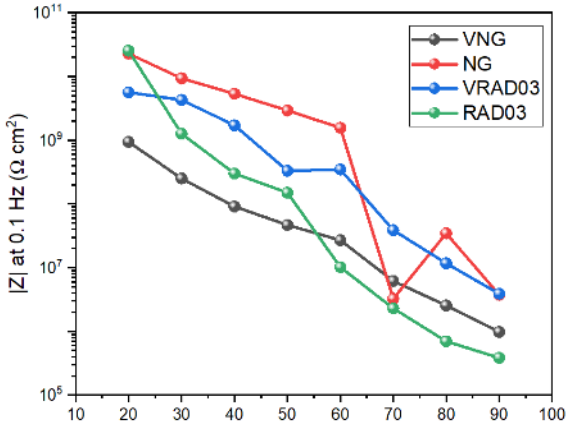

Figure 52 - Comparison of the |Z| collected at 0.1 Hz in the function of temperature obtained for VNG, NG, VRAD03, and RAD03.

The coatings VNG and VRAD03 formulated without fillers show |Z| values at 0.1 Hz lower than their relatives' containing fillers. The lower |Z| values for VNG and VRAD03 can be ascribed to the absence of fillers facilitating the electrolyte permeation inside the coating layer. VRAD03 shows |Z| values higher than VNG in the temperature range between 20 ˚C and 40 ˚C, likely due to the different curing technology. Solvents in VNG can create defective points when solvents evaporate during the curing process.

|Z| decrease in the function of temperature for VRAD03 occurs slower than RAD03, despite the absence of fillers. This behavior, at first counterintuitive, can be explained considering that fillers do increase the barrier properties of the UV-curable coating, as can be seen by the higher |Z| at room temperature of RAD03. However, they also decrease the overall crosslinking density by lowering the light penetration through the coating, as seen in Table 6 Section 6.1.2.2, consequently reducing glass transition temperature (T_g).

Despite RAD03 at 20 ˚C showing |Z| higher than NG, it decreases steeply, increasing the temperature: at 30 ˚C, the |Z| of RAD03 reaches 1.3 x10^9 Ω cm^2. |Z| decrease for NG coating is slower than RAD03; it reaches 1.6 x 10^9 Ω cm^2, heating up to 60 ˚C. The different rates of |Z| for RAD03 and NG coatings can be due to the different concentrations of fillers inside the coatings: RAD03 contains almost 20 % of fillers less than NG, allowing a less efficient barrier when temperature increase facilitates electrolyte permeation process inside the coating layer.

In the end, from the |Z| profiles plotted in the function of the temperature, each coating has a critical temperature between 50-60 ˚C at which a change of slope occurs. J. Li et al. (86) suggested that the temperature at which the slope change occurred is the temperature T_g of the aqueous electrolyte plasticized film, lower than the dry T_g. This temperature, named "wet T_g," represents the temperature at which the capacitive coating behavior turns resistive due to a more favorable water absorption into the coating. (79)

At temperatures higher than the wet T_g, the coatings undergo a swelling phenomenon due to electrolyte absorption, which consequently has a detrimental effect on their microstructure. This negatively affects their corrosion performance, as the decrease of |Z| suggests.

6.2.2 Accelerated Cyclic Electrochemical Test

6.2.2.1 Accelerated Cyclic Electrochemical Techniques (ACET)

ACET is a specialized method for evaluating the corrosion resistance of materials, particularly in aggressive environments where metals experience cycles of stress and recovery.

The main goal of ACET is to simulate real-world environmental conditions, such as alternating between corrosive exposure and recovery, to evaluate the material's susceptibility to corrosion. This helps assess the long-term durability and performance of metals or alloys, particularly in harsh environments like marine, industrial, or chemical applications.

Procedure:

The general procedure is the same as that used for the EIS test. Cyclic polarization sweeps are applied to the test specimen, repeatedly changing the electrochemical potential between the anodic at -4 V (corrosive) and cathodic at -1.5 V (passive or recovery) states. These cycles are designed to accelerate the corrosion processes, allowing quicker evaluation of the material's resistance to corrosion over time. Testing is performed in a chloride-containing solution (3.5 % NaCl), which simulates aggressive environments.

Standard.

ASTM Standard G199-09 (2014) - Accelerated Cyclic Electrochemical Techniques (ACET).

ACET often integrates existing electrochemical standards, combining aspects of cyclic electrochemical methods.

6.2.2.2 Analysis of Results

Impedance |Z| and phase angle vs. frequency (Bode Plot) at different numbers of cycles.

ACET method is usually applied to quickly evaluate protection performance when the coating is subjected to marine conditions. (87) (88) (89) The cathodic polarization drives two different processes into the coating layer:

The absorption and migration of electrolyte cations such as H^+ and Na^+ through the coating are due to the negative potential imposed at the metallic substrate surface. The concentration of positive charges in the coating must be neutralized by entering anions such as OH^- and Cl^-. The passage of ions (which can also be hydrated) through the coating can cause its deterioration and the formation of pores. (87)

The water reduction at a negative potential leads to H_2 gas evolution onto the metallic surface. The cathodic reaction is the following:

$$2H_2O + 2e^- \rightarrow H_2 + 2OH^- \qquad (7)$$

Water reduction will occur first if the electrolyte passes through the coating and reaches the interface. The evolution of H_2 increases local delamination, leading to the failure of the coating system, which is reflected in the impedance variation (90).

The successful occurrence of these two processes depends on the coating properties such as permeability to ions, adhesion to the substrate, local film delamination, susceptibility of the coating to form cracks because of its high rigidity, and, of course, the cathodic potential applied. Figures 53 to 56 report the ACET Bode plots of NG coating, VNG, RAD03, and VRAD03. The measurement indicated as n=0 is the measurement acquired before the first polarization.

The reference coating, NG coating, has shown excellent corrosion protection even after seven cycles at -4 V cathodic polarization and subsequent relaxation. Its Bode plot (Figure 53) shows negligible difference in impedance between the consecutive cycles, which is stable around 1 x 10^{11} Ω cm^2. Thus, the migration of electrolyte ions into the NG coating layers and the occurrence of water reduction reaction at the metal surface is hindered by its microstructure, which is made by the stacking of the fillers present in the coating. The importance of the filler is highlighted by the bode plot of VNG coating samples (Figure 54).

The VNG paint has poorer protection performance than NG coating with fillers. The impedance value remains around 1 x 10^7 Ω cm^2 during the ACET cycles, showing a negligible decrease. The electrochemical behavior of VNG coating is also different, as VNG has a less capacitive behavior. It agrees with the poorer corrosion protection performance due to the absence of fillers that can create a passive barrier and a more tortuous path for the electrolyte ion's migration through the coating layers. Thus, the lack of fillers in VNG favors the ion's absorption and migration process.

The Bode plot of RAD03 is reported in Figure 55. The Bode plot of RAD03 coating shows an impedance decrease from 2.6×10^{11} Ω cm^2 to 2.3×10^7 Ω cm^2 during the test. After the fourth cycle, the impedance has a negligible reduction and remains fixed around 2.3×10^7 Ω cm^2. It turns less performant after the second cycle of the experiment, suggesting a coating feature change upon the second cathodic polarization application. No blistering has been observed on the coating sample during the experiment. The Bode plot revealed only one process occurring, which could be related to ion absorption and migration inside the coating. The change in RAD03 behavior with fillers can be due to the shift in permeability to ions and coating surface porosity due to the cathodic polarization during the test.

In the end, Figure 56 shows the Bode plot of VRAD03. The shows a change in its electrochemical behavior upon the first cathodic polarization cycle. The faster-turning behavior of VRAD03 is likely due to the absence of fillers in its formulation, which favors the ion's absorption and migration process. This hypothesis is supported by only one process in the Bode plot and the absence of coating blistering during the experiment.

Another hypothesis is that a lower concentration of fillers can result in a less homogenous layer, which could lead to weak points in the coating. To develop this discussion, a separate, deeper study of the coating is necessary.

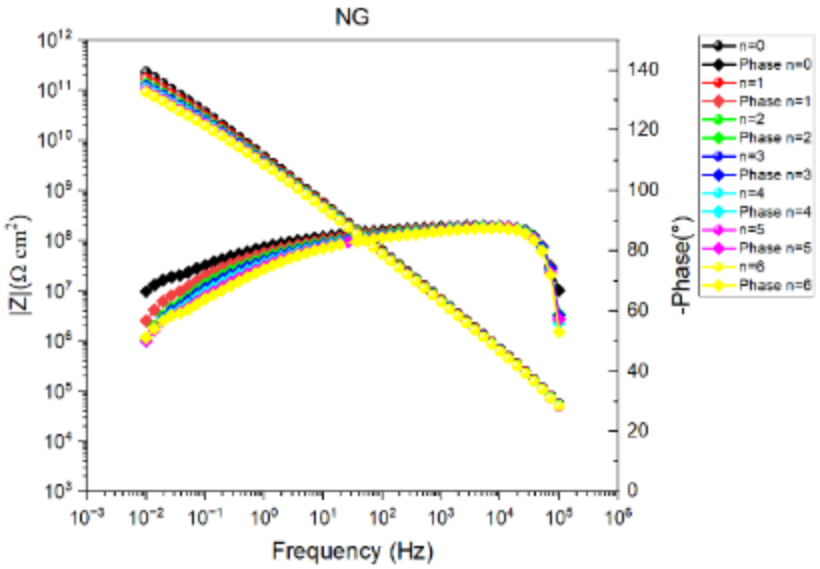

Figure 51 - ACET Bode plots of NG at different stress cycles.

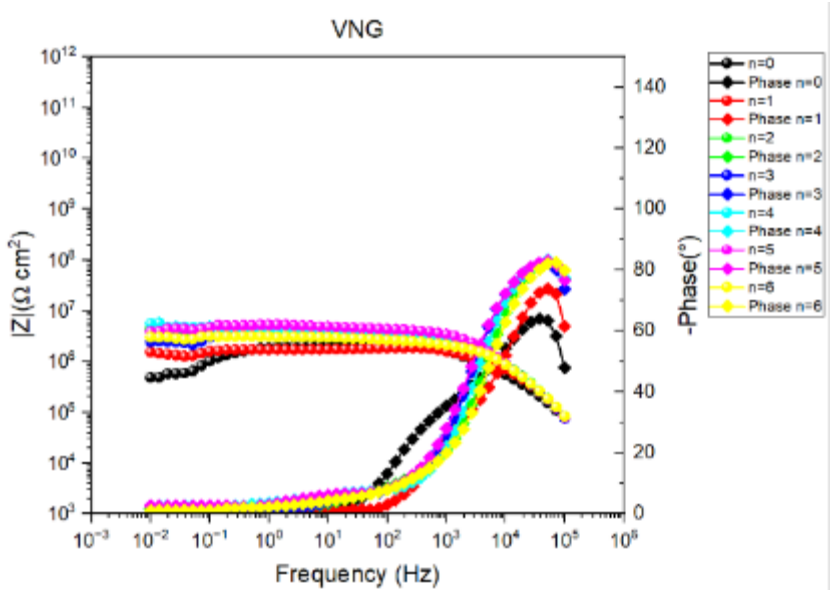

Figure 52 - ACET Bode plots of VNG at different stress cycles

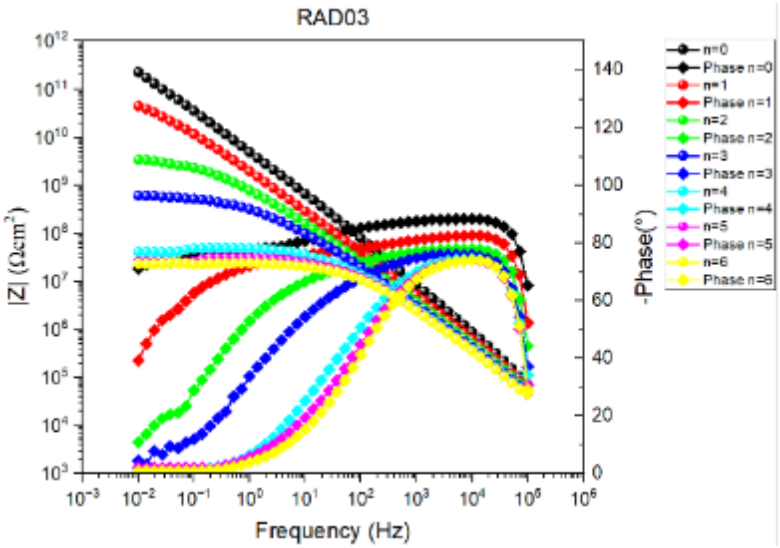

Figure 53 - ACET Bode plots of RAD03 at different stress cycles

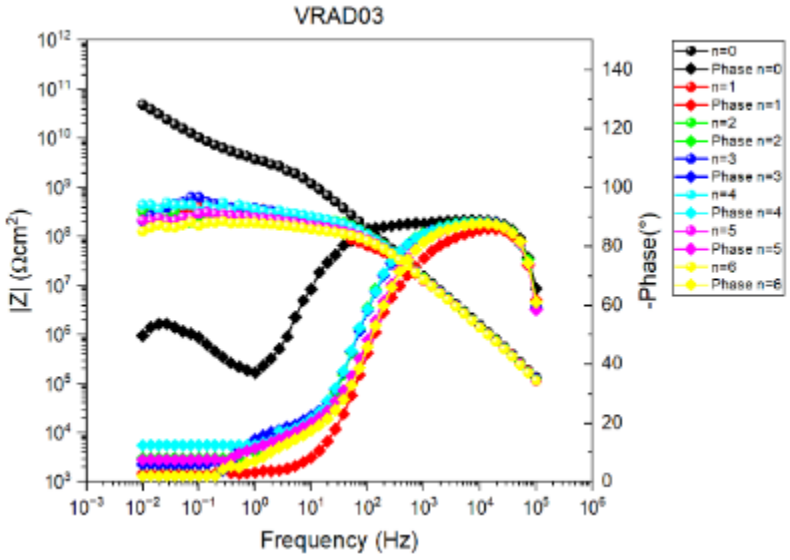

Figure 54 - ACET Bode plots of VRAD03 at different stress cycles

Impedance |Z| vs. number of cycles at fixed frequency

Figure 57 reports a plot of the |Z| profiles of each coating as a function of the number of cycles below to comprehend better the findings achieved by the ACET analysis.

As previously reported, by comparing the |Z| profiles as a function of the number of cycles performed during the ACET analysis, |Z| decrease among the consecutive cycles for NG coating is negligible, |Z| remains set in the order of 10^8 Ω cm^2. On the other hand, the reduction of |Z| RAD03 occurs faster within the first three cycles, reaching a plateau upon the fourth cycle. |Z| decrease of about four orders of magnitude.

Comparing the ACET findings achieved by investigating VNG and VRAD03, it is possible to observe that VRAD03 performs better than VNG. VRAD03 has |Z| values in the order of 10^8 Ω cm^2, while VNG has impedance in the order of 10^6 Ω cm^2. This resulted in an agreement with Curtarolo et al. (44) that accelerated corrosion testing on steel has shown superior corrosion resistance can be obtained with high-performance UV coatings compared to conventional epoxy and urethane corrosion resistance coating with much higher thicknesses.

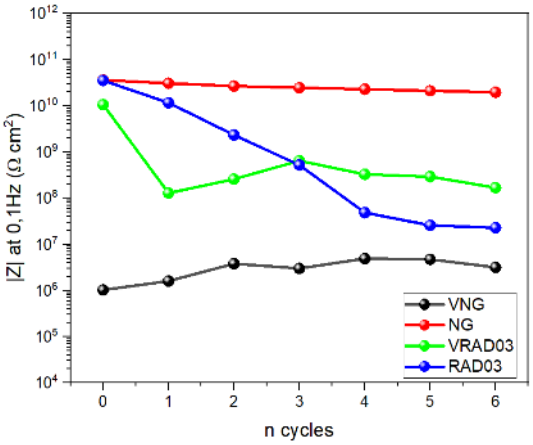

Figure 57 - Comparison of the |Z| collected at 0.1 Hz in the function of the number of cycles obtained for VNG, NG, VRAD03, and RAD03.

6.3 Conclusions of the Characterization

The characterization has provided valuable insights into the potential of replacing traditional thermal curing coating technology with more environmentally friendly UV curing coating technology. The technology developed for the UV-curable coating application has allowed us to treat the pipe specimens' inner surfaces effectively. By investigating RAD03 and comparing its performance to the established NG coating, we have demonstrated that UV coatings can provide comparable or superior corrosion protection. RAD03 showed stronger adhesion to steel substrates, even after exposure to acidic conditions, exceeding the performance of epoxy coatings.

However, considering the electrochemical characterization at different temperatures, RAD03 coating showed a faster decrease in impedance values than NG coating, reaching an impedance value lower than 1 x 10^8 Ω cm^2 at 90°C. This indicates the potential adverse effect of filler concentration on the overall barrier properties of the coating. Even after ACET analysis, it showed an impedance value lower than 1 x 10^8 Ω cm^2 upon the third cycle. Although the total concentration of fillers used in RAD03 was lower than in NG coating and ensured the complete curing of a 100 µm thick layer, further consideration should be given to the optimal total concentration of fillers. As demonstrated by the T_g values achieved by the DMTA analysis, the total amount of fillers used in RAD03 has detrimental effects on the uniformity of the cross-linking resin matrix.

Indeed, VRAD03, without fillers, displayed a capacitive behavior comparable to that of the NG coating even at temperatures as high as 90 °C, showing impedance values higher than 1 x 108 Ω cm2 and higher than the VNG coating when undergoing thermal stress, meaning higher corrosion

protection. Therefore, as demonstrated in this study, pure resin UV-curable coatings, applied at the same thickness as a traditional thermal curing coating, can provide comparable protective performance. However, a pure resin UV coating would not be a cost-effective product for the market; thus, filler use is preferable, and the optimal definition of its total concentration is necessary to obtain a filled UV-curable coating with improved protective performance than its relative without fillers and avoid possible detrimental effects during the UV curing reaction.

Ultimately, the strategy used in this study to easily convert a thermal curing coating into a UV curing coating achieved valid and exciting results, even if it should be improved in some aspects. These findings open promising avenues for future research. Subsequent studies may investigate the influence of various coating thicknesses and filler compositions on the corrosion protection behavior.

7 Conclusions and Related Work

Corrosion is an important issue during the design and development of new infrastructures and a significant cost of maintaining existing ones. Applying protective coatings to avoid corrosion is the most accessible and durable solution to corrosion issues. However, the application of thermal curing coating, particularly solvent-borne coating, has been demonstrated to have a detrimental impact on the environment and workplace health due to the emission of VOCs and the requirement of a large amount of energy for the curing process.

In this context, UV-curable coatings represent a promising solution since they overcome the main drawbacks of thermally cured coatings. They obtain process efficiency through reduced curing time (from hours to seconds), lower energy consumption, and improved environmental sustainability because of the absence of harmful VOCs in their formulation [14]. Despite their evident advantages, UV-curable coatings have rarely been applied to the inner surfaces of pipelines and narrow geometries due to the dimensional difficulties of bringing a UV light source inside these spaces.

During this research project, a novel and performant curing coating, a novel UV light source, and new equipment were designed, developed, and optimized to allow the application of UV technology to the corrosion protection of the inner surfaces of pipelines and narrow geometries.

The insights provided by the comparison study performed between RAD03, VRAD03 UV curable coatings, NG, and VNG as thermal curing coatings benchmark has demonstrated that UV curable coatings showed stronger adhesion to steel substrates, particularly RAD03, even after exposure to acidic conditions, exceeding the performance of NG thermal curing benchmark. Using the radical mechanism, and thus, applying UV LED in place of UV lamps, it has been possible to reduce the impact of the curing on the environment, avoiding mercury-containing waste production.

By electrochemical measurement, the corrosion protection performances have been evaluated and compared by using EIS characterization. The findings highlight the possible detrimental effects of the fillers' concentration used in RAD03 formulation, giving lower corrosion protection at increasing temperatures. This behavior can be ascribed to the decreased uniformity of the coating layer, which increases fillers' concentration. In the end, by comparing the features of the coating formulated without fillers, the role and performance of the resins used have been evaluated. VRAD03, when applied at the same thickness as a VNG, has been demonstrated to provide comparable protective performance. Notably, VRAD03 displayed a capacitive behavior similar to that of the NG coating even at temperatures as high as 90°C, showing impedance values higher than 1 x 108 Ω cm^2 and higher than the VNG coating when undergoing thermal stress, meaning higher corrosion protection.

The innovative UV LED light source here developed has been designed using a hexagonal model because it allowed the optimal equilibrium between a) dimensional requirements due to the minimal diameter characterizing pipes, b) the total number of LEDs for the array combination, and c) the minimum diameter of a cylindrical surface that could be uniformly irradiated considering the radial and linear radiation equal to 30 – 40 mm.

The source has been based on a 120 UV LEDs Luminus SST-10-UV array composed of 6 strips of 20 LEDs each, step 8 mm, fixed on a hexagonal aluminum support. The resulting radiant flux is Φ = 120 W with irradiation (or flux density) equal to 130 W/cm^2 calculated on a flat open surface and necessary to cross-link an epoxy photocuring paint.

In the end, the UV light source and the application of the rotary atomizer on the same equipment represent the innovative features of the equipment designed and developed here for applying and curing a UV-curable coating onto the pipe's inner surface.

The patent published by Legros et al. in 2015 reports a suitable system only for pipes with ID > 50 cm, using two UV lamps mounted onto a rail. As noted in this thesis, the equipment designed also allows for the treatment of pipes with an ID lower than 50 cm, using only one piece of equipment that can perform the paint application and the subsequent curing almost simultaneously.

The results achieved, thus, support the application of UV curable coatings to replace thermal curable coatings for the corrosion protection of the inner wall of pipes. In order:

a) further development studies of RAD03 formulation are ongoing to improve the formulation and test the so-prepared optimized RAD03 coating on the field;

b) Optimize the equipment working settings, particularly the UV light source and rotary atomizers, to improve the curing process and increase the quality of the UV-cured coring obtained.

The innovative characteristics of the technology investigated during this study project and reported in this thesis bring a step ahead into the field of steel corrosion protection. The application of UV technology to this field has fundamental innovative aspects concerning traditional thermal technology:

a) involves a smaller amount of energy;
b) involves lower amount of coating to cover the same number of pipes;
c) It allows maintenance operations to be performed directly on the field.

The pivotal features of UV technology for corrosion protection applications have been studied and developed, achieving innovative findings about:

- UV coating formulation;
- UV coating curing light source
- UV coating application;
- Design of equipment for application and curing of UV paint inside pipes.

A UV-curable coating formulation has been developed by evaluating the optimal amount of filler concentration to obtain a fully cured film of 100 µm thickness after exposure to 640 mW/cm2 for 60 seconds.

The insights provided by the comparison study performed on RAD03, VRAD03, NG, and VNG support what has been observed in the previous studies concerning the performance of UV-curable and thermal-curing coatings. UV curable coatings showed stronger adhesion to steel substrates, particularly RAD03, even after exposure to acidic conditions, exceeding the performance of NG. The corrosion protection performances have been evaluated and compared by using EIS characterization. The findings highlight the potential detrimental effects of the fillers' concentration used in RAD03 formulation, giving lower corrosion protection at increasing temperatures. This phenomenon can be ascribed to decreased uniformity of the coating layer, which increases fillers' concentration. In the end, by comparing the features of the coating formulated without fillers, the role and performance of the resins used have been evaluated. VRAD03, when applied at the same thickness as a VNG, has been demonstrated to provide comparable protective performance. Notably, VRAD03 displayed a capacitive behavior similar to that of the NG coating even at temperatures as high as 90°C, showing impedance values higher than 1 x 108 Ω cm^2 and higher than the VNG coating when undergoing thermal stress, meaning higher corrosion protection.

The results obtained support the application of UV curable coatings to replace thermal curable coatings for the corrosion protection of the inner wall of pipes. Further development studies of RAD03 formulation are ongoing to improve the formulation and test the so-prepared optimized RAD03 coating on the field.

The definition of a correct UV LED source is necessary to adequately cure a UV polymer used for protective organic coatings.

Regarding the curing of inner pipes using a UV LED light source, no one device able to provide practical, uniform irradiation respecting the dimensional constraints due to the dimensional features of the entry hole of gas cylinders and the tubes used for pipes and welling was available on the market. An innovative UV LED light source has been developed here. The hexagonal model selected among different geometrical models allows the optimal equilibrium between a) dimensional requirements due to the minimal diameter characterizing pipes, b) the total number of LEDs for array combination, and c) the minimum diameter of a cylindrical surface that could be uniformly irradiated considering the radial and the linear radiation equal to 30 – 40 mm.

The source is based on a 240 UV LED Luminus SST-10-UV array comprising six strips of 40 LEDs each, step 8 mm, fixed on a hexagonal aluminum support. The resulting radiant flux is Φ = 240 W with irradiation (or flux density) equal to 640 mW/cm^2 calculated on a 60 mm diameter 200 mm long pipe, which is necessary to cross-link an epoxy photocuring paint.

8 Bibliography

1. NACE International. (2023). “NACE international impact: NACE International report”. https://impact.nace.org/documents/Nace-International-Report.pdf (Accessed: April 17, 2023).

2. Pérez, T. E. (2013). Corrosion in the oil and gas industry: An increasing challenge for materials. “JOM”, “65”(11), 1033-1042.

3. Askari, M., Aliofkhazraei, M., Jafari, R., Hamghalam, P., & Hajizadeh, A. (2021). Downhole corrosion inhibitors for oil and gas production – A review. “Applied Surface Science Advances”, “6”, 100128. https://doi.org/10.1016/j.apsadv.2021.100128

4. Migahed, M. A., & Nassar, I. F. (2008). Corrosion inhibition of tubing steel during acidization of oil and gas wells. “Electrochimica Acta”, “53”(10), 2877-2882. https://doi.org/10.1016/j.electacta.2007.10.070

5. Sridhar, N., Thodla, R., Gui, F., Cao, L., & Anderko, A. (2017). Corrosion-resistant alloy testing and selection for oil and gas production. “Corrosion Engineering, Science and Technology”, “53”(1), 1-15. https://doi.org/10.1080/1478422X.2017.1384609

6. Alabtah, F. G., Mahdi, E., & Elyian, F. F. (2021). The use of fiber reinforced polymeric composites in pipelines: A review. “Composite Structures”, “276”, 114595. https://doi.org/10.1016/j.compstruct.2021.114595

7. Fan, L., Reis, S. T., Chen, G., & Koenigstein, M. L. (2018). Corrosion resistance of pipeline steel with damaged enamel coating and cathodic protection. “Coatings”, “8”(5), 185. https://doi.org/10.3390/coatings8050185

8. Hussain, A. K., Seetharamaiah, N., Pichumani, M., & Chakra, C. S. (2021). Research progress in organic zinc-rich primer coatings for cathodic protection of metals – A comprehensive review. “Progress in Organic Coatings”, “153”, 106040. https://doi.org/10.1016/j.porgcoat.2021.106040

9. Pourhashem, S., Ghasemy, E., Rashidi, A., & Vaezi, M. R. (2019). A review on the application of carbon nanostructures as nanofillers in corrosion-resistant organic coatings. “Journal of Coatings Technology and Research”, “17”(1), 19-55. https://doi.org/10.1007/s11998-019-00275-6

10. Cunningham, M. F., Campbell, J. D., Fu, Z., Bohling, J., Leroux, J. G., Mabee, W., & Robert, T. (2019). Future green chemistry and sustainability needs in polymeric coatings. “Green Chemistry”, “21”(20), 4919-4926. https://doi.org/10.1039/C9GC02462J

11. Dick, F. D. (2006). Solvent neurotoxicity. “Occupational and Environmental Medicine”, “63”(3), 221-226. https://doi.org/10.1136/oem.2005.022400

12. Schoff, C. K. (2005). Organic coatings: The paradoxical materials. “Progress in Organic Coatings”, “52”(1), 21-27. https://doi.org/10.1016/j.porgcoat.2004.05.001

13. Javadi, A., Mehr, H. S., Sobani, M., & Soucek, M. D. (2016). Cure-on-command technology: A review of the current state of the art. “Progress in Organic Coatings”, “100”, 2-31. https://doi.org/10.1016/j.porgcoat.2016.02.014

14. Khan, A., Balakrishnan, K., & Katona, T. (2008). Ultraviolet light-emitting diodes based on group three nitrides. “Nature Photonics”, “2”(2), 77-84. https://doi.org/10.1038/nphoton.2007.293

15. Li, D., Jiang, K., Sun, K., & Guo, C. (2018). AlGaN photonics: Recent advances in materials and ultraviolet devices. “Advanced Optical Materials”, “10”(1), 43-110. https://doi.org/10.1364/AOP.10.000043

16. Wang, Z., Tang, W. Z., Sillanpää, M., & Li, J. (2022). UV disinfection sensitivity index of spores or protozoa: A model to predict the required fluence of spores or protozoa. “Water Science and Technology”, “86”(9), 2820-2833. https://doi.org/10.2166/wst.2022.391

17. Dreyer, C., & Franziska, M. (2016). Application of LEDs for UV curing. In “III-Nitride Ultraviolet Emitters” (Vol. 227, pp. 415-434). https://doi.org/10.1007/978-3-319-24100-5_15

18. Stowe, R. W. (1999). Practical aspects of irradiance and energy in UV curing. “IAEA Publications”. https://inis.iaea.org/collection/NCLCollectionStore/_Public/31/016/31016357.pdf

19. Brondel, D., Edwards, R., Hayman, A., Hill, D., Mehta, S., & Semerad, T. (1994). Oilfield review, “4”-18.

20. Tuttle, R. N. (1987). J. Pet. Technol., “756”-762.

21. Cole, I. S., & Marny, D. (2012). Corrosion science. “Journal of Corrosion Science”, “56”(1), 5-16.

22. Lyon, S. B. (2017). Progress in organic coatings. “Progress in Organic Coatings”, “102”, 2-7.

23. Mayne, J. E. O. (1954). Anti-corrosion methods and materials. “Anti-Corrosion Methods and Materials”, “1”, 286-290.

24. Kenig, S., Deflorian, F., & Cafagna, R. (2010). “Proceedings of the 30th FATIPEC Conference”. Genoa, Italy: s.n.

25. Nguyen, T., Hubbard, J. B., & Pommersheim, J. M. (1996). Journal of coatings technology. “Journal of Coatings Technology”, “68”, 45-56.

26. Kinsella, E. M., & Mayne, J. E. O. (1969). British Polymer Journal. “British Polymer Journal”, “1”, 173-176.

27. Mayne, J. E. O., & Scantlebury, J. D. (1970). British Polymer Journal. “British Polymer Journal”, “2”, 240-243.

28. Jamali, S. S., & Mills, D. J. (2013). Corrosion engineering, science and technology. “Corrosion Engineering, Science and Technology”, “48”, 489-495.

29. P. Legross, V. Stone, E. Gonzales (2015). US 2015/0167706 United States.

30. Kjoller, K., Felts, J. R., Cook, D., Prater, C. B., & King, W. P. (2010). “Nanotechnology”, “21”.

31. Morsch, S., Lyon, S. B., Greensmith, P., Smith, S. D., & Gibbon, S. R. (2015). Faraday discussions. “Faraday Discussions”, “180”, 527-542.

32. Morsch, S., Liu, Y., Lyon, S. B., & Gibbon, S. R. (2016). Applied materials and interfaces. “Applied Materials and Interfaces”, “8”, 959-966.

33. Funke, W. (1979). Journal of oil color and chemical association. “Journal of Oil Color and Chemical Association”, “63”.

34. Funke, W., & Leidheiser, H. (1987). Journal of oil color and chemical association. “Journal of Oil Color and Chemical Association”, “70”, 121.

35. Harun, M. K., Marsh, J., & Lyon, S. B. (2005). Progress in organic coatings. “Progress in Organic Coatings”, “54”, 317-321.

36. Hughes, A. E., Birbilis, N., Mol, J. M. C., Garcia, S. J., Zhou, X., & Thompson, G. E. (2011). Z. Ahmad Edition.

37. Hughes, A. E., Boag, A., et al. (2006). “Proceedings of Aluminium Surface Science and Technology”, ATB Metallurgie, Beaune, France: s.n. “45”, 551-556.

38. Marsh, J., Scantlebury, J. D., & Lyon, S. B. (2001). Corrosion science. “Corrosion Science”, “43”, 829-852.

39. ur Rahman, O., Kashif, M., & Ahmad, S. (2015). Progress in organic coatings. “Progress in Organic Coatings”, “80”, 77-86.

40. Kim, J., Lim, W., Lee, Y., Kim, S., Park, S. R., Suh, S. K., & Moon, I. (2011). Industrial & engineering chemistry research. “Industrial & Engineering Chemistry Research”, “50”, 8272-8277.

41. Wang, S., Ang, H., & Tade, M. O. (2007). Environmental international. “Environmental International”, “33”, 694-705.

42. Giuliani, A., Giunta, D., & Condini, A. (2020). “ADIPEC 2020”. Abu Dhabi: s.n.

43. Noè, C., Iannucci, L., Malburet, S., Graillot, A., Sangermano, M., & Grassini, S. (2021). Macromolecular materials and engineering. “Macromolecular Materials and Engineering”, “306”.

44. Curtarolo, B. (2014). “Rad Tech”. Berea, OH, USA: s.n. UV technology for protection of surface.

45. Golden, R. (2005). Low-emission technology: A path to greener industry. “RadTech 2005”, 14-18.

46. Deflorian, F., & Fedel, M. (n.d.). UV-curable organic polymer coatings for corrosion protection of steel. pp. 530-559.

47. Engberg, D. (2019). Market overview 2019. “RadTech 2019”. Monaco: s.n.

48. O'Kefee, M., Fahrenholtz, W., & Curatarolo, B. (2010). Multifunctional UV (MUV) curable corrosion coatings for aerospace applications. “Metal Finishing”, 28-31.

49. Li, T., Zhang, Z. P., Rong, M. Z., & Zhang, M. Q. (2019). Journal of applied polymer science. “Journal of Applied Polymer Science”, “136”(26), 47700.

50. Jafarzadeh, S., Adhikari, A., Sundall, P., & Pan, J. (2011). Progress in organic coatings. “Progress in Organic Coatings”, “70”, 108-115.

51. Rahman, O., Kashif, M., & Ahmad, S. (2015). Progress in organic coatings, 80, 77-86.

52. Dreyer, C., & Mildner, F. (2016). Applications of LEDs for UV curing. In “Advances in polymer science” (pp. 415-434). Springer International Publishing.

53. Gaidukovs, S., Medvids, A., Onufrijevs, P., & Grase, L. (2018). Express polymer letters, 12, 918-929.

54. Liu, G., Zhu, X., Xu, B., Qian, X., Song, G., & Nie, J. (2013). “Journal of the American Chemical Society”, 130, 3698-3703.

55. Noè, C., Iannucci, L., Malburet, S., Graillot, A., Sangermano, M., & Grassini, S. (2021). Macromolecular materials and engineering, 306.

56. Varela Caselisa, J. L., Rubio Rosas, E., Santamaría Juárez, J. D., Galicia Aguilar, J. A., Sánchez Cantú, M., Olivares Xometl, O., & Morales Sánchez, M. (2018). Corrosion engineering, science and technology, 53(5), 362-369.

57. Peng, C., Chang, K., Weng, C., Lai, M., Hsu, C., Hsu, S., Li, S., Weib, Y., & Yeh, J. (2013). Polymer chemistry, 4, 926.

58. Skinner, D. (2019). "RadTech 2019". Monaco: s.n.

59. Strehmel, B. (2013). CHEManager, 6.

60. Uhl, A., Mills, R. W., & Vowels, R. W. (2002). Journal of biomedical materials research, 63, 729-738.

61. Vandewalle, K. S., Roberts, H. W., & Nadrus, J. L. (2005). Journal of esthetic and restorative dentistry, 17, 244-255.

62. Neckers, D. C., Federov, A. V., & Anayaogu, K. C. (2007). Journal of applied polymer science, 105, 803-808.

63. Salleh, N., Ghazali, N., Mohd, Y., Azman, H., Aznizam, B., & Munirah, M. (2009). The effect of radiation dosages and UV/EB radiation on the properties of nanocomposite coatings. "International Journal of Polymeric Materials", 58, 384-399. https://doi.org/10.101.

64. Moreno, I., & Viveros-Méndez, P. X. (2021). Modeling the irradiation pattern of LEDs at short distances. "Optics Express", 29, 6845-6853. https://doi.org/10.1364/OE.419428.

65. Optical modeling for the LED radiation patterns. Retrieved from http://rportal.lib.ntnu.edu.tw:8080/server/api/core/bitstreams/2d2f1c3f-2779-4056-bae9-11567a2860c9/content (accessed April 17, 2023).

66. Moreno, I., & Sun, C. (2008). Modeling the irradiation pattern of LEDs. "Optics Express", 16, 1808-1819. https://doi.org/10.1364/OE.16.001808.

67. Rachev, I., Djamiykov, T., Marinov, M., & Hinov, N. (2019). Improvement of the approximation accuracy of LED radiation patterns. "Electronics", 8, 337. https://doi.org/10.3390/electronics8030337.

68. H. Ramli, N. Zainal, M. Hess, C. Chan, (2022). Chem. Teach. Int., Vol. 4, p. 307-326.

69. Ye, Q., & Pulli, K. (2017). Numerical and experimental investigation on the spray coating process using a pneumatic atomizer: Influences of operating conditions and target geometries. "Coatings", 7(1), 13. https://doi.org/10.3390/coatings.

70. Venkata Krishna, W., Liu, W., & Owkes, M. (2023). High-fidelity simulations of a rotary bell atomizer with electrohydrodynamic effects. "International Journal of Multiphase Flow", 168, 104566.

71. Domnick, J., Scheibe, A., & Ye, Q. (2006). The simulation of electrostatic spray painting process with high-speed rotary bell atomizers. "Particle and Particle Systems Characterization". https://doi.org/10.1002/ppsc.200601018.

72. Soma, T., Katayama, T., Tanimoto, J., Saito, Y., Matsushita, Y., Aoki, H., Nakai, D., Kitamura, G., Miura, M., Asakawa, T., Daikoku, M., Haneda, T., Hatayama, Y., & Shirota, M. (Year). Liq.

73. Asbeck, W. K., & Van Loo, M. (1949). Critical pigment volume relationships. “Industrial & Engineering Chemistry”, 41, 1470-1475.

74. Shagh, P. K., & Stansbury, J. W. (2014). Role of filler and functional group conversion in the evolution of properties in polymeric dental restoratives. “Dental Materials”, 30, 586-593.

75. Gheith, M. H., Aziz, M. A., Ghory, W., Saba, N., Asim, M., Jawaid, M., & Alothman, O. (2019). Flexural, thermal, and dynamic mechanical properties of date palm fibres reinforced epoxy composites. “Journal of Materials Research and Technology”, 8, 853-860.

76. Ramli, H., Zainal, N., Hess, M., & Chan, C. (2022). Basic principle and good practices of rheology for polymers for teachers and beginners. “Chemistry Teacher International”, 4, 307-326.

77. Toft, M. (2011). The effect of crystalline morphology on the glass transition and enthalpic relaxation poly(ether-ether-ketone) (Unpublished master’s thesis). University of Birmingham, Birmingham, UK.

78. Brondel, D., Edwards, R., Hayman, A., Hill, D., Mehta, S., & Semerad, T. (1994). Corrosion in the oil industry. “Oilfield Review”, 4-18.

79. Giuliani, A., Giunta, D., & Condini, A. (2020). Advancing in liquid coatings: High performant liquid epoxy coating for oil well tubing, high temperature and high pressure resistant. “ADIPEC”.

80. Verma, C., Olasunkanmi, L. O., Akpan, E. D., Quraishi, M. A., Dagdag, O., El Gouri, M., Sherif, M., & Ebenso, E. E. (2020). Epoxy resins as anticorrosive polymeric materials: A review. “Reactive and Functional Polymers”, 156, 104741.

81. Wei, H., Xia, J., Zhou, W., Zhou, L., Hussain, G., Lin, Q., & Ostrikov, K. (2020). Adhesion and cohesion of epoxy-based industrial composite coatings. “Composite Part B: Engineering”, 193.

82. Gray, G. S. L., & Bernard, R. (2003). EIS: Electrochemical impedance spectroscopy: A tool to predict remaining coating life? “Journal of Protective Coatings & Linings”, 20, 66-74.

83. Noè, C., Iannucci, L., Malburet, S., Grallot, A., Sangermano, M., & Grassini, S. (2021). New UV-curable anticorrosion coatings from vegetable oils. “Macromolecular Materials and Engineering”, 306.

84. Cristoforetti, A., Rossi, S., Deflorian, F., & Fedel, M. (2023). On the limits of the EIS low-frequency impedance modulus as a tool to describe the protection of organic coatings exposed to accelerated aging tests. “Coatings”, 13.

85. Margarit-Mattos. (2020). ICP EIS and organic coatings performance: Revisiting some key points. “Electrochimica Acta”, 354, 136725.

86. Li, J., Jeffcoate, C. S., Bierwagen, G. P., Mills, D. J., & Tallman, D. E. (1998). Thermal transition effects and electrochemical properties in organic coatings: Part 1—Initial studies on corrosion protective organic coatings. “Corrosion”, 54, 763-771.

87. Gimeno, M. J., Puig, M., Chamorro, S., Molina, J., March, R., Oro', E., Pérez, P., Gracenea, J. J., & Suay, J. J. (2016). Improvement of the anticorrosive properties of an alkyd coating with zinc

88. Gimeno, M. J., Chamorro, S., March, R., Oró, E., Pérez, P., Gracenea, J., & Suay, J. (2014). Anticorrosive properties enhancement by means of phosphate pigments in an epoxy 2K coating: Assessment by NSS and ACET. “Progress in Organic Coatings”, 77, 2024-2030.

89. D'Elia, M. F., Magni, M., Romanò, T., Trasatti, S. P. M., Niederberger, M., & Caseri, W. R. (2022). Smart anticorrosion coatings based on poly(phenylene methylene): An assessment of the intrinsic self-healing behavior of the copolymer. "Polymers", 14, Article 3457.

90. Gracenea, J. J. (2011). The fast lane to failure. "European Coatings Journal", 3.

91. Li, J., Jeffcoate, C. S., Bierwagen, G. P., Mills, D. J., & Tallman, D. E. (1998). Thermal transition effects and electrochemical properties in organic coatings: Part 1—Initial studies on corrosion protective organic coatings. "Corrosion", 54, 763-771.

92. Nyborg, R. (2009). CO_2 corrosion models for oil and gas production systems. "Corrosion", NACE International.

93. El-Meligi, A. A. (2010). Corrosion prevention strategies as a crucial need for decreasing environmental pollution and saving economics. "International Journal of Electrochemical Science", 5(2), 199-215.

94. Revie, R. W., & Uhlig, H. H. (2008). "Corrosion handbook". John Wiley & Sons.

95. Palmer, A. C., & King, R. A. (2004). "Subsea pipeline engineering". PennWell Corporation.

96. Fontana, M. G. (2005). "Corrosion engineering". McGraw-Hill.

97. Sinnott, R. K., & Towler, G. (2009). "Chemical engineering design: Principles, practice and economics of plant and process design". Butterworth-Heinemann.

98. Roberge, P. R. (2008). "Corrosion engineering: Principles and practice". McGraw-Hill Professional.

99. Davis, J. R. (2000). "Corrosion: Understanding the basics". ASM International.

100. Decker, C. (2001). UV-radiation curing chemistry. "Pigment & Resin Technology", 30(5), 278-286.

101. Czajkowski, W., & Marciniak, H. (2009). UV-curable coatings in corrosion protection. "Progress in Organic Coatings", 65(2), 284-292.

102. Musa, A. Y., Mohamad, A. B., & Kadhum, A. A. H. (2012). Corrosion protection of metals by UV-curable coatings: A review. "Journal of Coatings Technology and Research", 9(4), 385-393.

103. Pappas, S. P. (2013). "UV curing: Science and technology". Technology Marketing Corporation.

104. Stowe, R. A., & Hadjiiski, L. (2003). Radcure coatings: UV curing technology and applications. "Journal of Coatings Technology", 75(940), 57-62.

105. Sangermano, M., Malucelli, G., & Bongiovanni, R. (2002). UV-curable epoxy systems containing reactive diluents for coating applications. "Macromolecular Materials and Engineering", 287(8), 529-536.

106. Hirayama, C., Ruzik, D., & Yoshikawa, K. (2017). Recent advances in UV-curable coatings with enhanced performance characteristics. "Progress in Organic Coatings", 104, 1-16.

107. Bongiovanni, R., Sangermano, M., & Priola, A. (2001). UV-curing of epoxy resins in the presence of cationic photoinitiators: Kinetics and properties of coatings. "Journal of Applied Polymer Science", 81(12), 2939-2946.

108. Yu, Z., Yan, Z., Zhang, F., Wang, J., Shao, Q., Murugadoss, V., Alhadhrami, A., Mersal, G. A. M., Ibrahim, M. M., El-Bahy, Z. M., Li, W., & Guo, Z. (2019). Epoxy-based coatings for internal corrosion protection of steel pipes: Advances and challenges. “Progress in Organic Coatings”, 132, 65–77.

109. Genescá, M. J., Rodríguez-Gómez, F. J., & Ramírez-Salgado, D. (2020). Evaluation of epoxy coatings for internal protection of pipelines transporting oil and gas. “Surface and Coatings Technology”, 385, 125382.

110. Ram, M. K., Kumar, R., & Jain, R. (2020). Internal application of fusion-bonded epoxy coatings in pipelines: Properties and challenges. “Coatings”, 10(6), 554.

111. Al-Khaldi, T., Al-Jumah, A., & Al-Rashed, F. (2019). Corrosion protection of oil and gas pipelines using internal FBE coatings. “Journal of Pipeline Systems Engineering and Practice”, 10(1), Article 04018038.

112. Sun, Z., Wang, Y., Li, X., & Zhang, J. (2018). Polyurethane coatings for internal corrosion protection of water pipelines. “Journal of Materials in Civil Engineering”, 30(4), Article 04018052.

113. Cruz, J., & Andrade, F. (2019). Cement mortar linings for corrosion protection of water pipelines: A review of performance and durability. “Journal of Water Supply: Research and Technology—AQUA”, 68(1), 1-18.

114. Li, H., Wang, Y., Liu, H., Zhang, Y., Zhang, Y., & Li, Y. (2020). Internal cement mortar lining for steel water pipes: Mechanisms of corrosion protection. “Water Science and Technology”, 81(10), 1969-1981.

115. Shen, S., Dai, P., Xia, Y., & Cao, Z. (2019). Organic corrosion inhibitors for internal corrosion protection of steel pipelines: A comprehensive review. “Corrosion Science”, 158, 108-118.

116. Tamalmani, K., & Husin, H. (2019). Internal corrosion inhibitors for oil and gas pipelines: Performance under multiphase flow conditions. “Journal of Natural Gas Science and Engineering”, 63, 203-211.

117. Vakili, M., Koutník, P., & Kohout, J. (2021). Advances in corrosion inhibitors for CO_2 and H_2S-induced internal corrosion in pipelines. “Corrosion Reviews”, 39(4), 305-324.

118. Cheng, Y. F. (2018). Internal cathodic protection of pipelines: Principles and applications. “Corrosion Engineering, Science and Technology”, 53(2), 157-166.

119. Muresan, L. M., & Barbu-Tudoran, L. (2020). Nanocomposite coatings for enhanced internal corrosion protection of steel pipelines. “Progress in Organic Coatings”, 145, Article 104647.

120. Healy, B., Yu, T., da Silva Alves, D., & Breslin, C. B. (2021). Graphene-based coatings for internal protection of steel pipelines: Advances and future perspectives. “Carbon”, 177, 1-21.

121. Jeong, Y.-J., Rubab, M., & Oh, D.-H. (2019). Development of self-healing coatings for internal corrosion protection of pipelines. “Coatings”, 9(9), Article 554.

122. Zhang, S., Xie, J., Huang, Y., Cheng, H., Zhang, Z., & Wu, Z. (2020). Smart coatings with self-healing functionality for corrosion prevention in oil and gas pipelines. “Journal of Materials Science”, 55(12), 4663-4680.

123. Bhandari, A., & Hossain, M. A. (2019). A study on the efficiency of airless spray coating technology for industrial applications. *Journal of Coatings Technology and Research, 16*(4), 919–926. https://doi.org/10.1007/s11998-019-00287-4

124. Li, C., Zhao, Y., & Wang, Y. (2018). Development of air spray painting technology in industrial applications: An overview. *International Journal of Advanced Manufacturing Technology, 97*(1-4), 99–113. https://doi.org/10.1007/s00170-018-1952-0

125. Fuchs, J. H., & Matz, M. (2020). The impact of rotary atomizer technology on the quality of coatings in industrial applications. *Surface and Coatings Technology, 399*, 126043. https://doi.org/10.1016/j.surfcoat.2020.126043

126. Zhang, Y., & Zhang, Q. (2021). Review on the advancements in coating technologies for corrosion protection. *Journal of Materials Science & Technology, 67*, 197–210. https://doi.org/10.1016/j.jmst.2020.09.046

127. Martinez, E., & Gonzalez, A. (2022). Electrostatic spray painting: Principles and applications in industry. *Progress in Organic Coatings, 160*, 106368. https://doi.org/10.1016/j.porgcoat.2021.106368

128. Williams, J. R. (2020). Trends in industrial coating applications: From air atomization to rotary atomizers. *Coatings, 10*(9), 865. https://doi.org/10.3390/coatings10090865